UNIVERSITY OF SOUTHAMPTON

Moments of Light-Meson Distribution Amplitudes from Lattice QCD

by

Michael Anthony Donnellan

A thesis submitted for the degree of

Doctor of Philosophy

School of Physics and Astronomy

September 2008

Dedicated to my parents.

UNIVERSITY OF SOUTHAMPTON

ABSTRACT

FACULTY OF SCIENCE

SCHOOL OF PHYSICS AND ASTRONOMY

Doctor of Philosophy

Moments of Light-Meson Distribution Amplitudes from Lattice QCD

Michael Anthony Donnellan

The distribution amplitudes of mesons parameterize their structure in partonic terms, at least insofar as that structure is relevant to collinearly-factorized exclusive processes: they essentially describe the valence Fock state's momentum distribution. Early applications were to form factors such as $F_\pi^{\rm em}(Q^2)$ and $F_{\gamma\gamma^*\pi}(Q^2)$, but the development of QCD factorization and the Soft Collinear Effective Theory has led to renewed interest motivated by flavour physics.

The lowest moments of the distribution amplitudes can be calculated using Lattice QCD. As part of the UKQCD/RBC collaborations' $N_f = 2+1$ domain-wall fermion phenomenology programme, we calculate the first two moments for the pseudoscalar mesons π and K and the (longitudinally-polarized) vector mesons ρ, K^* and ϕ, as well as the ratios of vector meson couplings f_ρ^T/f_ρ, $f_{K^*}^T/f_{K^*}$ and f_ϕ^T/f_ϕ. We obtain the desired quantities with a good precision and our results are in reasonable agreement with other recent lattice and QCD sum rule calculations (but with significantly smaller errors in the latter case). In particular, we are able clearly to discern the expected quark-mass dependence of SU(3) flavour breaking effects.

An important part of this research programme is the non-perturbative renormalization of lattice operators using the RI/MOM technique. We describe both our successful renormalization of the quark bilinears (necessary for the vector meson couplings) and our ongoing efforts to overcome some fundamental issues with RI/MOM which currently prevent us from using non-perturbative renormalization for the distribution amplitude moments.

Contents

List of Figures

List of Tables

Preface

The work described in this thesis was carried out as part of the broader UKQCD/RBC $N_f = 2+1$ domain-wall fermion phenomenology programme. Some of the results presented here have appeared in:

- P. A. Boyle, M. A. Donnellan, J. M. Flynn, A. Juttner, J. Noaki, C. T. Sachrajda and R. J. Tweedie [UKQCD Collaboration], "A lattice computation of the first moment of the kaon's distribution amplitude," Phys. Lett. B **641** (2006) 67 [arXiv:hep-lat/0607018].

- Y. Aoki *et al.*, "Non-perturbative renormalization of quark bilinear operators and B_K using domain wall fermions," Phys. Rev. D **78** (2008) 054510 [arXiv:0712.1061 [hep-lat]].

- C. Allton *et al.*, "Physical Results from 2+1 Flavor Domain Wall QCD and SU(2) Chiral Perturbation Theory," arXiv:0804.0473 [hep-lat]. (Accepted for publication in Phys. Rev. D).

The complete set of results for the low moments of light-meson distribution amplitudes will appear in a forthcoming UKQCD/RBC publication.

No claim to originality is made for the content of Chapters 1 - 3, which consist of background material compiled using a variety of other sources, including for example refs. [1–4], as well as a general description of the UKQCD/RBC simulations and datasets.

Of the original work contained in the remaining chapters, I worked directly on the bare calculations for both the vector meson couplings and the distribution amplitude moments, as well as on the non-perturbative renormalization of the quark bilinear operators.

Acknowledgments

Firstly, I would like to thank my supervisors Jonathan Flynn and Chris Sachrajda for their patient encouragement, advice, and support. I am grateful also to Rainer Sommer, both for bringing me to DESY Zeuthen and for allowing me time to write up.

It has been a pleasure to work with Conrado Albertus Torres, Dirk Brömmel, and Andreas Jüttner, each of whom I thank for their enthusiasm and helpfulness, extending of course far beyond things LQCD.

I would also particularly like to thank James Ettle, Andrew Tedder and Martin Wiebusch for their help and... comradeship(?). But mostly for keeping the whole thing interesting and amusing.

I am eternally grateful for Friederike's extremely generous help and support on making the transition to Berlin, without which it would all have gone very differently.

My experience in Southampton would not have been what it was without Sarah, to whom I will always be grateful for most of the best bits of those years.

Most of all I thank my parents.

Chapter 1

Introduction

The Standard Model (SM) embodies our current understanding of the fundamental structure of matter, successfully describing physical phenomena on scales down to around 10^{-16}cm. It is a quantum theory of fields, with a field corresponding to each of the known types of elementary particle (plus the as-yet-undiscovered Higgs field) and with the quantized excitations of those fields representing the particles themselves. The SM represents the culmination of decades of interplay between, on the one hand, theoretical efforts to reconcile quantum mechanics with special relativity, and on the other, painstaking experimental investigation of the sub-nuclear world. With a structure determined largely by fundamental principles of symmetry and renormalizability, the SM is a framework of impressive (if not totally satisfactory) underlying simplicity: all matter is composed of a few basic types of spin-1/2 fermion interacting via spin-1 'gauge' fields, the latter being formulated around non-Abelian generalizations of the local U(1) symmetry possessed by Maxwell's electromagnetic field equations.

As is typical of quantum field theories, the SM's Lagrangian actually defines an unphysical theory in which 'ultraviolet' divergences (infinities originating in its short-distance structure) are ubiquitous, a sign that it fails as a description of Nature on the smallest of scales. Given that it was constructed on the basis of experimental observations made up to limited energy

scales, this is unsurprising. In addition, its complicated structure and 19 free parameters hint at some deeper origin, it says nothing at all about gravity, and it offers no explanations for such relatively recent experimental discoveries as neutrino oscillations and dark matter. So the SM does not provide a complete description of Nature, and indeed it would have been unrealistic to have expected it to include all of the substructure present at as-yet-unreachable scales, and which presumably renders some true theory finite.

Nevertheless, the SM can be regarded as an 'effective field theory' that provides a valid description of physics up to some cutoff energy scale above which the new, currently-unknown physics becomes important. The effects of the missing ultraviolet physics on the low-energy physics are then encoded in the values of the free parameters. Within its range of validity, the Standard Model provides a predictive calculational framework independently of the cutoff if it is 'renormalized': calculations must be performed in a 'regularized' theory which is finite and from which the formally-defined theory is recovered in some limit, with some physical quantities that are divergent in the 'bare' unregularized theory - rather than the parameters appearing in the Lagrangian - held fixed at experimentally-determined values as that limit is taken.

In this way the theory may be defined, although the standard techniques, such as dimensional regularization, do so only at a perturbative level. Such perturbative definitions of the theory, however, make possible the calculation of a vast array of physical cross-sections and decay rates using renormalized perturbation theory. It is as a result of the accumulation of a broad range of such calculations, and their successful comparison with experimental results, that we have acquired such confidence in the SM and the basic principles upon which it is built.

One approach to seeking signs of physics beyond the SM is the somewhat indirect one of precision study of relatively low-energy processes which are particularly sensitive to the short-distance structure. In this way, it is hoped that it will be possible to overconstrain the

SM's parameters. In particular, in 'flavour physics' one wants to overconstrain the CKM matrix which describes how quark flavours mix under the weak interaction and which is the sole source of CP violation in the SM (ignoring the strong CP problem). These parameters must, however, be determined by studying weak decays of hadrons, which necessarily involve both the weak interactions and the strong interactions at low energy. This is an extremely difficult phenomenological problem because, whilst perturbation theory has been tremendously successful when applied to the electroweak interactions, its usefulness for the strong interactions is limited to high energies.

In the SM, the strong interactions are described by Quantum Chromodynamics (QCD), according to which strongly interacting matter consists of quarks and gluons which interact more and more weakly on smaller and smaller length scales (asymptotic freedom). This is compatible with the observation of Bjorken scaling in deep-inelastic scattering (DIS) experiments and with the success of the Feynman parton model of hadrons, and perturbative QCD (pQCD) may be used to describe some aspects of such processes with good accuracy. QCD also possesses the property of confinement, however: the interactions between quarks and gluons become stronger as the length scale is increased, to the extent that individual quarks or gluons cannot be separated from the bound-states and are never observed. Hadrons are therefore unique amongst composite objects, since their constituents do not exist in isolation.

The strong interactions, then, are unavoidably non-perturbative, and this will almost always be relevant to physical processes - if only because hadrons are present in the initial and final states. The non-perturbative physics of hadronization obscures the clean electroweak physics of weak hadronic decays, and in fact the dominant uncertainty in our description of such processes is often the theoretical uncertainty on the relevant hadronic matrix elements.

Lattice QCD (LQCD) provides a non-perturbative definition of QCD and the possibility of determining such hadronic matrix elements from first principles, thereby making it possible to

see past the soft, nonperturbative strong interaction physics and to extract signals for the underlying electroweak physics. There are a variety of quantities which in some sense parameterize hadron structure in terms of quarks and gluons. Light-cone distribution amplitudes are one such quantity, entering the theoretical description of exclusive processes at large momentum transfer. As we shall discuss, they are an important non-perturbative input in flavour physics. In this work, we use LQCD to improve upon our knowledge of the leading-twist distribution amplitudes of light mesons, via the calculation of their lowest moments.

The remainder of this thesis is structured as follows:

- In Chapter 2 we discuss in some generality the QCD Lagrangian and its symmetries. We describe how Light-Cone Distribution Amplitudes arise in the factorization of hard exclusive processes, what they can tell us about hadronic structure, how they are studied, and what is currently known about them. We also discuss some related non-perturbative quantities: the vector meson couplings to the vector and tensor currents, f_V and f_V^T.

- In Chapter 3 we review LQCD. We discuss the lattice formulation of fermion and gauge fields, focussing in particular on the domain wall fermion (DWF) action used in this study. We also outline the associated numerical and theoretical techniques, such as the RI/MOM non-perturbative renormalization approach which we employ in this work. We give the simulation and measurement parameters which describe the UKQCD/RBC datasets with which we work.

- In Chapter 4 we describe the bare lattice calculations we have performed for the ratios of vector meson couplings, f_V^T/f_V, and present our unrenormalized results.

- In Chapter 5 we discuss the non-perturbative renormalization of the fermion bilinear operators on our lattices, with emphasis on the calculation of the renormalization constants necessary for our vector meson couplings calculation. We also present our final f_V^T/f_V

results.

- In Chapter 6 we describe the bare lattice calculations in which we obtain values for the first 2 moments of the leading-twist distribution amplitudes for the pseudoscalar mesons π and K and for the vector mesons ρ, K^* and ϕ. We present the bare results and discuss the chiral extrapolation of our data.

- Chapter 7 contains a discussion of the renormalization necessary for the distribution amplitude moments, beginning with the perturbative calculations and moving on to the current status of our attempts at non-perturbative renormalization.

- In Chapter 8 we present our final results for the distribution amplitude moments and summarize what has been done so far. We discuss both the prospects for further refinement of these results and for the future of lattice studies of distribution amplitudes more generally.

Chapter 2

QCD and Light-Cone Distribution Amplitudes

In this chapter, we begin by introducing QCD and outlining some of its more general properties, focussing on those aspects which are of most direct relevance to this work. We then discuss the issues and challenges involved in actually using QCD to do strong interaction phenomenology, describing the most important calculational approaches and their usefulness and limitations in understanding physical processes.

We move on to explain the phenomenological origin and physical interpretation of the hadronic quantities of primary interest in this work, the light-cone distribution amplitudes. In addition, we also discuss the (very closely-related) vector meson couplings to the vector and tensor currents, which we also study on the lattice. We attempt both to place the distribution amplitudes in context in the larger picture of hadron structure studies, as well as to emphasize their more recently-acquired importance for flavour physics analyses - and therefore ultimately for the understanding of CP violation and the search for new physics as described in chapter 1. We discuss the theoretical approaches currently used in the study of distribution amplitudes and summarize the present status of our knowledge and understanding of them.

Table 2.1: Current quark mass estimates [5].

q	m_q
u	1.5 - 3.3 MeV
d	3.5 - 6 MeV
s	104^{+26}_{-34} MeV
c	$1.27^{+0.07}_{-0.11}$ GeV
b	$4.2^{+0.17}_{-0.07}$ GeV
t	171.2 ± 2.1 GeV

2.1 QCD

QCD is, at least at the classical level, fully defined by its Lagrangian density:

$$\mathscr{L} = -\frac{1}{4} F^a_{\mu\nu} F^{a\mu\nu} + \sum_i^{N_f} \bar{\psi}_i (i\gamma^\mu D_\mu - m_i)\psi_i. \tag{2.1}$$

Here we have suppressed all spacetime arguments and both the spin and color indices of the fermionic fields ψ_i. The flavour index i runs over the number of flavours N_f, which appears to be 6 in Nature, with each flavour consisting of a triplet of Dirac spinors transforming in the defining representation of the gauge group SU(3) and being characterized by a mass parameter m_i. There is a very clear hierarchy in these masses[1], and recent estimates for their values are given in table 2.1.

The "gamma matrices" γ^μ satisfy the Dirac algebra (i.e., the Clifford algebra of the Lorentz group SO(3,1)):

$$\{\gamma^\mu, \gamma^\nu\} = 2\eta^{\mu\nu}, \tag{2.2}$$

where $\eta^{\mu\nu}$ is the Minkowski metric. Classically, then, the quark fields would have as their

[1] Since the quarks are confined, of course, there is some ambiguity in precisely how their masses are defined. Nevertheless, the existence of a very definite quark mass hierarchy is well-established.

equation of motion the Dirac equation, except that the ordinary spacetime derivative has been replaced by the gauge covariant derivative D_μ, which introduces a coupling to the gauge fields A^a_μ through the dimensionless parameter g, the gauge coupling:

$$D_\mu \equiv \partial_\mu - igA^a_\mu(x)T^a. \tag{2.3}$$

The T^a appearing here are the generators, for the defining representation, of the Lie algebra of SU(3), which is defined by:

$$[T^a, T^b] = if^{abc}T^c, \tag{2.4}$$

where the f^{abc} are the structure constants. They are conventionally normalized such that:

$$\mathrm{Tr}[T^aT^b] = \frac{1}{2}\delta^{ab} \tag{2.5}$$

The gauge field A^a_μ transforms in the adjoint representation of SU(3), and its dynamics are specified via the field strength tensor

$$F^a_{\mu\nu} \equiv \partial_\mu A^a_\nu - \partial_\nu A^a_\mu + gf^{abc}A^b_\mu A^c_\nu, \tag{2.6}$$

the structure of which clearly leads to self-interactions among the gluons.

The form of the QCD Lagrangian is largely determined by a few fundamental principles - it is constructed such that it possesses a local SU(3) symmetry corresponding to the field transformations:

$$\psi(x) \rightarrow \psi'(x) = \Lambda(x)\psi(x) \tag{2.7}$$

$$A_\mu(x) \equiv A^a_\mu(x)T^a \rightarrow A'_\mu(x) = \Lambda(x)A_\mu\Lambda^{-1}(x) + (\partial_\mu\Lambda(x))\Lambda^{-1}(x) \tag{2.8}$$

for any differentiable field of SU(3) matrices $\Lambda(x)$ acting on the colour indices. This requirement, as well as the demand that the theory be renormalizable, essentially determines the structure of the QCD Lagrangian.

2.1.1 Symmetries

The symmetries of the QCD Lagrangian are crucial to an understanding of its relation to strong interaction phenomenology. As we shall discuss, however, those symmetries are for the most part approximations only, being subject either to an explicit breaking which is in some sense small or else to spontaneous breaking or breaking by quantum effects.

The quark masses are the only scales present in the QCD Lagrangian, and so QCD with massless quarks would appear to be scale invariant. In fact, the Lagrangian possesses a slightly larger symmetry known as conformal symmetry. This symmetry, however, is a symmetry of the classical theory only and is broken in the quantum theory (even in the absence of quark masses) because, although it holds for the Lagrangian, it does not hold for the path integral measure that is required to define the full quantum theory. Nonetheless, conformal symmetry can be a useful tool for the phenomenologist, as we shall discuss when we introduce the conformal expansion in section 2.5.

This breaking of conformal symmetry by quantum effects is known as the 'conformal anomaly', and can be illustrated by the non-zero value of the β-function, defined via:

$$\beta(g) \equiv g\frac{\partial g}{\partial \mu}\,, \tag{2.9}$$

where g is a renormalized coupling and μ the corresponding renormalization scale. A one-loop perturbative calculation for a general gauge group SU(N_c) yields:

$$\beta(g) = -\frac{g^3}{16\pi^2}\left[\frac{11}{3}N_c - \frac{2}{3}N_f\right] \tag{2.10}$$

Since we can define a scale by specifying a particular value taken by the renormalized coupling (i.e., we must introduce a constant of integration), the quantum theory actually generates a scale ('dimensional transmutation'). This scale, known as $\Lambda_{\rm QCD}$, serves as a measure of the point at which QCD becomes non-perturbative, and has a value of approximately 0.5 GeV.

It is with this dynamically-generated scale that the quark masses, and the differences between them, must be compared. It is usual to divide the quark flavours into the light quarks (u,d,s) whose masses lie below Λ_{QCD} and the heavy quarks (c,b,t) whose masses lie above it. The heavy flavours are so much heavier, in fact, that it is often appropriate to work in an effective theory in which they have been integrated out and their influence has been absorbed into the values of the free parameters. This is the approach we take in our $N_f = 2+1$ simulations, and in this work we restrict our attention to light-quark physics (although, as we shall discuss, our results do have relevance to heavy flavour physics).

Similarities in the light quark masses endow QCD with some approximate flavour symmetries. As can be seen from table 2.1, there appears to be a significant mass difference between the u and d quarks. Nevertheless, predictions based upon SU(2) isospin symmetry hold at approximately the 1% level, since both masses are so much less than Λ_{QCD}. Similarly, even SU(3) flavour symmetry holds at approximately the 30% level, despite the strange quark being much more massive than either the u or the d, because the masses of each of the quarks (u,d,s) is well below the QCD scale.

In the massless-quark limit, the flavour symmetries are chiral - i.e. they hold separately for left- and right-handed quarks, giving an $SU(3)_L x SU(3)_R$ symmetry. This symmetry is spontaneously broken in QCD, however, leading to the appearance of 'approximately massless' bosons in accordance with Goldstone's theorem (the pseudoscalar mesons are much lighter than the other hadrons and may be regarded as pseudo-Goldstone bosons). By expanding simultaneously in the momenta and quark masses, it is possible to write an effective theory for the low energy physics of QCD in terms of these pseudo-Goldstone bosons - chiral perturbation theory (χPT) [6, 7]. χPT can often provide some theoretical guidance for the quark mass extrapolations that are necessary for LQCD simulations, which at present are are only computationally-feasible with excessively-heavy light-quarks.

2.2 Factorization

Since hadronic processes necessarily involve the long-distance, strongly-coupled behaviour of QCD, very little strong interaction physics can be described directly in perturbation theory. Inclusive cross sections without hadrons in the initial-state, such as the total cross section for e^+e^- annihilation into hadrons (or even into jets) are the exception. In such cases, the non-perturbative physics associated with hadronization drops out and a quark-gluon level calculation suffices because, when the details of the hadrons in the final state are ignored, all outgoing quark-gluon states contribute.

For most processes involving the strong interactions, however, some means of systematically disentangling the short- and long-distance contributions (factorization) is necessary in order for pQCD to be useful. Almost all applications of pQCD rely to some extent upon one of the several factorization theorems which have been established to varying degrees of rigour [8]. These factorization theorems are essentially extensions of the operator product expansion (OPE) [9], which allows for the separation of scales in a physical amplitude by re-expressing a product of operators as a product of a local operator (whose hadronic matrix elements contain the non-perturbative effects) and a Wilson-coefficient (which can be calculated in perturbation theory).

The factorization of a QCD process amounts to isolating a perturbatively-calculable quark-gluon level subprocess from the surrounding soft physics. The full QCD process is then described by combining the perturbative contribution, calculated at some order in $\alpha_s = g^2/(4\pi)^2$, with a non-perturbative quantity which supplies the relevant hadron structure information (i.e., whichever aspect of the hadronic wavefunction controls the process in question). These non-perturbative quantities can be measured experimentally, and ideally they will be defined independently of the details of a given process, thereby making possible a unified interpretation of

a broad range of experiments. Lattice QCD, of course, provides a non-perturbative definition of QCD and a corresponding calculational method, and therefore allows in some cases for the ab initio calculation of such quantities.

Light-cone distribution amplitudes, the subject of this work, are an important class of non-perturbative hadronic quantities, showing up in the analysis of hard exclusive processes (i.e., processes in which we do concern ourselves with the hadronic reaction products in the final state) to which "collinear factorization" theorems apply. In this section, before giving a formal definition of the distribution amplitudes, we attempt to establish the phenomenological contexts in which they arise, their relation to other quantities which parameterize hadron structure, and their physical interpretation [10,11]. We therefore compare, within the physically-intuitive framework of the quark-parton model, factorization in the inclusive and exclusive cases. We will later show how Light-Cone Quantization can unify the description of inclusive and exclusive processes and can bridge the gap between the physically-intuitive notion of what DAs are and their field-theoretic definition.

2.2.1 Inclusive Processes

The study of inclusive processes has dominated the development of QCD phenomenology. Both experimentally and theoretically, inclusive processes are more accessible than exclusive processes: the cross sections and branching ratios fall off much more slowly with momentum transfer, detection of the final state is simpler, and factorization is naturally more straightforward when particular hadronic final states are not distinguished.

We restrict ourselves here to a brief discussion of perhaps the most important and familiar of inclusive processes: deep-inelastic lepton hadron scattering (DIS) [12]. A lepton l (in the simplest case, an electron) exchanges a large momentum Q^2 with a hadron H which breaks up: $l^{\pm}H \rightarrow l^{\pm}X$, with X representing any final state of the hadronic remnant. The differential cross

section at a given energy is measured with respect to the lepton's energy and angle of deflection only.

In the parton model, the hadron is assumed to consist of a cluster of collinear, almost-free pointlike constituents. At sufficiently high energies, the relative velocities of the participating particles are nearly lightlike, and so the hadronic binding processes are highly time-dilated in the rest frame of the leptonic probe, and the partonic state of the hadron can be considered to be "frozen" for the duration of the scattering process. Furthermore, by considering the process in the "infinite momentum frame", in which the hadron has a very large momentum along the opposite direction to the virtual boson and is therefore seen to be highly Lorentz contracted, it is to be expected that the virtual boson couples to a single parton. At large momentum transfer it is likely that the struck parton is 'knocked out' of the hadron. The process therefore has two characteristic timescales: there is a fast elastic scatter involving the lepton and a single parton, and a much slower hadronization process, with the struck parton being knocked well clear of the others before the impact can be communicated to them. There is therefore a lack of quantum interference between the long-distance, hadronic binding and the short-distance momentum transfer.

The inclusive cross section is concerned only with the outgoing lepton, and the hadronization process which "dresses up" the hadronic remnants into colourless states is irrelevant. The arguments above suggest that the deflection of the lepton will be determined by the charge and momentum of the struck parton, however, and will be otherwise insensitive to that parton's relation to the other hadronic constituents. The relevant hadron structure information is then simply the probability of the probe encountering a charged parton of type i, in a given hadron H, carrying a fraction x of the hadron's momentum, $f_{i/H}(x, Q^2)$. These are the parton distribution functions (pdfs). The DIS cross-section is given by a convolution of the pdfs with a perturbatively calculable cross-section for the hard subprocess.

The pdfs are process-independent and intrinsic to a given hadron. They can therefore also be used to describe other inclusive processes, such as Drell-Yan processes like $H_1 + H_2 \rightarrow \mu^+ + \mu^- + X$. The pdfs, however, are single-particle probabilities. They are not sensitive either to particular Fock states within the hadron or to correlations between quarks and gluons. Thus, the study of hard inclusive reactions does not provide information about hadronic structure at the amplitude level, but rather is limited to telling us about the partonic content of hadrons.

2.2.2 Exclusive Processes

Although the study of exclusive processes involving hadrons has been somewhat overshadowed by the study of the inclusive reactions, the possibility of applying pQCD to exclusive processes was established some time ago, with the framework of collinear factorization [13]. Exclusive processes provide new and complimentary information on hadron dynamics: they allow for the study of QCD processes at the amplitude level, and - whereas inclusive reactions reveal only the partonic content of hadrons - the exclusive reactions can actually tell us about the structure of the bound states. As we will discuss below, this is because exclusive processes are dominated by specific, rare configurations of the partonic constituents: either only the valence-quarks contribute, or else one of the partons carries most of the hadron's momentum (known as the soft overlap or Feynman mechanism). The study of exclusive processes is now coming to the fore of QCD phenomenology [14], especially in the light of the development of approaches for the theoretical description of hadronic B decays, given their importance for constraining the CKM matrix and for studies of CP-violation.

As an example we discuss the simplest case, elastic scattering $e^- \pi \rightarrow e^- \pi$, which is described by the pion's electromagnetic form factor:

$$\langle \pi(p_2)|V_\mu(0)|\pi(p_1)\rangle = F_\pi(Q^2)(p_1 + p_2)_\mu, \tag{2.11}$$

where $V_\mu(0) = (\frac{2}{3} e \bar{u}\gamma_\mu u - \frac{1}{3} e \bar{d}\gamma_\mu d)$ is the electromagnetic current for the light quarks and $Q^2 =$

$-q^2 > 0$ is the squared-momentum of the virtual photon. There is no term proportional to $(p_1 - p_2)_\mu$ because the electromagnetic current is conserved. The form factor $F_\pi(Q^2)$ contains both the perturbative and the non-perturbative dynamics of the process. It is a reasonably intuitive quantity, describing the departure from point (Rutherford) scattering, and in a non-relativistic analysis it can be shown to be essentially the Fourier transform of the hadron's charge density.

As with the inclusive reactions, the quark-parton model provides a good starting point for reasoning about factorization in exclusive processes. Again, the partonic state of the hadron can be considered to be 'frozen' for the duration of the scattering process, and the photon couples to a single parton. Because we are now interested in a particular final state, however, we must consider specific Fock states within the hadron. It is unlikely that the outgoing partons will reform into a pion unless they are collinear, and this will not be the case if the struck parton is unable to communicate the impact to the others. It is clear, therefore, that hard gluon exchange must take place in order to turn all the partons of a given Fock state to the final direction, and since more partons require more hard gluons, the process is dominated by the valence Fock state.

In fact, there is a caveat to the argument presented above. If one of the partons carries almost all of the hadron's momentum, then the remaining partons have very long wavelengths and can have a significant overlap with any outgoing direction. In this case, the gluon exchange argument does not hold and the valence Fock state is not guaranteed to dominate. This is known as the 'soft overlap' or Feynman mechanism, and threatens the applicability of collinear factorization.

The relevant hadron structure information for this hard exclusive processes, then, is the overlap of the pion state with the valence Fock state in which the collinear quark and antiquark pair have small transverse separation and carry longitudinal momentum fractions u and $\bar{u} =$

$1-u$. This is the pion distribution amplitude $\phi_\pi(u,Q^2)$. At large Q^2, we can then write the pion's electromagnetic form factor as a convolution of DAs for the incoming and outgoing pions with a perturbatively-calculable hard-scattering kernel T_H:

$$F_\pi(Q^2) = \int_0^1 dx \int_0^1 dy\, \phi_\pi(y,Q^2) T_H(x,y,Q^2) \phi_\pi(x,Q^2) \tag{2.12}$$

2.3 Meson Distribution Amplitudes

We have seen how hadronic light-cone distribution amplitudes arise in the QCD analysis of those "classical" hard exclusive processes, such as the pion's electromagnetic form factor and the $\gamma\gamma^* - \pi$ transition form factor, to which collinear factorization was shown to apply by Brodsky, Lepage and others [13, 15–17] almost 30 years ago. The study of DAs - along with that of the Generalized Parton Distributions (GPDs) [18, 19], which are closely related - is crucial to the extension of QCD's descriptive power beyond the inclusive processes through which it historically proved its value as a fundamental theory.

In addition to their conceptual value as components of the hadronic wavefunction, and their phenomenological uses in describing these "classical" processes, however, the distribution amplitudes have acquired new relevance and importance as a result of field-theoretical developments that have taken place in recent years. The development of two competing approaches to the subtle problem of factorization in B decays, in both of which the distribution amplitudes play an important role, and the detailed study of such processes at the B-factories BaBar and Belle, makes the accurate determination of DAs particularly pressing, since now they are important for the measurement of the CKM matrix, for the study of CP violation, and in the search for new physics.

Factorization is more difficult to establish in B-physics because the hard and soft mechanisms contribute at the same order in $1/m_b$. It has been shown, however, that collinear

factorization can be applied, to leading order in $1/m_b$, to a large class of nonleptonic B-decays [20–22]. This framework, known as "QCD factorization", makes use of meson DAs to parameterize the nonperturbative physics. Secondly, DAs also play a crucial role in the soft-collinear effective theory (SCET) [23–25], which aims to provide a unified theoretical framework for the factorization of both hard-collinear and soft effects. In this work, we shall focus on the distribution amplitudes of light mesons, specifically the pseudoscalars and vectors. These are relevant for decays such as $B \to \pi\pi$ and $B \to \pi K$. They also appear in light-cone sum rule (LCSR) expressions for the form factors of semileptonic decays such as $B \to \pi l \nu$.

Our discussion in the previous section actually applies to the distribution amplitudes of leading-twist, which control cross-sections and decay rates at leading-order in Q^2. The higher-twist DAs are associated with power-suppressed contributions, and originate, for example, in higher Fock states [26]. We shall consider only the leading, twist-2 distribution amplitudes in this work.

The light-cone DAs are defined via vacuum-to-meson matrix elements of quark-antiquark light-cone operators, which are essentially non-local continuations of those which define the decay constants. In the pseudoscalar case at leading-twist, we have for example:

$$\langle 0|\bar{q}(z)\gamma_\rho\gamma_5\mathscr{P}(z,-z)q(-z)|\pi(p)\rangle|_{z^2=0} \equiv f_\pi(ip_\rho)\int_0^1 du\, e^{i(u-\bar{u})p\cdot z}\phi_\pi(u,\mu) \tag{2.13}$$

where

$$\mathscr{P}(z,-z) = \mathscr{P}\exp\left\{-ig\int_{-z}^{z} dw^\mu A_\mu(w)\right\}, \tag{2.14}$$

is the path-ordered exponential which is necessary to maintain gauge invariance, and f_π is the pion decay constant defined by the local matrix element $\langle 0|\bar{q}\gamma_\mu\gamma_5 q|\pi(p)\rangle = if_\pi p_\mu$. The DA's normalization is such that:

$$\int_0^1 du\,\phi_\pi(u,\mu) = 1\,. \tag{2.15}$$

In hard exclusive processes involving the light vector mesons ρ, K^* and ϕ, polarization-

dependence provides many opportunities to study the underlying dynamics, with the longitudinally and transversely polarized final vector meson states often corresponding to different weak interaction physics [27]. Particularly important examples of such processes are the exclusive semileptonic $B \to \rho l \nu_l$, rare radiative $B \to \rho\gamma$ or nonleptonic, $B \to \pi\rho$ etc. decays of B-mesons, which are crucial for extracting CKM matrix elements.

The theoretical description of such processes requires knowledge of the vector meson distribution amplitudes and their normalizations, the vector meson decay constants. The leading-twist vector meson DAs, in the longitudinally-polarized case, are given by:

$$\langle 0|\bar{q}(z)\gamma_\mu \mathscr{P}(z,-z)q(-z)|\rho(p;\lambda)\rangle|_{z^2=0} \equiv f_\rho m_\rho p_\mu \frac{\varepsilon_{(\lambda)}\cdot z}{p\cdot z}\int_0^1 du\, e^{i(u-\bar{u})p.z}\phi_\rho^{\parallel}(u,\mu)\,, \quad (2.16)$$

where p and λ are the momentum and polarization state of the vector meson $V(p;\lambda)$ and $\varepsilon_{(\lambda)}$ is the corresponding polarization vector. In addition to the vector meson decay constant f_ρ there is also its coupling to the tensor current, f_ρ^T. These quantities are of phenomenological interest in their own right, and we now address their definitions and importance.

2.3.1 Vector Meson Couplings

In this section, we discuss the couplings of the light vector mesons V to the vector and tensor currents. These couplings f_V and f_V^T are defined through the matrix elements:

$$\langle 0\,|\,\bar{q}_2(0)\gamma^\mu q_1(0)\,|\,V(p;\lambda)\rangle \;=\; f_V\, m_V\, \varepsilon^\mu_{(\lambda)} \quad (2.17)$$

$$\langle 0\,|\,\bar{q}_2(0)\sigma^{\mu\nu} q_1(0)\,|\,V(p;\lambda)\rangle \;=\; i f_V^T(\mu)\left(\varepsilon^\mu_{(\lambda)}p^\nu - \varepsilon^\nu_{(\lambda)}p^\mu\right), \quad (2.18)$$

where we note that $\varepsilon^\mu_{(\lambda)}p_\mu = 0$ and $\sigma^{\mu\nu} \equiv \frac{i}{2}[\gamma^\mu,\gamma^\nu]$. The tensor bilinear operator $\bar{q}_2\sigma^{\mu\nu}q_1$ (and hence $f_V^T(\mu)$) depends on the renormalization scheme and scale μ (we will ultimately quote our final results, in chapter 5, in the $\overline{\rm MS}$ scheme at $\mu = 2\,{\rm GeV}$).

The decay constants f_V can be determined experimentally. For the charged ρ and K^* mesons, one can use τ decays to deduce f_ρ and f_{K^*} as illustrated by the diagram in fig. 2.1,

Figure 2.1: The diagram illustrating how τ decays can be used to deduce f_ρ and f_{K^*}.

where the curly line represents the W-boson. From the measured branching ratios one obtains the following values for the decay constants [28]:

$$\mathrm{Br}(\tau^- \to \rho^- \nu_\tau) = (25.0 \pm 0.3)\% \quad \Rightarrow \quad f_{\rho^-} \simeq 208\,\mathrm{MeV} \tag{2.19}$$

$$\mathrm{Br}(\tau^- \to K^{*-} \nu_\tau) = (1.29 \pm 0.05)\% \quad \Rightarrow \quad f_{K^{*-}} \simeq 217\,\mathrm{MeV}\,, \tag{2.20}$$

where, as in ref. [28], we display only the central values. One can also determine f_{ρ^0} from the width of the decay of the ρ^0 into e^+e^- which gives $f_{\rho^0} = 216(5)$ MeV. Similarly from the width of the decay $\phi \to e^+e^-$ one deduces $f_\phi \simeq 233$ MeV.

The couplings f_V^T can not be obtained directly from experiment but are used as inputs in sum-rule calculations (see, for example, refs. [29,30]) and other phenomenological applications to B-decays (see, for example, refs. [31–34]). They can of course also be determined from sum rule analyses, but as the uncertainties due to the sum rule approach are difficult to quantify, it would be preferable to have a lattice determination. Previous lattice results for the vector meson couplings will be discussed in chapter 5; determinations obtained using QCD sum-rules are reviewed in [29]. In chapters 4 and 5, we present our calculation and results for f_V^T/f_V, which can then be combined with the experimental values of f_V to obtain f_V^T. As described in ref. [28], the ratio is itself an important non-perturbative input in sum rule expressions for form factors for processes such as $B \to \rho l \nu$, which in turn are important in the extraction of CKM matrix elements.

2.4 Light-Cone Quantization

We have been discussing the factorization of both inclusive and exclusive hadronic processes within the context of the parton model, which enabled us to make qualitative physical arguments as to which aspects of the hadronic wavefunction control these processes. In particular, we have argued that the distribution amplitudes which control hard exclusive processes essentially describe the momentum distribution of the valence quarks.

This discussion of the hadronic wavefunction may seem somewhat poorly motivated, however, and in particular a discussion in terms of individual Fock states could seem dubious from a field theoretic perspective. In the standard formulation of QCD - or indeed any relativistic quantum field theory, confining or not - a constituent picture of bound states is problematic because the physical vacuum of an interacting theory is not in general the Fock vacuum, and the wavefunction must describe states with an arbitrary number of quanta having arbitrary momenta and helicities. Furthermore, boosting such a wavefunction is as complex a problem as initially solving the bound state problem in the rest frame.

In this section we briefly introduce light-cone quantization (LCQ) [35,36], an alternative to the usual equal-time quantization (ETQ) formulation of relativistic quantum field theories. LCQ possesses a number of unique features which make it particularly suitable for the composite description of bound states, and allows us to formulate QCD such that it resembles as far as possible the parton model. LCQ allows for a unified description of inclusive and exclusive reactions and should clarify our discussion of the hadronic wavefunction and the isolation of individual Fock states, as occurs in the distribution amplitudes.

LCQ originates in a 1949 paper by Dirac [37]), in which the three distinct, reasonable choices for a 'time' parameter in relativistic Hamiltonian dynamics are identified. The 'instant form' of dynamics corresponds to ETQ and is implicitly used in most field theory work, whilst

the 'front form' is the basis for LCQ. Comparatively little work is done in the 'point form'. Dirac showed that in this front form of Hamiltonian dynamics a maximum number of Poincare generators become independent of the interaction, including certain Lorentz boosts.

In LCQ, then, the quantization surface is a null plane tangent to a light-front. It is convenient to introduce light-cone coordinates:

$$x^{\pm} \equiv x^0 \pm x^3 \quad x_{\perp} = (x^1, x^2), \tag{2.21}$$

such that the magnitude of a 4-vector x is given by $x^2 = x_+ x_- - \vec{x}_{\perp}^2$. We may then take $x^+ = 0$ to define the quantization surface. To contrast this approach with ETQ, we consider a simple scalar field theory. In canonical quantization, we define our field operators in the Heisenberg Picture by specifying that the canonical commutation relations:

$$[\phi(\mathbf{x}), \pi(\mathbf{y})] = i\delta^{(3)}(\mathbf{x}-\mathbf{y}) \tag{2.22}$$

$$[\phi(\mathbf{x}), \phi(\mathbf{y})] = [\pi(\mathbf{x}), \pi(\mathbf{y})] = 0 \tag{2.23}$$

hold on a surface of constant time t for some inertial frame [1]. The field operators in the rest of spacetime are then determined in the usual way, by the generator of time translations - the Hamiltonian:

$$\phi(x) = e^{iHt}\phi(\mathbf{x})e^{-iHt} \tag{2.24}$$

This choice corresponds to a choice of a Fock basis, however, and the different field operators obtained by using a different quantization surface will operate differently on the Fock space, creating and destroying different quanta.

2.4.1 The Fock State Expansion and Hadronic Wavefunctions

The most remarkable feature of this formalism is the apparent simplicity of the vacuum state - since the total light-cone momentum $P^+ > 0$ and is conserved, the physical vacuum appears to

coincide with the Fock vacuum. There is thus no spontaneous creation of massive fermions in the ground state, and all constituents in a physical eigenstate are directly related to that state and not to disconnected vacuum fluctuations. The LCQ Fock state expansion therefore provides a complete relativistic many-particle basis for diagonalizing the full theory.

Using the light-cone Fock basis, it is possible to define universal, process-independent, frame-independent hadronic wavefunctions encoding all possible quark and gluon correlations:

$$\langle n; x_i, \vec{k}_{\perp i}, \lambda_i | \psi_H \rangle = \psi_{n/H}(x_i, \vec{k}_{\perp i}, \lambda_i) \tag{2.25}$$

where $x_i \equiv k_i^+ / p^+$.

It is now possible to make more definite statements about the physical interpretations we have offered for pdfs and DAs. The pdfs may be expressed as both an integration over transverse degrees of freedom and a sum over Fock states:

$$q(x, Q^2) = \sum_n \int d^2 k_\perp \sum_\lambda \left| \psi_n(x_i, \vec{k}_{\perp i}, \lambda_i) \right|^2 . \tag{2.26}$$

and the (leading-twist) pion distribution amplitude may be written as an integration over transverse momenta for the valence Fock state only:

$$\phi_\pi(x, Q^2) \equiv \int^{Q^2} d^2 k_\perp \psi_{q\bar{q}/\pi}(x_i, \vec{k}_{\perp i}, \lambda) . \tag{2.27}$$

2.5 Parameterization of DAs via Moments

Light-cone distribution amplitudes have traditionally been parameterized in terms of their moments, defined in the usual way:

$$\langle \xi^n \rangle_\pi(\mu^2) = \int_{-1}^{1} d\xi \, \xi^n \phi_\pi(\xi, \mu^2), \tag{2.28}$$

where we have introduced the difference between the longitudinal momentum fractions, $\xi \equiv u - \bar{u} = 2u - 1$.

It is because the ordinary moments may be related to matrix elements of local operators [38] that we may study the distribution amplitudes using lattice QCD (the light-cone matrix elements which define the DAs themselves are of course not amenable to the standard lattice techniques, since in Euclidean space the light-cone has been rotated to the complex direction). By expanding the non-local operators on the light cone, we obtain symmetric, traceless twist-2 operators (the twist of an operator being the difference between its dimension and its spin). The moments can then be obtained from matrix elements such as:

$$\langle 0|\bar{q}(0)\gamma_\rho\gamma_5\overleftrightarrow{D}_\mu s(0)|K(p)\rangle = \langle\xi^1\rangle_K f_K p_\rho\, p_\mu, \tag{2.29}$$

$$\langle 0|\bar{q}(0)\gamma_\rho\gamma_5\overleftrightarrow{D}_\mu\overleftrightarrow{D}_\nu q(0)|\pi(p)\rangle = -i\langle\xi^2\rangle_\pi f_\pi p_\rho p_\mu p_\nu, \tag{2.30}$$

$$\langle 0|\bar{q}(0)\gamma_\rho\overleftrightarrow{D}_\mu s(0)|K^*(p,\lambda)\rangle = \langle\xi^1\rangle^{\parallel}_{K^*} f_{K^*} m_{K^*}\frac{1}{2}\left(p_\mu\varepsilon_\nu^{(\lambda)} + p_\nu\varepsilon_\mu^{(\lambda)}\right), \tag{2.31}$$

$$\langle 0|\bar{q}(0)\gamma_\rho\overleftrightarrow{D}_\mu\overleftrightarrow{D}_\nu q(0)|\rho(p,\lambda)\rangle = -i\langle\xi^2\rangle^{\parallel}_\rho f_\rho m_\rho\frac{1}{3}\left(\varepsilon_\rho^{(\lambda)}p_\mu p_\nu + \varepsilon_\mu^{(\lambda)}p_\nu p_\rho + \varepsilon_\nu^{(\lambda)}p_\rho p_\mu\right). \tag{2.32}$$

We note that the same operators also appear in studies of moments of GPDs (in that case, however, we require meson-meson matrix elements rather than meson-vacuum matrix elements).

In more modern analyses, especially those based upon the technique of QCD sum rules (which we discuss in the next section), one deals instead with the 'Gegenbauer moments' which arise from a conformal expansion [39,40]. The conformal expansion is analogous to the partial wave expansion in ordinary quantum mechanics, in which we make use of the rotational invariance of a spherically-symmetric potential to separate angular degrees of freedom from radial ones.

In the partial wave decomposition, all dependence on the angular coordinates is included in spherical harmonics $Y_m^l(\theta,\phi)$, which form an irreducible representation of O(3), and the dependence on the remaining radial coordinate is governed by a one-dimensional Schrödinger

equation:

$$\psi(r,\theta,\phi) \to R(r)\sum_{m,l} Y_m^l(\theta,\phi) \tag{2.33}$$

In the conformal expansion, one uses instead the conformal invariance of massless QCD to separate longitudinal and transverse degrees of freedom. All dependence on the longitudinal momentum fractions is described by orthogonal polynomials that form an irreducible representation of the 'collinear subgroup' of the conformal group, SL(2,$\mathbb{R}$). The transverse-momentum dependence is represented as the scale-dependence of the relevant operators and is governed by RG equations.

Give that the anomalous breaking of conformal symmetry is a rather characteristic feature of QCD, it may seem somewhat surprising that a conformal expansion is found to be a useful tool. In fact, the different 'partial waves', labelled by different "conformal spins", do mix but not to leading-logarithmic accuracy. Conformal spin is thus a good quantum number in hard processes up to small corrections of order α_s^2.

The asymptotic $Q^2 \to \infty$ DA is known from perturbative QCD: $\phi_{as} = 6u\bar{u}$. For the leading-twist quark-antiquark DAs that we are interested in, the conformal expansion can then be written:

$$\phi(u,\mu^2) = 6u\bar{u}\sum_{n=0}^{\infty} a_n(\mu^2) C_n^{3/2}(2u-1), \tag{2.34}$$

where $C_n^{3/2}(2u-1)$ are Gegenbauer polynomials. Since the partial waves of different conformal spin do not mix to leading-order accuracy, the Gegenbauer moments renormalize multiplicatively:

$$a_n(\mu) = a_n(\mu_0)\left(\frac{\alpha_s(\mu)}{\alpha_s(\mu_0)}\right)^{(\gamma_{(n)}-\gamma_{(0)})/\beta_0}. \tag{2.35}$$

The one-loop anomalous dimensions are:

$$\gamma_{(n)} = \gamma_{(n)}^{\parallel} = C_F\left(1 - \frac{2}{(n+1)(n+2)} + 4\sum_{j=2}^{n+1} 1/j\right), \tag{2.36}$$

$$\gamma_{(0)}^{\perp} = C_F\left(1 + 4\sum_{j=2}^{n+1} 1/j\right) \tag{2.37}$$

As they are positive and increase with n, the effects of higher-order Gegenbauers are damped at higher scales as the DAs approach their asymptotic form, and the conformal expansion may be truncated. Alternatively, we can say, with reference to convolutions such as that in eq. 2.12, that for the slowly varying kernels T_H which are often encountered for interesting processes, the strongly-oscillating higher-order Gegenbauers will be washed out. The same conclusion is reached by considering, rather than the conformal expansion, the diagonalization of the ERBL equations [13,16,41,42] which govern the evolution of the DAs much as the DGLAP equations [43–46] govern the evolution of pdfs.

For the lowest moments, the ordinary and Gegenbauer moments are connected by simple algebraic relations, e.g.:

$$a_1 = \frac{5}{3}\langle\xi\rangle, \quad a_2 = \frac{7}{12}\left(5\langle\xi^2\rangle - 1\right), \quad \text{etc.} \tag{2.38}$$

Thus, we can effectively obtain values for the Gegenbauer moments on the lattice.

2.6 Status of Distribution Amplitudes

In this section, we summarize what is currently known about (leading-twist) light-meson distribution amplitudes. We can make some conclusions immediately, based on symmetry arguments alone: for mesons of definite G-parity, there is a symmetry under the interchange $u \leftrightarrow \bar{u}$ of the 2 momentum fractions. In these cases, the distribution amplitude is an even function of $\xi = u - \bar{u}$ and the odd moments vanish. Thus, $\langle\xi^1\rangle_\pi$, $\langle\xi^1\rangle_\rho^\parallel$ and $\langle\xi^1\rangle_\phi^\parallel$ all vanish, and $\langle\xi^1\rangle_K$ and $\langle\xi^1\rangle_{K^*}^\parallel$ are SU(3) flavour breaking effects.

We note that since $\langle\xi^1\rangle_K$ is essentially the average difference between the fractions of longitudinal momentum carried by the strange and light quarks:

$$\langle\xi^1\rangle_K(\mu) = \int_0^1 du(2u-1)\,\phi_K(u,\mu) = \langle 2u-1\rangle, \tag{2.39}$$

we would expect from constituent quark model insights that the sign of $\langle \xi^1 \rangle_K = \frac{3}{5} a_1^K$ would be positive. We shall see that this appears to be the case.

In fact, $\langle \xi^1 \rangle_K$ is a rather important SU(3) breaking parameter - perhaps the most important after f_K/f_π - and is important for predictions of B-decay rates such as $B \to K$, K^* [47]. For example, from light-cone sum rule expressions for semileptonic form factors, we have:

$$\frac{F^{B\to K}}{F^{B\to\pi}} = \frac{f_K}{f_\pi}(1 + c_1 a_1^K) + \dots , \tag{2.40}$$

where $c_1 \sim O(1)$. There are furthermore some cases, such as the weak radiative decays $B \to \rho\gamma$ vs. $B \to K^*\gamma$, where the main theoretical error comes from such SU(3) breaking effects. The ratio of these decay rates is studied at the B factories Belle and BaBar and allows for the measurement of the ratio of CKM matrix elements $|V_{ts}|/|V_{td}|$.

There have been three main approaches to the study of DAs: extraction from experimental data, direct calculations using QCD sum rules, and most recently lattice calculations. The overall normalizations of DAs are given by local hadronic matrix elements, essentially the decay constants, which have already been discussed and are partly accessible experimentally, and partly have to be calculated theoretically. The shapes of the leading-twist distribution amplitudes, in the form of the Gegenbauer moments, can be determined from experiments by analysing data on form factors such as $F_{\gamma\gamma^*\pi}$ (which was studied by the CLEO experiment), and F_π^{em}. There is a lack of sufficiently accurate data, however, and it is difficult to avoid contamination from other hadronic uncertainties and higher twist effects. As a result, the existing experimental constraints are not very stringent.

Distribution amplitude moments, then, must largely be determined from theory. They have been the subject of many studies using a range of nonperturbative approaches, of which the two most important have been QCD sum rules, which we have mentioned several times now, and Lattice QCD. Lattice studies have until quite recently been limited to the second moment of the pion's distribution amplitude [48–51], but the earliest studies were largely exploratory

and gave results that were not quite phenomenologically useful.

The main tool for studying light meson DAs has been QCD sum rules [52–54], whose application to the study of moments of DAs was pioneered by Chernyak and Zhitnitsky [10]. In this approach, analyticity is used to relate the operator product expansion of a correlation functions of two currents:

$$\Pi = i \int d^4y e^{iqy} \langle 0|T J_1(y) J_2(0)|0\rangle = \sum_n C_n(q^2)\langle O_n\rangle \equiv \Pi^{\rm OPE} \tag{2.41}$$

around $y = 0$, to its dispersion relation in terms of hadronic contributions:

$$\Pi = \int_0^\infty ds \frac{\rho(s)}{s - q^2 - i0} \equiv \Pi^{\rm had}, \tag{2.42}$$

where $\rho(s)$ is the spectral density of the correlation function along its physical cut. The OPE yields a series of local operators of increasing dimension whose expectation values in the vacuum are the condensates. There is unfortunately an irreducible error of $\sim 20\%$ associated with the sum rule approach (it is not possible to properly isolate the hadronic states because, unlike in the non-perturbative lattice formulation, the limit of large Euclidean time cannot be taken). The first moment of the kaon's distribution amplitude, for example, has in the past been determined mainly from QCD sum rules, and recent, representative results include:

$$a_1^K(1\,{\rm GeV}) = 0.05(2)\ [55],\quad 0.10(12)\ [56],\quad 0.050(25)\ [57]\quad \text{and}\quad 0.06(3)\ [58]. \tag{2.43}$$

These results all have the expected sign, but the uncertainties are around 50%. The reduction of such uncertainties is the chief motivation of the lattice programme. We note that in addition to the UKQCD/RBC $N_f = 2+1$ domain wall fermion programme for the calculation of distribution amplitude moments on the lattice, there is a UKQCD/QCDSF programme using $N_f = 2$ improved Wilson quarks.

Chapter 3

Lattice QCD

As discussed in Chapter 1, in order to attempt the determination of Standard Model parameters, and thereby to investigate the extent to which the SM is able to describe experimental results, it is essential that we are able to extract predictions for hadronic physics from QCD. Thus, we require a non-perturbative definition of QCD and a corresponding calculational method. Currently, the only known way to define QCD non-perturbatively is via lattice regularization - an approach first suggested by Wilson in 1974 [59].

Wilson's original intention was to make some of the intuition and analytical techniques of statistical mechanics (specifically, the high-temperature/strong-coupling expansion) applicable to quantum field theories [60]. Within a few years, however, the Monte Carlo simulation techniques used in statistical mechanics had also been adapted to Lattice QCD [61], and today it is with large-scale numerical computations that LQCD is most often associated. When combined with Monte Carlo estimation of the Euclidean path integral, the lattice formulation of QCD allows for the numerical 'solution' of the theory in the sense that it is possible to obtain quantitative predictions for physical observables, within statistical errors which can in principle be made arbitrarily small, and without the introduction of any additional assumptions.

Of course, this last statement ought to be qualified in several ways. The statistical errors

allowed by current computational resources are far from negligible, and for many physical quantities are in fact prohibitive. More troublesome, however, are the systematic uncertainties introduced by the several extrapolations that must be made, and the control of these errors is the main challenge in producing phenomenologically-useful results on the lattice. Extrapolations are necessary both because we are unable to simulate at physical light quark masses or at sufficiently small lattice spacing (for reasons of computational expense), and because the simulations themselves introduce additional parameters - such as the finite volume - whose effects must be accounted for. As we will discuss below, there are also many physical observables whose calculability in LQCD has been established only recently, and, even for those quantities most suited to the lattice approach, it is only in recent years that lattice calculations have had real phenomenological impact. After approximately 20 years of developments in computer hardware, algorithms, and field theory techniques, however, LQCD is now emerging as the pre-eminent non-perturbative tool for studying the strong interactions.

In this chapter, we introduce the essentials of LQCD and its associated numerical techniques, focussing especially on those aspects relevant to the calculations performed in this work. We also describe the simulations in which our datasets were generated and give the most general details of the measurements that were performed.

3.1 Euclidean Path Integrals

Lattice QCD is based on Feynman's path integral (or functional integral) approach to quantization, which has a number of advantages over the older canonical quantization procedure. Most obviously, the Lagrangian-based path integral formalism is manifestly relativistic, whereas the Hamiltonian-based alternative is not (although this comes at the expense of the loss of manifest unitarity). There are a number of other, formal advantages to the functional integral approach, but as we shall now discuss, the point most relevant to LQCD is that the Euclidean path integral

allows us to relate a quantum field theory to a classical statistical field theory, and thus LQCD can be thought of as a particularly complicated Ising-type model.

Starting from the expression for the transition amplitude in terms of a superposition of equally-weighted amplitudes for all possible classical paths, with phases given by the corresponding classical action, it is possible arrive at a path integral expression for the vacuum expectation value of a multi-local operator $O(x_1,x_2,\ldots,x_n)$ consisting of a time-ordered product of quark and gluon fields [1]:

$$\langle 0|O(x_1,x_2,\ldots,x_n)|0\rangle = \frac{1}{Z}\int \mathscr{D}A_\mu \mathscr{D}\psi \mathscr{D}\bar{\psi}\; O(x_1,x_2,\ldots,x_n)\, e^{iS} \tag{3.1}$$

where

$$Z = \int \mathscr{D}A_\mu \mathscr{D}\psi \mathscr{D}\bar{\psi}\; e^{iS}, \tag{3.2}$$

and S is the QCD action. Such 'correlation functions' or 'Greens functions' contain essentially all of the physical content of the theory.

The functional integral is defined formally as the continuum limit of the well-defined integral appearing in discretized spacetime, and the fermionic fields are represented by (anti-commuting) Grassmann numbers. The complex exponential, of course, produces oscillatory behaviour, and one may suspect that there will be problems with the convergence of such an integral. It is profitable for the purposes of both theoretical analysis and numerical calculations to perform a 'Wick rotation', i.e. an analytic continuation to imaginary time. One begins by defining new coordinates:

$$x^0 = -ix_E^4, \quad x^i = x_E^i, \tag{3.3}$$

and then restricting these new coordinates to the real line.

The Euclidean gamma matrices are then related to the Minkowski gamma matrices by:

$$\gamma_i^E = i\gamma_i, \quad \gamma_4^E = \gamma_0, \tag{3.4}$$

and satisfy the Clifford algebra of SO(4):

$$\{\gamma_\mu^E, \gamma_\nu^E\} = 2\delta_{\mu\nu}. \tag{3.5}$$

The path integral expression now contains a minus sign rather than the imaginary factor:

$$\langle 0|O(x_1,x_2,...,x_n)|0\rangle = \frac{1}{Z}\int \mathcal{D}A_\mu \mathcal{D}\psi \mathcal{D}\bar{\psi}\, e^{-S_E} O(x_1,x_2,...,x_n) \tag{3.6}$$

where S_E is the Euclidean action. The Euclidean action of QCD is, fortunately, real and bounded from below, and we therefore do not need to worry as much about the convergence of the path integral, which can be treated as a probability system with a Boltzmann weight e^{-S_E}. Henceforth, we work implicitly in Euclidean space, and will suppress the subscript 'E' in our notation.

In this way, QCD is made more amenable to manipulation and to calculation, but at the expense of obscuring the physics (although this is offset to some extent by the availability of analogies with, and intuition from, statistical mechanics). In principle, one would now like to calculate Euclidean correlation functions and then analytically continue them back to Minkowski space, which should be easier than calculating the Minkowski space correlation functions directly. Correlation functions on a Euclidean lattice, however, are clearly not analytical functions, and this approach is totally impractical numerically.

Fortunately, hadronic masses and certain matrix elements may be obtained directly in the Euclidean theory, and this is the approach taken in LQCD. Essentially, the hadronic states that can be isolated are the lowest-energy eigenstates of the Hamiltonian with a given set of quantum numbers. The calculation of scattering amplitudes and, for example, $K \to \pi\pi$ matrix elements is thus beyond the standard techniques [62], but there are interesting theoretical developments in this area [63]. The extraction of hadronic masses and matrix elements from lattice correlation functions is outlined in the next chapter for the case of vector meson two-point functions, which can be thought of as a 'next-to-simplest' case

3.2 Lattice Regularization and Finite Volume

A quantum field theory defined on a spacetime lattice is regularized (i.e., devoid of UV divergences) because, since it does not possess field degrees of freedom at arbitrarily small spacetime separation, it cannot support field oscillations with arbitrarily high frequencies (i.e., it has a momentum cutoff). Since, as we have already said, the functional integral itself is defined via spacetime discretization, this is in a sense the most conceptually economical regularization. In the simplest and most common case of a hypercubic lattice of spacing a, consisting of the points $\{x : x \in a\mathbb{Z}^4\}$, all physical 4-momenta can be represented by those lying within the first Brillouin zone, defined by $-\pi/a < p_\mu \leq \pi/a$. Any theory formulated on such a lattice therefore has a UV cutoff:

$$\Lambda = \frac{\pi}{a}. \tag{3.7}$$

Functional integrals in the infinite-volume lattice theory possess a denumerable but infinite set of integration variables. Since we anticipate performing numerical calculations, however, it will be necessary also to restrict the theory to a finite spacetime volume, thereby reducing the functional integrals to well-defined multi-dimensional integrals. Typically, one has a box of 4-volume L^3T with periodic boundary conditions, where the extent T in the (Euclidean) time direction is chosen to be greater than the spatial extent L since we are particularly interested in the limit of large Euclidean time.

A side-effect of going to a finite volume is that the components p_i of hadronic momenta on the lattice are restricted to integer multiples of $2\pi/L$. Typically, this leads to a momentum resolution of order a few hundred MeV. The most important phenomenological disadvantages of this restriction arise in relation to momentum-dependent quantities such as the form factors of weak semileptonic decays of hadrons. The recent theoretical development of 'partially-twisted boundary conditions', however, makes it possible to access intermediate momenta, without

excessive computational effort, by introducing a phase angle into the fermionic boundary conditions only [64–67].

The quantization of momentum is an important issue for the work presented here, in two main respects. Firstly, this feature of lattice kinematics has important consequences for hadronic resonances, which as we shall discuss in chapter 4 are often stable in lattice simulations as a result. Secondly, and as will be discussed in chapter 6, we must sometimes induce some hadronic momentum in order to access our desired matrix elements, and this can push us uncomfortably close to the lattice cutoff, thereby introducing more serious discretization errors and also more statistical uncertainty. Of course, finite volume effects can also be a source of systematic error, but as they fall off exponentially they are rarely as worrying as discretization errors, which we discuss more fully in the next section.

3.3 Formulating Lattice Actions

A nonperturbative regularization of QCD may now be defined by transcribing appropriate degrees of freedom onto the spacetime lattice and specifying a Lagrangian in which integrations are replaced by sums and derivatives by finite differences. Any such system from which the formal QCD Lagrangian can be recovered in the continuum limit $a \to 0$, and in which the fermion doubling problem (to be described below) is solved, is in principle acceptable - there is no unique discretization. In the remainder of this chapter, we will discuss in detail several specific issues which arise when formulating LQCD with numerical simulations in mind. Computational cost is for example an important practical consideration. At this point, however, we introduce two more general, conceptual issues that are involved in designing lattice regularizations.

The first such issue, which applies also to the choice of a regulator for continuum perturbative calculations, is that it is desirable to preserve as far as possible the symmetries of the formal

Lagrangian in the regularized theory. As we will discuss below, in the lattice regularization it is possible to preserve exact gauge invariance at finite a, but Lorentz invariance is of course sacrificed and instead the spacetime symmetries are those of the finite hypercubic group of reflections and $\pi/2$ rotations, $\mathscr{H}_4$. This fact has important consequences for our calculations, as we shall discuss in chapter 6. Particularly important is the presence of chiral symmetry on the lattice, which is perhaps the central consideration in formulating lattice fermion fields, as we discuss in the next section.

The second issue does not arise for analytic, perturbative calculations, but is relevant to LQCD because we anticipate performing numerical simulations in the regularized theory. As a consequence, and because of the constraints imposed by limited computational power on the lattice spacing a at which simulations may be performed, it is important that the regularized theory approaches QCD as quickly as possible as a is reduced, i.e. that our lattice formulation remains as QCD-like as possible for as large a lattice spacing as possible.

Since asymptotic freedom implies that the bare coupling vanishes as the continuum limit is taken, lattice perturbation theory may be used to achieve some analytic control over the approach to that limit. In Symanzik's analysis of the continuum limit in perturbation theory [68], the lattice spacing dependence is made explicit by constructing an effective continuum theory, with non-renormalizable terms proportional to some power of the lattice spacing, which matches the lattice theory at scales well below the cutoff. With $\mathscr{L}_0$ the continuum QCD Lagrangian, we then have:

$$S_{\text{eff}} = \int d^4x \left\{ \mathscr{L}_0(x) + a\mathscr{L}_1(x) + a^2\mathscr{L}_2(x) + ... \right\}, \tag{3.8}$$

where the $\mathscr{L}_k$'s for $k > 0$ are linear combinations of local operators, of dimension $4+k$, which are invariant under the symmetries of the lattice theory. For the 'standard' formulation of LQCD with Wilson fermions, the discretization errors begin at $O(a)$ (and at $O(a^2)$ in the pure Yang-Mills case).

This analysis suggests the possibility of constructing 'improved' actions, where the discretization effects begin at $O(a^2)$ rather than at $O(a)$, by adding counterterms with coefficients tuned in order to cancel the discretization effects. Numerically, this can make the difference between a systematic error of around 13% and a systematic error of around 1.5%.

3.4 Lattice Fermions

The formulation of lattice fermion fields is more problematic than that of lattice gauge fields, mainly because it is extremely difficult to preserve chiral symmetries at finite lattice spacing. Since this discussion is so much more involved, and since the choice of a lattice fermion action is perhaps the most important decision to be made when embarking upon a programme of simulations - with the choice of a gauge field action a secondary consideration - we address the issue of putting quark fields on the lattice first.

Transcription of the fermionic degrees of freedom onto the lattice is straightforward enough: we assign Grassmann numbers, in the appropriate spinorial representation of the Lorentz group, to each lattice site. We may then proceed in the obvious way, by replacing spacetime derivatives ∂_μ with finite differences Δ_μ (which can be made gauge covariant using the link variables, since as we will discuss they are the parallel transporters associated with gauge invariance). In this way, a 'naive' lattice fermion action is obtained.

By Taylor expanding the naive action and dropping higher order terms in a, it can be shown that the correct continuum action is recovered with discretization errors starting at $O(a^2)$. 'Naive' lattice fermions do possess the expected chiral symmetries, but unfortunately they suffer from the 'fermion doubling problem': the action describes $2^d = 16$ fermionic states rather than one. The momentum space free propagator has a pole at each corner of the Brillouin zone, and the extra 15 fermion modes are lattice artefacts that do not disappear in the continuum limit.

The standard way of removing the doublers proposed by Wilson involves adding to the action an irrelevant term (which of course cannot ruin the continuum limit). The doublers then acquire masses proportional to $1/a$ and decouple as $a \to 0$. But the Wilson term also introduces an explicit breaking of chiral symmetry (even in the absence of bare quark masses), which can now be recovered only in the continuum limit. Consequently, quark masses are not protected against an additive renormalization, making it difficult to simulate at small quark mass. Large subtractions must be performed in order to keep the renormalized mass close to the bare mass, and there is the problem of 'exceptional configurations': large additive mass renormalizations can make the renormalized mass negative, in which case the run must be thrown out. The renormalization of lattice operators also becomes much more complicated, as operators of different chirality may now mix. The number of operators and the mixings amongst them can make renormalization difficult, and even impossible in practice.

Despite the many disadvantages to the loss of chiral symmetry, it appeared to be an inevitable consequence of solving the doubling problem. This is formalized in the Nielsen-Ninomiya 'no-go' theorem [69], which states that the following four conditions cannot hold simultaneously for a fermionic theory on the lattice:

- D(x) is local;
- the Fourier transformed D behaves for $p \ll 1$ as $i\gamma^\mu p^\mu + \mathcal{O}(p^2)$;
- there are no doublers;
- $\gamma_5 D + D\gamma_5 = 0$;

3.4.1 The Ginsparg-Wilson Relation

The loophole that enables these apparent consequences of the no-go theorem to be avoided was actually hinted at in work which came not long after that of Nielsen and Ninomiya. By

considering the block-spin RG in QCD, Ginsparg and Wilson arrived at a relation which, if satisfied by a lattice Dirac operator, provided for a 'remnant chiral symmetry' [70]:

$$\gamma_5 D + D\gamma_5 = aD\gamma_5 D \tag{3.9}$$

Any lattice Dirac operator satisfying the Ginsparg-Wilson relation is also automatically O(a)-improved.

As the Ginsparg-Wilson relation was incompletely understood, however, and as it appeared that it would be extremely difficult to find a solution for the interacting case, it did not receive a lot of attention until more recently. In fact, several solutions are now known: domain wall fermions (DWF) [71–73], overlap fermions [74–77] and fixed-point ("classically-perfect") fermions [78,79]. As a result, the Ginsparg-Wilson relation has been reexamined and is now much better understood. It in fact allows for the existence of a lattice chiral symmetry which reduces to the usual continuum chiral symmetry in the continuum limit, but which provides all of the important consequences of chiral symmetry at finite lattice spacing. It has been shown [80] that the infinitesimal lattice chiral transformations can be written:

$$\psi \to \psi + \varepsilon\gamma^5(1 - aD)\psi \tag{3.10}$$

$$\bar{\psi} \to \bar{\psi} + \varepsilon\bar{\psi}(1 - aD)\gamma_5 \tag{3.11}$$

These are very complicated transformations, and in particular they involve the gauge fields because of the presence of D.

The Nielsen-Ninomiya no-go theorem still holds, of course, but its original interpretation can now be seen as having been overly restrictive in the assumption that chiral symmetry had to be realized in the same way on the lattice as in the continuum. General overviews are given in refs. [81–83].

3.4.2 Domain Wall Fermions

Domain wall fermions are the most numerically tractable of Ginsparg-Wilson fermions, and provide a tunable chiral symmetry which allows a balance between computational cost and lattice chiral symmetry to be achieved. In fact, domain wall fermions as used in numerical simulations do not exactly satisfy the Ginsparg-Wilson equation, but serve as a controlled approximation to the exact overlap formulation.

The domain wall construction was originally studied in the continuum. A Dirac fermion in 5 dimensions, with a mass term depending on the 5th coordinate s and having the form of a step function (or a tanh function - the mechanism is robust), has zero modes of a given chirality bound exponentially to the domain wall (or 'mass defect'), giving rise to a single Weyl fermion in the 4D theory.

This construction also works on the lattice, and if a 5D Wilson term is included doublers are absent from the 4D theory. The mechanism also works in the presence of gauge fields, and on the lattice one has 4D gauge fields (and so the 5th dimension is perhaps best viewed as a kind of flavour space). In this case, the domain walls are replaced by Dirichlet boundary conditions at either end of the 5th dimension, and the modes of opposite chirality are bound to the opposing walls. The length of the fifth dimension in units of the lattice spacing, L_s, then controls the amount of residual chiral symmetry breaking, and in the $L_s \to \infty$ limit, the Ginsparg-Wilson relation is satisfied and the overlap formulation is recovered. To leading-order in the lattice spacing a, the only effects of the finite L_s are the appearance of an additive mass renormalization m_{res}, known as the residual mass. The number of points in the 5th dimension, L_s, can also be taken as an approximate cost factor, relating the number of floating point operations required for domain wall simulations to the equivalent Wilson fermion calculations. Thus, even quenched DWF simulations are computationally quite intensive.

With an input quark mass m_f, the 5-dimensional DWF lattice action is given by:

$$S_f = \sum_{x,x',s,s'} \bar{\Psi}_{x,s} M_{x,s;x',s'} \Psi_{x',s'} \tag{3.12}$$

where:

$$M_{x,s,;x',s'} = \delta_{s,s'} D^{\parallel}_{x,x'} + \delta_{x,x'} D^{\perp}_{s,s'} \tag{3.13}$$

and:

$$D^{\parallel}_{x,x'} = -\frac{1}{2}\sum_{\mu}\left[(1-\gamma_\mu)U_\mu(x)\delta_{x+\hat{\mu},x'} + (1+\gamma_\mu)U^{\dagger}_{\mu}(x')\delta_{x-\hat{\mu},x'}\right] + (4-M_5)\delta_{x,x'}, \tag{3.14}$$

$$\begin{aligned} D^{\perp}_{s,s'} = & -\frac{1}{2}\left[(1-\gamma_5)\delta_{s+1,s'} + (1+\gamma_5)\delta_{s-1,s'} - 2\delta_{s,s'}\right] \\ & + \frac{m_f}{2}\left[(1-\gamma_5)\delta_{s,L_s-1}\delta_{0,s'} + (1+\gamma_5)\delta_{s,0}\delta_{L_s-1,s'}\right]. \end{aligned} \tag{3.15}$$

3.5 Lattice Gauge Fields

On the lattice, gauge fields are formulated not in terms of vector fields taking on values in the Lie algebra of the gauge group, as is the case in perturbation theory, but rather in terms of variables living on directed links between lattice sites and taking on values in the gauge group itself. Thus, the 'link variable' $U_\mu(x)$ is an SU(3) matrix living on the link directed from the site x to the site $x+\hat{\mu}$, with $\hat{\mu}$ a unit lattice vector in the μ-direction. The lattice formulation of gauge fields is closely related to the geometrical picture of gauge theories, in which the vector gauge fields A^a_μ are thought of as a connection, and the lattice's link variables are in fact the discrete analogue of the parallel transporters (or "Wilson lines") associated with gauge invariance in the continuum. A parallel transporter $L(x,y)$ connecting the spacetime points x and y is related to the usual vector field through the path-ordered exponential:

$$L(x,y) = \mathscr{P} e^{\int_y^x igA^{a\mu}(z)T^a dz_\mu}. \tag{3.16}$$

The gauge transformation of such a path-ordered exponential depends only on the gauge rotations V at its end points:

$$L(x,y) \rightarrow V(x)U_\mu(x)V^{-1}(y). \tag{3.17}$$

So in the discrete case, we may relate the link variables to the gauge fields through:

$$U_\mu(x) = e^{iagA^b_\mu(x+a\hat{\mu}/2)T^b}, \tag{3.18}$$

and under a gauge transformation the links transform as

$$U_\mu(x) \rightarrow V(x)U_\mu(x)V^\dagger(x+a\hat{\mu}). \tag{3.19}$$

It is clear from the gauge transformation properties of link variables that traces of closed loops formed from them will be gauge invariant, which suggests an approach to writing down both an action for the gauge fields and operators for physical observables involving them. The simplest closed loop is the 1×1 plaquette:

$$P_{\mu\nu}(x) = U_\mu(x)U_\nu(x+a\hat{\mu})U^\dagger_\mu(x+a\hat{\nu})U^\dagger_\nu(x)\,. \tag{3.20}$$

The original and simplest lattice action for gauge fields, proposed by Wilson, is in fact a sum over all possible 1×1 plaquettes:

$$S_g = \beta \sum_{x,\mu,\nu} \Re\left[1 - \frac{1}{3}\mathrm{Tr}P_{\mu\nu}(x)\right], \tag{3.21}$$

where $\beta = 6/g^2$. Expanding the right-hand side in powers of the lattice spacing, it is possible to show that this gives the correct continuum limit, with discretization errors beginning at $\mathcal{O}(a^2)$.

The definition of lattice gauge fields is not complete without an integration measure, and we use an invariant group measure, the Haar measure defined by:

$$\int dU f(U) = \int dU f(UV) = \int dU f(WU) \tag{3.22}$$

where U, V and W are elements of gauge group SU(3) and $f(U)$ is an arbitrary function over the group.

3.5.1 Iwasaki Gauge Action

More complicated gauge actions than the Wilson action may be formed by taking into account more complicated closed loops of link variables. In particular, the next object to consider after the plaquette would be the 1×2, 6-link lattice rectangle R. Taking the traces and real parts implicitly, we can then write a general lattice action:

$$S_g = -\frac{\beta}{3}\left[(1-8c_1)\sum_{x,\mu<\nu} P_{\mu\nu}(x) + c_1 \sum_{x,\mu\neq\nu} R_{\mu\nu}(x)\right], \tag{3.23}$$

where the constant c_1 may be determined, for example, using Schwinger-Dyson equations (known as the doubly-blocked Wilson, or DBW2 action) or from renormalization group flow (which gives the Iwasaki action [84–86]).

With DWF, the choice of gauge action impacts the amount of residual chiral symmetry breaking arising from the finite value of L_s. The greater the presence of lattice dislocations, the larger m_{res} tends to be. Lattice dislocations, however, also drive the change in toplogical charge - an important measure of the ergodicity and decorrelation of the simulations. A balance must therefore be sought. The UKQCD/RBC collaborations have compared the Iwasaki and the DBW2 actions, and have found the Iwasaki action to be the best choice overall [87].

3.6 Numerical Methods

Having formulated a non-perturbative regularization of QCD, it should be possible to establish some means of performing non-perturbative calculations with it. As we have seen in section 3.2, the correlation functions (which embody the physical content of the theory) can be expressed as ratios of integrals over all field degrees of freedom, and so the task is to be able to perform these integrations. In practice, very different approaches are taken for the integrations over the fermionic fields, which can be done analytically, than for the gauge field integrations, for which we must resort to a numerical approach.

Since the fermionic contribution to the LQCD action can always be written $S_f = \int d^4x\, \bar{\psi} M \psi$, for some Dirac operator M, the Grassmann variable integrations take a standard form. Using the properties of Grassmann variables they can be reduced essentially to the rules of Wick contraction, which are familiar from perturbation theory: all fermionic observables can be expressed in terms of the quark propagator $S(x|y)$ by performing all possible contractions. For quarks of flavour q we have:

$$\overbrace{q^a_\alpha(x)\bar{q}^b_\beta}(y) = (S_q)^{ab}_{\alpha\beta}(x|y). \tag{3.24}$$

The propagator is obtained by inverting the Dirac operator, with the appropriate quark mass, on a particular background gauge configuration:

$$(S_q)^{ab}_{\alpha\beta}(x|y) = (M^{-1})^{ab}_{\alpha\beta}(x|y) \tag{3.25}$$

This step is so computationally expensive (with the cost increasing strongly as the quark mass decreases) that one generally has to fix the position of one end of the propagator. Since the propagator also has the property $\gamma_5 S^\dagger(x|y)\gamma_5 = S(y|x)$, however, this is not as problematic a restriction as it initially seems. Ongoing theoretical and algorithmic developments (in addition, of course, to improvements in hardware) are making the calculation of 'all-to-all' propagators a more feasible goal [88].

The gauge field integrations are in general not Gaussian in form and therefore cannot be handled so easily. Since these integrals are finite-dimensional when defined on a finite volume lattice, however, we would expect that in principle at least it would be possible to perform them numerically.

3.6.1 Monte Carlo

The remaining integration over the gauge fields involves a very large number of integration variables, but it is nevertheless a perfectly well-defined multi-dimensional integral, and because

of the exponential damping introduced by the e^{-S} factor it is absolutely convergent. Typically, there will be something like 100m integration variables in current lattice simulations, and so it is immediately apparent that numerical quadrature will be impossible and one must resort to Monte Carlo methods.

Monte Carlo integration would, however, be hopelessly inefficient without importance sampling. Fortunately, the e^{-S} factor means that only a very small part of the integration space makes a significant contribution to the integral, and LQCD is therefore particularly well-suited to this approach: by generating a set of N_{cf} gauge configurations U_α according to the appropriate probability distribution, a Monte Carlo estimator for a correlation function is obtained:

$$\langle 0|\Gamma|0\rangle \approx \frac{1}{N_{cf}} \sum_{\alpha=1}^{N_{cf}} \Gamma[U_\alpha] \tag{3.26}$$

The law of large numbers guarantees that in the limit of a very large sample the true correlation function is obtained, and the central limit theorem guarantees that the sample mean has a Gaussian distribution about this true correlation function, with a standard deviation proportional to $1/\sqrt{N_{cf}}$. In order to obtain an estimate for the statistical uncertainty on the Monte Carlo estimator, it is necessary to resort to some statistical resampling technique, such as the jackknife or bootstrap, in which new samples are generated by drawing from the existing samples but with omissions or duplications.

In order to perform this sampling, usually Markov chains are used, as they can often be constructed such that their equilibrium probability distribution [89] is the probability distribution desired. Consecutive samples generated from a Markov chain are not independent, however, and this threatens the reliable estimation of the statistical error. The extent of the 'autocorrelation' must somehow be quantified, and only configurations which some adequate separation in the Monte Carlo history can then be taken as independent samples.

Lattice QCD is one of the most intensive applications of Monte Carlo methods, and the bulk of the computational effort usually goes into the generation of gauge configurations. The

quark field integrations introduce the highly non-local fermionic determinant - which contains the dynamical effects of sea quarks - into the probability measure for the sampling of gauge fields. The inclusion of these effects is particularly costly, and the 'quenched' approximation in which they are neglected is an uncontrolled approximation which seems to introduce an error of $\sim 20\%$. In practice, the inversion of the Dirac matrix can be substituted for the calculation of its determinant, but since the condition number of the Dirac matrix increases as $1/m_f^2$, simulations cannot be carried out at physical light quark masses. The algorithmic "state-of-the-art" is represented by Hybrid Monte Carlo (HMC) [89], which benefits from the efficient exploration of the integration space that can be achieved by incorporating molecular dynamics methods, without the introduction of a systematic error which characterized previous techniques.

3.7 Renormalization

Having established both a non-perturbative regularization of QCD and a calculational method by which hadronic masses and matrix elements may be obtained at finite lattice spacing[1], it is now necessary to consider how to take the physical continuum limit and so make contact with experimental observations.

We must first set the free parameters of the model, thus making it well-defined and predictive, by holding a corresponding number of physical observables fixed (at experimentally-determined values) whilst the continuum limit is taken. For QCD, the natural way to do so non-perturbatively is via the hadronic spectrum. In order to perform a simulation, of course, bare values of all Lagrangian parameters must be supplied. However, we need only put in dimensionless numbers - the bare coupling g_0 and quark masses am in units of the lattice spacing - and do not set the lattice spacing a directly. Conceptually, basic renormalization [90]

[1] In practice, of course, there are obstacles both theoretical and computational which place limits on the set of hadronic observables that can be calculated on the lattice.

then involves adjusting the input quark masses such that ratios of hadronic masses match their physical values:

$$(am_H)/(am_p) = m_H^{\text{exp}}/m_p^{\text{exp}}, \tag{3.27}$$

and then 'setting the lattice scale', i.e. calculating the value of the lattice spacing a by, for example, setting the lattice proton mass to its physical value:

$$a = (am_p)/m_p^{\text{exp}}. \tag{3.28}$$

As we discuss in the next section, what is done in practice will usually be more complicated - we have merely outlined the basic procedure at a conceptual level here. There are a variety of suggestions for the optimal approach to setting the lattice scale under different circumstances, and the results obtained can exhibit significant dependence on the method used.

For most observables of phenomenological interest, further renormalization is necessary because in general normalizations of lattice operators must also be adjusted (and the operators may mix) as the continuum limit is taken:

$$O_i(\mu) = \sum_j Z_{ij}(\mu a, g(a))O_j(a) \tag{3.29}$$

In particular, hadronic matrix elements calculated on the lattice often arise in an operator product expansion, and the corresponding Wilson coefficients are usually evaluated in the $\overline{\text{MS}}$ scheme of dimensional regularization at the standard, reference renormalization scale $\mu = 2$ GeV. In such cases, it is necessary to match the lattice operators to those defined in the same scheme and at the same scale. Since every lattice formulation defines a different regularization, the renormalization constants Z_{ij} must be calculated separately for each discretization.

3.7.1 Continuum Extrapolations

Before proceeding to discuss the calculation of renormalization constants, however, we make a brief remark on the necessity (or, at least, the desirability) of continuum extrapolations of lattice results. It can initially be surprising that, whilst in the context of continuum perturbative calculations renormalized quantities are often said to be independent of the cutoff (or of whatever regularization parameter is used), on the lattice we must nevertheless extrapolate our spacing-dependent renormalized quantities to the continuum limit.

The reason for this difference has already been discussed in section 3.3, where we explained the importance of the 'improvement' of lattice formulations. It is a consequence of our restriction to performing numerical simulations at lattice spacings which are smaller, but not much smaller, than the physical scales relevant to the observables in which we are interested. The issue does not arise in continuum perturbative calculations because then we have analytical control over the regularization-parameter dependence, and can therefore always remove it to a region where it does not affect the physics (i.e. it is not a problem to take the cutoff much higher than the physical scales of interest). The concept of the effective continuum theory allows for a clear interpretation via the renormalization group: if we had to perform continuum perturbative calculations using a Lagrangian having additional, non-renormalizable interactions with couplings proportional to a parameter a that could not be set to zero, we would want to work only at scales low-enough such that the non-renormalizable terms had negligible effect.

3.7.2 Perturbative Renormalization of Lattice Operators

We can use any convenient states to fix the normalizations of lattice operators, and since we are able to fix the Lagrangian parameters non-perturbatively, we would hope to be able to

do the same for operator normalizations[2]. In fixing the free parameters we used a hadronic scheme, however, and it is usually undesirable to apply hadronic renormalization conditions to operators. Firstly, this is because it is not helpful when we want to match to a perturbative scheme, and secondly, it is because we must then incur an unnecessary loss of predictivity due to having used additional experimental input after fixing the free parameters (i.e., the value for the hadronic matrix element which goes on the r.h.s of the renormalization condition can only come from experiment, since we have no means other than LQCD by which to evaluate it a priori).

Since renormalization concerns UV structure, the asymptotic freedom of QCD implies that perturbation theory could be useful for this problem, and indeed the 'traditional' method for renormalizing lattice operators relies upon lattice perturbation theory [91]. One treats the lattice regularization as a renormalization scheme with a renormalization scale of (usually) $\mu = 1/a$, and simply matches to, say, the $\overline{\text{MS}}$ scheme at this scale by comparing the calculations of amputated quark two-point functions, with an insertion of the relevant operator, in continuum and in lattice perturbation theory. It is important for the success of this approach, of course, that the lattice spacing is fine enough that $1/a$ is within the perturbative regime.

Since the lattice operators are defined such that (at least for $p \ll \pi/a$) their tree-level matrix elements are the same as those of the original continuum operators, we can write the one-loop expressions:

$$\langle q|O_i^{lat}|q\rangle = \sum_j \left(\delta_{ij} + \frac{g_0^2}{16\pi^2}\left(-\gamma_{ij}^{(0)}\log a^2p^2 + R_{ij}^{lat}\right)\right)\cdot\langle q|O_j^{tree}|q\rangle \qquad (3.30)$$

$$\langle q|O_i^{\overline{\text{MS}}}|q\rangle = \sum_j \left(\delta_{ij} + \frac{g_{\overline{\text{MS}}}^2}{16\pi^2}\left(-\gamma_{ij}^{(0)}\log\frac{p^2}{\mu^2} + R_{ij}^{\overline{\text{MS}}}\right)\right)\cdot\langle q|O_j^{tree}|q\rangle, \qquad (3.31)$$

where the finite constants R_{ij}^{lat} and $R_{ij}^{\overline{\text{MS}}}$ are to be evaluated by applying the appropriate Feynman

[2]Of course, in those cases where we ultimately want matrix elements of operators defined in a perturbative, continuum scheme, we cannot avoid having to perform a perturbative matching step at some point.

rules. The relation between the lattice and continuum operators can then be written:

$$\langle q|O_i^{\overline{\rm MS}}|q\rangle = \sum_j \left(\delta_{ij} - \frac{g_0^2}{16\pi^2}\left(-\gamma_{ij}^{(0)}\log a^2\mu^2 + R_{ij}^{lat} - R_{ij}^{\overline{\rm MS}}\right)\right)\cdot\langle q|O_j^{lat}|q\rangle, \tag{3.32}$$

and the differences $\Delta R_{ij} = R_{ij}^{lat} - R_{ij}^{\overline{\rm MS}}$ determine the matching factors:

$$Z_{ij}(a\mu, g_0) = \delta_{ij} - \frac{g_0^2}{16\pi^2}\left(-\gamma_{ij}^{(0)}\log a^2\mu^2 + \Delta R_{ij}\right), \tag{3.33}$$

Having obtained these factors, one can match and then run perturbatively to the desired scale on the $\overline{\rm MS}$ side.

The reliance upon lattice perturbation theory is a major disadvantage of this approach. Lattice Feynman rules tend to be extremely complicated, and the presence of a cutoff invalidates many of the standard continuum tricks. As a result, perturbation theory on the lattice is approximately '1-loop more complicated' than in the continuum, and there are relatively few calculations going beyond 1-loop order. Convergence is also usually poorer than in the continuum, even when tools such as mean-field improvement are used to resum some of the larger contributions (typical n-loop corrections being numerically of $O(\alpha_s^n)$ rather than of $O((\alpha_s/4\pi)^n)$), and there is an ambiguity in the choice of coupling between, for example, some tadpole-improved lattice coupling and the $\overline{\rm MS}$ coupling, which can make a significant difference to the results obtained at 1-loop.

It can also be difficult to estimate the uncertainty present in perturbative renormalization, and it is in particular impossible to disentangle renormalization-scale dependence from cutoff effects, as any variation of a is also a variation of the renormalization scale μ. For calculations with domain-wall fermions, the Feynman rules are certainly complicated, and there is the added complication that the renormalization coefficients can depend sensitively on the domain wall height, which being essentially a Wilson fermion mass is additively renormalized. We outline (mean field improved) lattice perturbation theory with domain wall fermions in section 5.6.

Lattice perturbation theory does have advantages, of course. It can make operator mixing

more transparent than the non-perturbative methods that we discuss in the next subsection, although when operators mix with those of a lower dimension, power divergences arise which must be subtracted non-perturbatively and then this approach fails entirely.

3.7.3 Non-Perturbative Renormalization of Lattice Operators

Non-perturbative approaches to the renormalization of lattice operators [92] involve renormalizing initially in an intermediate scheme which can be applied both perturbatively and non-perturbatively. The use of lattice perturbation theory is then avoided, but continuum perturbation theory can still be used to match to a standard perturbative scheme. There is therefore a requirement for the existence of a window in lattice momenta such that:

$$\Lambda_{\rm QCD} \ll |p| \ll a^{-1}, \tag{3.34}$$

which can be relaxed in principle at the upper limit by performing 'step scaling' [93], i.e. by matching the renormalization conditions successively to finer (and also smaller in physical units) lattices. There are two main non-perturbative renormalization (NPR) techniques: the Rome-Southampton RI/MOM approach [94] and finite volume approaches (in which one takes $\mu = L^{-1}$) based on the Schrödinger Functional (SF) [95,96]. We will only discuss the RI/MOM method in this work.

It is clear from the previous subsection that in order to renormalize non-perturbatively without sacrificing predictivity, one must calculate non-perturbatively on the lattice a quantity that can also be calculated in perturbation theory (rather than a hadronic quantity). In the RI/MOM approach, one chooses simple renormalization conditions that can be implemented in any regularization (i.e. they are regularization independent (RI)). The amputated vertex function of an operator between external quark states with large virtualities is calculated non-perturbatively on the lattice and is set equal to its tree-level value, thus mimicking the perturbative matching procedure. For example, if we consider the generic two-quark operator $O_\Gamma = \bar{\psi}\Gamma\psi$, we may

impose the condition

$$Z_\Gamma \langle p|O_\Gamma|p\rangle|_{p^2=-\mu^2} = \langle p|O_\Gamma^{\text{tree}}|p\rangle, \tag{3.35}$$

where Γ is one of the Dirac matrices. This determines the operator renormalization constant Z_Γ up to the quark wave function renormalization. The latter is then determined by considering the vertex function of a conserved current. The renormalization constant is usually assumed to be quark mass independent, which can be achieved by imposing the renormalization condition in the chiral limit.

Since we have external quark states, of course, this calculation must be done in a fixed gauge (usually Landau gauge). As with any non-perturbative gauge-fixing procedure, however, there will inevitably be some uncertainty associated with Gribov copies [97]. This is generally found to be much less than the statistical error [98].

This approach has the advantage that it provides an adaptable, general framework that can be used for a wide variety of renormalization problems, including the subtraction of power divergences. The RI/MOM technique works particularly well with domain-wall fermions [99] as the DWF improvement and suppression of chiral symmetry breaking occur both on- and off-shell.

3.8 Simulation Details

The results described in this thesis represent a part of the broader UKQCD/RBC domain wall fermion phenomenology programme. Our numerical calculations are based upon gauge field configurations drawn from the joint UKQCD/RBC datasets, which were generated in simulations with $N_f = 2+1$ flavours of dynamical domain wall fermions and with the Iwasaki gauge action. These were in fact the first $2+1$ flavour DWF simulations, and followed earlier, quenched RBC studies.

As we have already stated, the DWF formulation is very expensive computationally, and the chief benefit of such chiral formulations of LQCD is the avoidance of mixing of operators with those of a different chirality. Quantities for which one profits most from the computational effort associated with these simulations are, for example, the neutral-kaon mixing parameter B_K [100,101] and the kaon matrix elements of the $\Delta S = 1$ weak effective Hamiltonian [102]. Thus, although domain wall fermions are in some sense the characteristic feature of our simulations, we do not claim that this is a formulation that would be chosen specifically for the calculation of moments of distribution amplitudes.

The inclusion of the strange quark presents a technical problem for the generation of gauge configurations, as the HMC algorithm requires there to be pairs of degenerate flavours. The alternative Polynomial HMC and R algorithms have the disadvantages of relative inefficiency and inexactness (i.e., having an inherent systematic error) respectively. The simulations described here therefore relied upon the Rational Hybrid Monte Carlo (RHMC) [103] algorithm, which was developed specifically in order to avoid these problems - it allows for the inclusion of an arbitrary number of quark flavours and yet is both exact and has the efficiency of HMC. This is accomplished by the use of rational functions to approximate the matrix square root appearing in the action. All configurations were generated on the purpose-designed QCDOC computer [104–106], using the Columbia Physics System software.

Our set of gauge configurations includes data with 2 different volumes but at a single lattice spacing, thus giving us some indication of the size of finite volume effects but no ability to perform a continuum extrapolation. We therefore have an unavoidable systematic error which is, however, formally of $O(a^2\Lambda^2_{QCD}) \simeq 2.5\%$ due to the automatic $O(a)$-improvement of the DWF action and operators. For both volumes, we have attempted to fix the strange quark mass to the physical strange mass, but have produced several independent ensembles with differing light-quark masses, all heavier than those found in nature. The hadronic spectrum

Table 3.1: Lattice scale and unrenormalized quark masses in lattice units. Note $\tilde{m}_X \equiv m_X + m_{\text{res}}$. Only the statistical errors are given here.

a^{-1} [GeV]	a [fm]	m_{ud}	$\tilde{m}_{ud}$	m_s	$\tilde{m}_s$	$\tilde{m}_{ud} : \tilde{m}_s$
1.729(28)	0.1141(18)	-0.001847(58)	0.001300(58)	0.0343(16)	0.0375(16)	1:28.8(4)

and other properties of these configurations have been studied in detail and the results have been presented in ref. [107] (for the lattice volume $(L/a)^3 \times T/a = 16^3 \times 32$) and ref. [108] (for the lattice volume $24^3 \times 64$). In both cases the length of the fifth dimension is $L_s = 16$.

The choice of bare parameters in our simulations is $\beta = 2.13$ for the bare gauge coupling, $am_s = 0.04$ for the strange quark mass and $am_q = 0.03$, 0.02, 0.01 and, in the 24^3 case only, 0.005 for the bare light-quark masses. Our strange quark mass corresponds to 1.150 times the physical strange quark mass (this was of course not known until after the simulations were complete). With this choice of simulation parameters the lattice spacing is $a^{-1} = 1.729(28)$ GeV [108], giving physical volumes of $(1.83\text{ fm})^3$ and $(2.74\text{ fm})^3$. The lattice spacing was obtained using the masses of the π and K pseudoscalar mesons and the triply-strange Ω baryon (which, of course, is relatively insensitive to the light-quark physics). The quark masses obtained in the 24^3 study are shown in table 3.1. Due to the remnant chiral symmetry breaking, the quark mass has to be corrected additively by the residual mass in the chiral limit, $am_{res} = 0.00315(2)$ [108]. The physical pion masses are as follows:

$$ma = 0.03\ (m_\pi \simeq 670\text{MeV}); \qquad ma = 0.02\ \ (m_\pi \simeq 555\text{MeV});$$

$$ma = 0.01\ (m_\pi \simeq 415\text{MeV}); \qquad ma = 0.005\ (m_\pi \simeq 330\text{MeV}).$$

Measurements were performed using the Chroma LQCD library [109] and the SciDAC

Table 3.2: Calculation parameters for our 16^3 dataset, which corresponds largely to that of [107]. The range and measurement separation Δ are specified in molecular dynamics time units. N_{meas} is the number of measurements for each source position t_{src}. The total number of measurements is therefore $N_{\text{meas}} \times N_{\text{src}}$, where N_{src} is the number of different values for t_{src}. In the right-most column, XY-XY denotes contraction of two quark propagators with X-type smearing at source and Y-type smearing at sink. G = Gaussian wavefunction. L = point.

m_l	Range	Δ	N_{meas}	$t_{\text{src locations}}$	Smearing
0.01	500-3990	10	350	0,8,16,24	GL-GL
0.02	500-3990	10	350	0,8,16,24	GL-GL
0.03	4030-7600	10	358	0,16	GL-GL

Table 3.3: Calculation parameters for the two separate 24^3 datasets, DEG and UNI.

m_l	Dataset	Range	Δ	N_{meas}	$t_{\text{src locations}}$
0.005	DEG	900-4460	40	90	0,32
	UNI	900-4480	20	180	0,32,16
0.01	DEG	1460-5020	40	90	0,32
	UNI	800-3940	10	315	0,32
0.02	DEG	1800-3560	40	45	0,32
	UNI	1800-3580	20	90	0,32
0.03	DEG	1260-3020	40	45	0,32
	UNI	1260-3040	20	90	0,32

Table 3.4: The different source and sink contractions of the quark propagators for the UNI dataset. $V = \gamma_i$ $(i = 1,2,3)$ is one of the spatial components of the vector current and $T = \sigma_{4i}$ are the calculated components of the tensor current. XY-XY denotes contraction of two quark propagators with a X-type smearing at source and a Y-type smearing at sink. H=hydrogen S-wave, G=Gaussian wave function (cf. [87]), and L=point.

Contraction	UNI Dataset	
$\langle \mathcal{O}_{snk} \mathcal{O}_{src} \rangle$	m=0.005, 0.02, 0.03	m=0.01
$\langle V,V \rangle$	HL-HL	GL-GL
	LL-HL	LL-GL
	HL-LL	GL-LL
$\langle T,V \rangle$	HL-HL	GL-GL
	LL-HL	LL-GL
	HL-LL	GL-LL

software stack, again largely on the QCDOC. The details are summarized in tables 3.2 and 3.3. In this work, we restrict our analysis almost entirely to the unitary (UNI) data, in which the valence and sea quark masses are the same, despite partially-quenched data being used extensively in ref. [108]. Thus, we do not refer to the FPQ (Full Partially-Quenched) dataset of ref. [108] in table 3.3. We do, however, give the details of the DEG (Degenerate) dataset, which consists of hadron correlators with degenerate valence quark masses, including partially-quenched ones, since these were used in the vector meson mass fits presented in chapter 4. In the 16^3 case, our dataset differs from that used in ref. [107] in that the Markov chains have been extended for the heaviest light quark mass (due to the observation in correlation functions of features which suggest that the chains were not sufficiently equilibrated).

In order to improve the statistical sampling of correlation functions, on each configuration we averaged the results obtained from either 2, 3 or 4 sources spaced out along a lattice diagonal. This is equivalent, of course, to shifting the gauge fields - since the action is translation invariant, this does not ruin the probabilistic sampling, but when measuring operators which are localized we make more efficient use of the information available. In the 16^3 case, for example, the sources used are at the origin, at $(4,4,4,8)$, at $(8,8,8,16)$ and at $(12,12,12,24)$. Statistical errors for observables are estimated using single-elimination jackknife, with the measurements made on the same configuration but at different source positions put in the same jackknife bin due to the strong correlations expected between them. In order to lessen the effect of autocorrelations, we follow the same blocking procedures as in [107] and [108]. In the 16^3 case, the span of the measurements in each block covers 50 molecular dynamics time units. In the 24^3 case, for the $m_q a = 0.005$ and $m_q a = 0.01$ ensembles, each jackknife bin contains measurements from every 80 molecular dynamics time units, while for the $m_q a = 0.02$ and $m_q a = 0.03$ ensembles each bin contains measurements from every 40 molecular dynamics time units, in order to have a reasonable number of bins for the analysis.

In order to improve the overlap with the mesonic states, at the source we employ either hydrogen S-wavefunction smearing [110] with radius $r = 3.5$ in lattice units or gauge invariant Gaussian smearing [111] with radius $r = 4$.

Chapter 4

Vector Meson Couplings:

Bare Calculation

In section 2.3.1, we introduced the couplings of the light vector mesons ρ, K^* and ϕ to the vector and tensor currents, f_V and f_V^T respectively. These quantities are closely related to the corresponding light-cone distribution amplitudes (being essentially their normalizations) and enter the QCD description of hard exclusive processes involving vector mesons - we have already discussed their phenomenological applications and status. In particular, we have explained the usefulness of an accurate value of the ratio f_V^T/f_V, since as we shall discuss below, our data allow us to obtain this quantity with much better precision than the individual decay constants.

In the present chapter, we describe our bare lattice calculation of the ratios of vector meson couplings, and present the unrenormalized results. The calculation of the relevant renormalization constants is the subject of chapter 5, and it is there that we present our final results, quoted in the $\overline{\text{MS}}$ scheme at $\mu = 2\,\text{GeV}$, and compare them with previous lattice studies. This work is published in ref. [108], with preliminary results having appeared in ref. [112].

4.1 f_V^T / f_V from Lattice Correlation Functions

The meson-to-vacuum matrix elements occuring in the definitions given in equations 2.17 and 2.18, $\langle 0|V^\mu|V(p;\lambda)\rangle$ and $\langle 0|T^{\mu\nu}|V(p;\lambda)\rangle$, may be obtained via the following lattice 2-point functions:

$$C_{V_\mu V_\nu}(t,\vec{x}) \equiv \langle 0\,|V_\mu(t,\vec{x})V_\nu(0)\,|0\rangle\,, \tag{4.1}$$

and

$$C_{T_{\rho\mu}V_\nu}(t,\vec{x}) \equiv \langle 0\,|T_{\rho\mu}(t,\vec{x})V_\nu(0)\,|0\rangle\,, \tag{4.2}$$

where the local operators are given by

$$V_\mu(x) \equiv \bar{\psi}(x)\gamma_\mu\psi(x) \qquad T_{\rho\mu}(x) \equiv \bar{\psi}(x)\sigma_{\rho\mu}\psi(x)\,. \tag{4.3}$$

In each case, we have placed the operator in whose hadronic matrix element we are interested at the sink, whilst the vector currents situated at the sources of these correlation functions serve as interpolating operators for the creation of vector meson states, as we shall now discuss.

We begin by partially Fourier transforming each correlator:

$$C(t,\vec{p}) \equiv (1/L^3)\sum_{\vec{x}} e^{i\vec{p}\cdot\vec{x}}C(t,\vec{x})\,, \tag{4.4}$$

where L^3 is the lattice volume. By then using translation invariance to write the sink operator in terms of one sited at the origin, inserting the complete set of energy eigenstates, and going to the limit of large Euclidean time t, we obtain a projection onto the lowest-energy state having the momentum $\vec{p}$ and the quantum numbers of the vector current interpolating operator. These states are essentially the vector mesons, but there are some important qualifications which ought to be added to this statement, and which we now address.

Whilst the pseudoscalar mesons π and K are energy eigenstates of QCD and have electroweak decays only, the vector mesons are resonances and decay by the strong interaction.

The ρ decays to a $\pi\pi$ pair in a p-wave state with a branching ratio of $\sim 100\%$, the K^* decays similarly to $K\pi$, and the ϕ decays predominantly to KK states. Nonetheless, it is usually possible to project onto ρ meson states in lattice studies. One reason for this has been that its strong decay channels cannot occur in the quenched approximation, but even in full QCD studies such as ours the states can be isolated. Firstly, this is because, with the heavy quark masses used in lattice simulations, one usually has $m_\pi/m_\rho > 0.5$, and so the decay is energetically forbidden. Even when this is not the case, however, the ρ is stable on the lattice because the quantization of momentum occuring in finite volume leads to a large minimum non-vanishing momentum. It is certainly less than satisfactory, however, that we must extrapolate through the decay threshold in going to the physical quark mass and infinite volume limits, but at this point in time there is not a great deal that can be done about these issues.

Taking the above correlation functions at zero momentum, and making use of the definitions given in equations 2.17 and 2.18, as well as the completeness relation for the polarization vectors of massive vector particles:

$$\sum_\lambda \varepsilon_\mu^\lambda {}^* \varepsilon_\nu^\lambda = -g_{\mu\nu} + \frac{p_\mu p_\nu}{m^2}\,, \tag{4.5}$$

we can obtain bare lattice values for f_V and f_V^T, as well as the vector meson mass m_V, by fitting to the large t behaviour with particular choices of the Lorentz indices:

$$C_{VV}^{s_1 s_2}(t) \equiv \sum_{\vec{x},i} \langle 0 | V_i^{s_1}(t,\vec{x}) V_i^{s_2}(0) | 0 \rangle = 3 f_V^{s_1} f_V^{s_2} m_V e^{-m_V T/2} \cosh\left(m_V\left(T/2 - t\right)\right)\,, \tag{4.6}$$

$$C_{TV}^{s_1 s_2}(t) \equiv \sum_{\vec{x},i} \langle 0 | T_{4i}^{s_1}(t,\vec{x}) V_i^{s_2}(0) | 0 \rangle = 3 f_V^{T s_1} f_V^{s_2} m_V e^{-m_V T/2} \sinh\left(m_V\left(T/2 - t\right)\right)\,. \tag{4.7}$$

Here, $i = 1,2,3$ is a spatial index, and the labels s_1 and s_2 denote the smearing used at the sink and at the source of the correlation functions, respectively. The cosh and sinh factors occur because of the backwards propagating state that we get with periodic boundary conditions, and we get one or the other depending upon the behaviour of the operators under time-reversal symmetry T. We note that, in practice, we also make use of the corelation function C_{VT} in the

analysis.

From the ratio

$$R(t) \equiv \frac{C_{TV}^{Ls_2}}{C_{VV}^{Ls_2}} = \frac{f_V^T}{f_V} \tanh(m_V(T/2-t)), \tag{4.8}$$

in which the L signifies that we must take local operators at the sink, we can obtain the ratio of the couplings. In this case, we expect to obtain a better signal than for the individual correlation functions since there should be some suppression of statistical fluctuations in the Monte Carlo integration as a result of taking the ratio, and also some cancellation of systematic uncertainties such as the dependence on the lattice spacing. This is the approach taken in almost all lattice studies of these quantities, although the QCDSF collaboration have obtained f_V^T directly.

By choosing the appropriate quark flavours, we obtain results for each of the ρ, K^* and ϕ mesons. In principle, one obtains disconnected contributions in the ϕ case, when quark operators at the same point are contracted together. Such amplitudes are very challenging numerically, however, as they tend to be extremely noisy. We argue that these contributions are Zweig suppressed and can therefore be neglected.

4.2 Bare Results

In table 4.1, we summarize our results for the vector meson masses from fits to (4.6) on the DEG 24^3 data set (cf. table 3.3) and from fits to (4.6) and (4.7) on the UNI data set. In the latter case we average over various choices of the source smearing function (cf. table 3.4) while always using a point sink.

On the UNI data set, again averaging over the same choices for the source and the sink, we also evaluate the ratios f_V^T/f_V. In each case eq. (4.8) exhibits well pronounced plateaus which we fit to a constant. In table 4.2 we present the bare values of f_V^T/f_V. It can be seen that the measured results are obtained with excellent precision. We have also compared our results with

Table 4.1: Results for the measured vector meson masses (DEG and UNI data sets).

m_l^{sea}	m_x	m_y	DEG	UNI
0.005	0.005	0.005	0.5053(58)	0.507(19)
	0.005	0.04		0.5591(75)
	0.04	0.04	0.6227(19)	0.6183(48)
0.01	0.01	0.01	0.5288(45)	0.527(17)
	0.01	0.04		0.5887(89)
	0.04	0.04	0.6295(18)	0.6319(48)
0.02	0.02	0.02	0.5789(55)	0.584(16)
	0.02	0.04		0.612(13)
	0.04	0.04	0.6453(33)	0.6453(84)
0.03	0.03	0.03	0.6317(33)	0.6239(76)
	0.03	0.04		0.6447(83)
	0.04	0.04	0.6622(27)	0.6609(69)

Table 4.2: Results for the measured ratio of couplings f_V^T/f_V, and at the chiral point as given by linear extrapolation.

am_q	Volume	0.03	0.02	0.01	0.005	chiral	χ^2/d.o.f
f_ρ^T/f_ρ	24^3	0.6806(55)	0.6646(73)	0.645(13)	0.624(21)	0.619(15)	0.17
	16^3	0.6885(63)	0.6660(69)	0.6236(80)	-		
$f_{K^*}^T/f_{K^*}$	24^3	0.6893(55)	0.6781(56)	0.6667(43)	0.6570(68)	0.6498(62)	0.11
	16^3	0.6879(48)	0.6774(45)	0.6516(46)	-		
f_ϕ^T/f_ϕ	24^3	0.6947(36)	0.6933(38)	0.6881(22)	0.6866(32)	0.6838(33)	0.10
	16^3	0.7023(47)	0.6907(31)	0.6822(33)	-		

those obtained on the $16^3 \times 32 \times 16$ lattices for m_l =0.01, 0.02 and 0.03 [112]. No significant finite volume effects were found.

From fig. 4.1 it can be seen that the dependence of the bare f_V^T/f_V on the masses of the light quarks is very mild and so we restrict our chiral extrapolation to linear and quadratic functions in the quark mass as shown in the figure. For the ratio of bare couplings in the chiral limit we obtain:

$$\frac{f_\rho^T}{f_\rho} = 0.619(15)(18); \quad \frac{f_{K^*}^T}{f_{K^*}} = 0.6498(62)(60); \quad \frac{f_\phi^T}{f_\phi} = 0.6838(32)(22), \qquad (4.9)$$

where the central value corresponds to the linear extrapolation and the second error is the difference between the results from the linear and quadratic extrapolations.

The bare results in eq. (4.9) were obtained with the notional strange quark mass of m_h = 0.04 rather than the physical value of $m_s = 0.0343$ (see table 3.1). The values of the ratios in

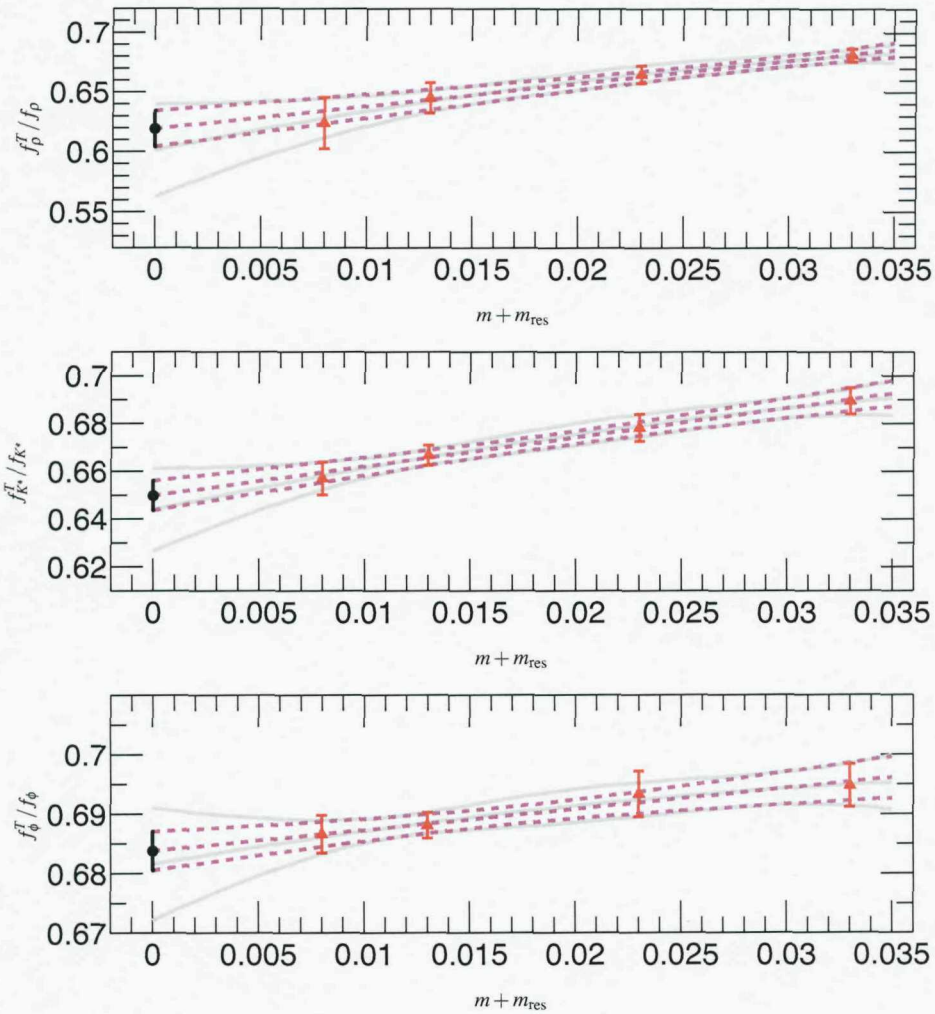

Figure 4.1: Chiral extrapolations for f_ρ^T/f_ρ, $f_{K^*}^T/f_{K^*}$ and f_ϕ^T/f_ϕ respectively. The broken red lines represent a linear fit to the mass behaviour and the solid grey lines a quadratic fit.

eq. (4.9) are very similar for the ρ, K^* and ϕ mesons and we correct for the change in m_s by linear interpolation in the valence quark mass (m_h is fixed at 0.04). Thus, for example, for the K^* meson we interpolate between the K^* and the ρ:

$$\frac{f_{K^*}^T}{f_{K^*}}(m_s = 0.0343) = \frac{f_{K^*}^T}{f_{K^*}}(m_h = 0.04) + \frac{\Delta}{(0.04 + m_{\rm res})}(0.0343 - 0.04), \tag{4.10}$$

where $\Delta = f_{K^*}^T/f_{K^*}(m_h = 0.04) - f_\rho^T/f_\rho$. After carrying out a similar extrapolation for f_ϕ^T/f_ϕ the corrected bare values are then:

$$\frac{f_\rho^T}{f_\rho} = 0.619(15)(18); \quad \frac{f_{K^*}^T}{f_{K^*}} = 0.6457(62)(60); \quad \frac{f_\phi^T}{f_\phi} = 0.6753(32)(22). \tag{4.11}$$

Chapter 5

Vector Meson Couplings: Renormalization

The bare results presented in the previous chapter for the vector meson coupling ratios f_V^T/f_V, calculated at our single lattice spacing of $a^{-1} = 1.73$ GeV, require renormalization. In order to obtain physical results, which should in principle be independent of both our cutoff and our choice of lattice formulation, we must multiply these values by the ratio of the renormalization constants for the tensor and axial currents, Z_T/Z_V, corresponding to some renormalization scheme - and ultimately we will want to quote our results in the standard $\overline{\text{MS}}$ scheme of dimensional regularization.

In this chapter, we discuss in general the non-perturbative renormalization, via the RI/MOM approach, of fermion bilinear operators using domain-wall fermions, and include a comparison of the results thus obtained with one-loop perturbative estimates for these coefficients. As explained in section 3.7, the RI/MOM technique is particularly appropriate for use with the domain-wall fermion formulation, especially given the sensitive additive renormalization of the domain wall height. We focus on the ratio Z_T/Z_V, and present here our final results for the vector meson couplings, matched perturbatively to the $\overline{\text{MS}}$ scheme at 2 GeV. The work

described in this chapter corresponds essentially to that published in ref. [101].

5.1 Simulation Details

It is one of the advantages of the Rome-Southampton approach to NPR that it does not require any additional simulations to be performed. For the non-perturbative calculation of renormalization coefficients in the intermediate RI/MOM scheme, one may reuse the same gauge field configurations that have been used for the measurement of hadronic masses and matrix elements (although this can of course introduce statistical correlations that ought properly to be taken into account). In principle, we would like to be able to vary the strange quark mass as well as the light quark masses, however, because - for compatibility with the perturbative calculations - the renormalization conditions ought to be imposed in the limit where all three masses vanish. As we do not have such data, we must accept this as a source of systematic error.

The non-perturbative calculations described below were carried out using lattices drawn from the 16^3 dataset detailed in section 3.8 (this is appropriate since we would not expect finite volume effects to be significant when considering the renormalization of local operators). The statistics are, however, somewhat different than those chosen for the bare measurements: for each of the three independent ensembles, with light sea quark masses 0.01, 0.02 and 0.03, we have used 75 configurations, starting from trajectory number 1000 and with trajectory separation 40. Since we take the 24^3 results for the bare vector meson couplings as our main results, we do not need to worry about correlations between the bare matrix elements and their non-perturbative renormalization coefficients.

Following the RI/MOM non-perturbative renormalization procedure outlined in subsection 3.7.3, the lattices are first fixed in Landau gauge. Then, on each gauge-fixed configuration, we measure the point-point quark propagators $S(x,x_0)$ with periodic boundary conditions in space

and time, where x_0 is the source position and x is the sink, by inverting the Dirac operator D on a point source:

$$\sum_{x'} D(x,x')S(x',y) = \delta_{x,y} \tag{5.1}$$

We will only need light-quark propagators for what follows. These are the basic building blocks for all of our subsequent calculations.

Using this 'point source' approach, therefore, we obtain with one inversion the quark propagator at all separations or momenta. There is however no volume-averaging - one end of the propagator is fixed on a particular site (which corresponds to the position of the local operator being renormalized), suggesting that we do not make full use of our sampled gauge fields. In order that we can make more efficient use of our lattices by averaging over several positions for the local operators, we have invested extra computational effort in inversions for four different sources, approximately equally-spaced along a lattice diagonal:

$$x_0 \in \{(0,0,0,0),(4,4,4,8),(7,7,7,15),(12,12,12,24)\}. \tag{5.2}$$

Next, a discrete Fourier transform is performed on the propagators,

$$S(p,x_0) = \sum_x S(x,x_0)\exp[-ip\cdot(x-x_0)], \tag{5.3}$$

where

$$p_\mu = \frac{2\pi}{L_\mu} n_\mu, \tag{5.4}$$

n_μ is a four-vector of integers and

$$L_x = L_y = L_z = 16 \quad L_t = 32. \tag{5.5}$$

For the n_μ we take values in the ranges

$$n_x, n_y, n_z \in \{-2,-1,0,1,2\} \qquad \text{and} \qquad n_t \in \{-4,-3,-2,-1,0,1,2,3,4\} \tag{5.6}$$

and require that the squared amplitude of the lattice momenta is in the range $0 \leq p^2 \lesssim 2.5$ (for simplicity of notation we frequently use lattice units for dimensionful quantities such as p

and m, but when we particularly wish to emphasize the nature of the discretization errors we explicitly reinstate the lattice spacing, writing for example, $(ap)^2$ or $(am)^2$).

5.2 Renormalization of Flavour Non-Singlet Fermion Bilinears

In ref. [101], a non-perturbative calculation of the renormalization coefficients for the quark bilinears and for the K - $\bar{K}$ mixing parameter B_K was presented. We do not discuss Z_{B_K} in this work, however, and where the quark bilinears are concerned we focus on the ratio Z_T/Z_V (which we need for the vector meson couplings calculation) rather than on the renormalization constants for the quark mass and wavefunction, Z_m and Z_q.

We now consider the renormalization, in the RI/MOM scheme, of quark bilinear operators of the form $\bar{u}\Gamma d$, where Γ is one of the 16 Dirac matrices. Because we take the flavour non-singlet case, we do not need to worry about 'disconnected' contributions. The corresponding renormalization constant Z_Γ is the factor relating the renormalized and bare bilinear operators:

$$[\bar{u}\Gamma d]_{\text{ren}}(\mu) = Z_\Gamma(\mu a)[\bar{u}\Gamma d]_0\,, \tag{5.7}$$

where μ is the renormalization scale and we treat only local operators where the lattice fields $\bar{u}$ and d in the bilinear operator $[\bar{u}\Gamma d]_0$ are evaluated at the same space-time point. For these relatively simple operators, there is no mixing under renormalization. Furthermore, $Z_{A,V}$ are determined by Ward Identities (which are respected by the RI/MOM scheme) because of chiral symmetry, and are scale independent.

Following the RI/MOM prescription, we define the bare Green functions between off-shell quark lines, and evaluate their momentum-space counterparts $G_{\Gamma,0}(p)$ on the lattice, averaged over all sources and gauge configurations,

$$G_{\Gamma,0}(p) = \frac{1}{N}\sum_{i=1}^{N}\left\{\frac{1}{n_{\text{source}}}\sum_{x_0}\left[S_i(p,x_0)\,\Gamma\left(\gamma_5 S_i(p,x_0)^\dagger\gamma_5\right)\right]\right\}. \tag{5.8}$$

We then amputate this Green function using the averaged propagators,

$$\Pi_{\Gamma,0}(p) = S^{-1}(p)\, G_{\Gamma,0}(p) \left(\gamma_5 \left[S^{-1}(p)\right]^\dagger \gamma_5\right), \tag{5.9}$$

where $S^{-1}(p)$ is calculated according to:

$$S(p)^{-1} = \left\{ \frac{1}{N} \sum_{i=1}^{N} \left[\frac{1}{n_{\text{source}}} \sum_{x_0} S_i(p, x_0) \right] \right\}^{-1} \tag{5.10}$$

and where $n_{\text{source}} = 4$ and $i \in \{1, 2, \cdots, N\}$ labels each configuration.

The bare vertex amplitudes are then obtained from the amputated Green functions as follows:

$$\Lambda_S(p) = \frac{1}{12} \text{Tr}\left[\Pi_1(p)\, 1\right] \tag{5.11}$$

$$\Lambda_P(p) = \frac{1}{12} \text{Tr}\left[\Pi_{\gamma_5}(p)\, \gamma_5\right] \tag{5.12}$$

$$\Lambda_V(p) = \frac{1}{48} \text{Tr}\left[\sum_\mu \Pi_{\gamma_\mu}(p)\, \gamma_\mu\right] \tag{5.13}$$

$$\Lambda_A(p) = \frac{1}{48} \text{Tr}\left[\sum_\mu \Pi_{\gamma_\mu \gamma_5}(p)\, \gamma_5 \gamma_\mu\right] \tag{5.14}$$

$$\Lambda_T(p) = \frac{1}{72} \text{Tr}\left[\sum_{\mu,\nu} \Pi_{\sigma_{\mu\nu}}(p)\, \sigma_{\nu\mu}\right]. \tag{5.15}$$

We estimate statistical errors for the bare vertex amplitudes using the standard single-elimination jackknife procedure. Because the results for different sources on a single configuration cannot be assumed to be statistically independent, however, we must include the results for all four sources in a single jackknife bin in order that correlations between them do not lead to these errors being underestimated. Thus, our approach of using multiple-sources is equivalent to averaging over different positions of the local operators, and is a valid way to improve the signal without additional gauge field sampling. The results from the different sources do appear to be reasonably independent, and a reduction in statistical error of approximately a factor of two has been gained by this quadrupling of the computational effort. In order to also have some confidence that autocorrelations between our configurations do not lead to

underestimation of the statistical errors, we have performed additional checks using jackknife bin widths of 3 and 5 consecutive configurations, and we obtain compatible results in those cases.

Results and statistical errors for all five bare vertex amplitudes, for each of the dynamical light quark masses, are presented in table 5.1 through table 5.3. With these results, by requiring that the renormalized vertex amplitudes satisfy

$$\Lambda_{i,\mathrm{ren}} = \frac{Z_i}{Z_q}\Lambda_i = 1\,, \qquad i \in \{S,P,V,A,T\}\,, \tag{5.16}$$

we have essentially obtained the renormalization constants for the quark bilinear operators in the RI/MOM scheme. We must now remove the Z_q factor by taking advantage of a conserved current, which yields Z_A, perform the perturbative running to the standard reference scale of 2 GeV (if necessary), and there match perturbatively to the $\overline{\mathrm{MS}}$ scheme.

Equations (5.7) through eq. (5.16), however, only describe the schematic procedure used to calculate the renormalization coefficients of quark bilinears. In practice, with finite quark masses and with a limited range of momenta, we must carefully consider lattice artefacts and other systematic uncertainties. We discuss the details in the next section, before continuing with the details of the calculation for the case of the tensor current operator.

5.3 The Renormalization 'Window', Chiral Symmetry Breaking and $Z_A - Z_V$

As explained in section 3.7, in order that our RI/MOM scheme renormalization constants are obtained at sufficiently high scales that perturbative running and matching to a continuum scheme can be applied, without there being excessive contamination by discretization effects, there must exist on the lattice a window of momenta such that

$$\Lambda_{\mathrm{QCD}} \ll |p| \ll a^{-1}. \tag{5.17}$$

Table 5.1: The five bare vertex amplitudes Λ_i, $i \in \{S,P,V,A,T\}$ averaged over four sources, with $m_l = 0.01$.

$(ap)^2$	Λ_S	Λ_P	Λ_V	Λ_A	Λ_T
0.347	2.125(86)	6.72(19)	1.1702(58)	1.0675(43)	0.8904(43)
0.617	1.945(51)	4.45(11)	1.1419(37)	1.0938(30)	0.9404(26)
0.810	1.856(37)	3.677(81)	1.1348(31)	1.1025(27)	0.9618(19)
1.079	1.758(27)	3.022(57)	1.1335(29)	1.1135(27)	0.9882(16)
1.234	1.715(24)	2.792(50)	1.1291(29)	1.1137(27)	0.9935(17)
1.388	1.677(21)	2.600(43)	1.1328(26)	1.1191(24)	1.0065(13)
1.542	1.642(19)	2.448(38)	1.1355(27)	1.1240(25)	1.0167(14)
1.851	1.599(16)	2.239(32)	1.1387(29)	1.1301(27)	1.0310(16)
2.005	1.578(15)	2.154(28)	1.1420(27)	1.1342(26)	1.0392(16)
2.467	1.532(13)	1.979(23)	1.1495(29)	1.1434(29)	1.0577(19)

Table 5.2: The five bare vertex amplitudes Λ_i, $i \in \{S,P,V,A,T\}$ averaged over four sources, with $m_l = 0.02$.

$(ap)^2$	Λ_S	Λ_P	Λ_V	Λ_A	Λ_T
0.347	1.828(45)	5.09(14)	1.1745(46)	1.0412(28)	0.8930(31)
0.617	1.774(30)	3.600(82)	1.1465(30)	1.0838(21)	0.9414(18)
0.810	1.721(24)	3.052(61)	1.1360(24)	1.0943(19)	0.9614(15)
1.079	1.655(19)	2.590(45)	1.1331(22)	1.1069(20)	0.9870(12)
1.234	1.637(16)	2.428(40)	1.1307(21)	1.1083(20)	0.9930(12)
1.388	1.608(15)	2.283(33)	1.1323(21)	1.1141(19)	1.0049(11)
1.542	1.581(14)	2.175(30)	1.1351(21)	1.1199(20)	1.0159(12)
1.851	1.552(11)	2.019(24)	1.1389(22)	1.1275(21)	1.0309(12)
2.005	1.532(11)	1.955(23)	1.1416(23)	1.1315(22)	1.0390(14)
2.467	1.4984(91)	1.819(18)	1.1498(26)	1.1422(25)	1.0580(17)

Table 5.3: The five bare vertex amplitudes Λ_i, $i \in \{S,P,V,A,T\}$ averaged over four sources, with $m_l = 0.03$.

$(ap)^2$	Λ_S	Λ_P	Λ_V	Λ_A	Λ_T
0.347	1.723(56)	4.10(14)	1.1809(56)	1.0357(23)	0.9020(24)
0.617	1.702(37)	3.049(87)	1.1457(37)	1.0769(19)	0.9451(17)
0.810	1.663(28)	2.658(66)	1.1356(31)	1.0886(17)	0.9642(14)
1.079	1.610(21)	2.307(49)	1.1325(27)	1.1015(18)	0.9883(12)
1.234	1.591(18)	2.182(42)	1.1294(25)	1.1050(20)	0.9951(12)
1.388	1.569(15)	2.076(37)	1.1312(25)	1.1105(20)	1.0061(11)
1.542	1.548(13)	1.991(33)	1.1337(26)	1.1157(21)	1.0161(12)
1.851	1.520(10)	1.869(27)	1.1366(26)	1.1228(22)	1.0300(13)
2.005	1.5065(96)	1.820(25)	1.1395(27)	1.1271(24)	1.0382(15)
2.467	1.4764(78)	1.717(20)	1.1464(27)	1.1371(26)	1.0561(17)

In practice, however, this condition is not easily satisfied, and violations of both restrictions lead to systematic uncertainties which must be quantified.

Due to the presence of spontaneous chiral symmetry breaking at low momenta, which can be seen in the non-trivial difference between Z_q/Z_A and Z_q/Z_V as we discuss below, we are forced to rely on the calculation in the relatively high momentum region, where $(ap)^2 \gtrsim 1$. Fortunately, the effects from breaking the restriction imposed by the finite lattice spacing a are small and predictable. They introduce an error of $\mathcal{O}\left((ap)^2\right)$ to the renormalization coefficients, which can be removed by quadratic fitting to the momentum dependence. A more detailed investigation of this issue was presented in an earlier, quenched RBC paper on NPR using domain wall fermions, ref. [99].

Since our calculations are necessarily carried out at finite momenta, the effects of both the low energy spontaneous chiral symmetry breaking present in QCD, and of our non-zero quark masses, are visible. In order to understand these effects, we study the difference between the off-shell vector and axial vector vertex functions. In the limit of a small mass and a large momentum, we expect

$$Z_A = Z_V, \tag{5.18}$$

or equivalently,

$$\Lambda_A(p^2) = \Lambda_V(p^2) \tag{5.19}$$

for $p^2 \gg \Lambda^2_{\rm QCD}, m^2$.

To determine the extent of chiral symmetry breaking in our calculation, we examine the relative difference between Λ_A and Λ_V. In figure 5.1 we plot the quantity $\frac{\Lambda_A - \Lambda_V}{(\Lambda_A+\Lambda_V)/2}$ as a function of momentum. To obtain the chiral limit here, we have performed a linear extrapolation $m_l + m_{\rm res} \to 0$. While a quadratic extrapolation gives a similar result, this linear choice generally leads to the smaller χ^2.

At relatively low momenta, $0.5 \leq (pa)^2 \leq 1$, we observe that this quantity is quite large

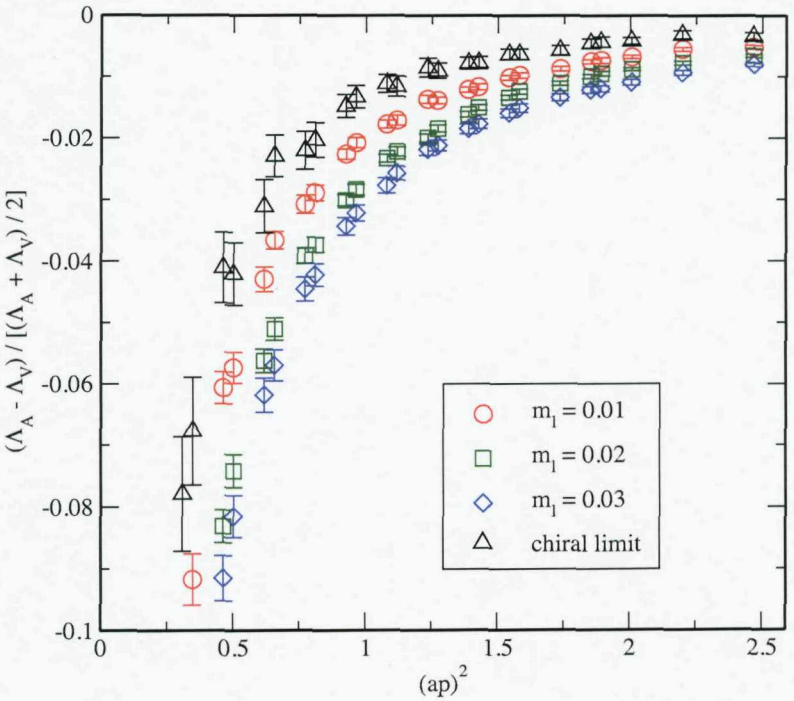

Figure 5.1: The ratio $\frac{\Lambda_A - \Lambda_V}{(\Lambda_A + \Lambda_V)/2}$ plotted as a function of momentum for each dynamical light-quark mass m_l, and in the chiral limit evaluated by linear extrapolation in m_l. The 5-10% difference at low momentum decreases rapidly as the momentum increases. At the scale $\mu \simeq$ 2 GeV, or $(ap)^2 \simeq 1.4$, the difference is about 1%, which contributes to the systematic error in our renormalization constants.

($\sim 5\%$). Furthermore, even when we extrapolate $\frac{\Lambda_A - \Lambda_V}{(\Lambda_A + \Lambda_V)/2}$ to the chiral limit, the difference between Λ_A and Λ_V does not vanish. As is discussed in some detail in ref. [101], this difference appears to represent the high-energy tail of QCD dynamical chiral symmetry breaking rather than coming from the finite value of L_s as might be suspected, since the explicit chiral symmetry breaking terms needed to split Λ_A and Λ_V can be argued to be $\mathcal{O}(m_{res}^2)$ and similar deviations are seen in quenched data where the finite-L_S effects are expected to be smaller. Naive power counting estimates, however, fail to account for the substantial difference we see, which appears to result from our use of "exceptional momenta" (i.e. kinematics where a momentum transfer is zero, which introduces an extra, infrared scale). This analysis is supported in ref. [101] by data calculated at non-exceptional momenta, showing that the chiral symmetry breaking vanished almost entirely at medium to large momenta.

While it would be more satisfactory to perform our calculations using non-exceptional momenta, the resulting RI/MOM renormalization conditions would not be consistent with those for which perturbative matching calculations have been done. There are also many more discrete lattice momenta that can be used in the exceptional momentum case.

At the scale which we are most interested in, that is $\mu \simeq 2$ GeV or $(ap)^2 \simeq 1.3$, Λ_A and Λ_V differ by about 1%. Since we have no way to determine which of the two quantities has less contamination from low energy chiral symmetry breaking, we take the average $\frac{1}{2}(\Lambda_A + \Lambda_V)$ as the central value for both Z_q/Z_A and Z_q/Z_V. The difference between Λ_A or Λ_V and $\frac{1}{2}(\Lambda_A + \Lambda_V)$ then provides an estimate for one systematic error in our final results. The value of $\frac{1}{2}(\Lambda_A + \Lambda_V)$ is plotted in figure 5.2.

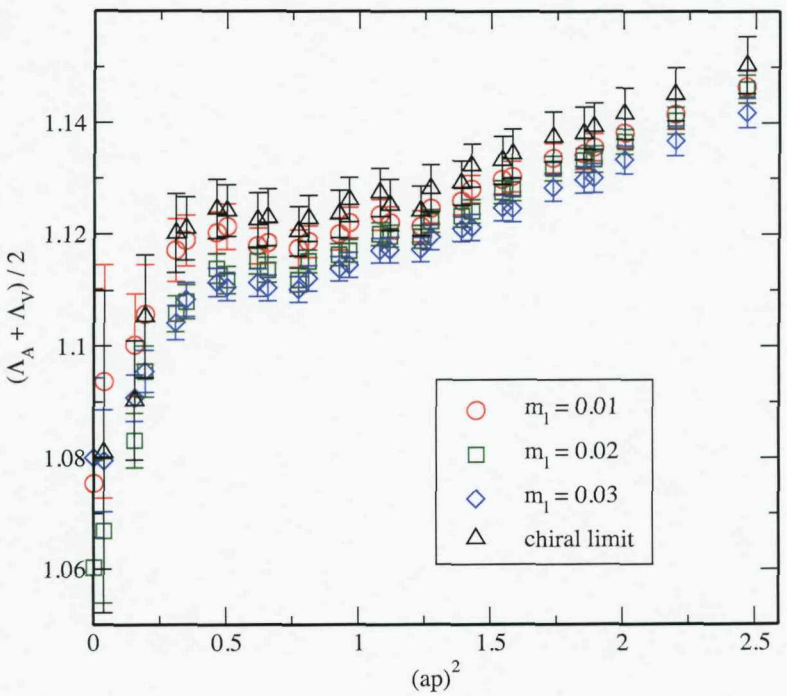

Figure 5.2: The average $\frac{1}{2}(\Lambda_A + \Lambda_V)$ plotted as a function of momentum and evaluated for each dynamical light-quark mass and in the chiral limit. The chiral limit is taken using a linear fit.

5.4 Tensor Current Renormalization and Renormalization Group Running

In section 5.2, we described the non-perturbative calculation, using bare lattice correlation functions, of the quantity $\Lambda_T(p) = Z_q^{\mathrm{RI/MOM}}(p)/Z_T^{\mathrm{RI/MOM}}(p)$. In order to obtain the tensor current renormalization constant Z_T, or the ratio Z_T/Z_V, we must remove the Z_q factor. For each dynamical quark mass, therefore, we combine the ratios $\Lambda_T = Z_q/Z_T$ and $\frac{1}{2}(\Lambda_A + \Lambda_V) = Z_q/Z_{A,V}$ in order to obtain the ratio of Z_T to Z_V in the RI/MOM scheme:

$$\frac{Z_T^{\mathrm{RI/MOM}}}{Z_A}(p) = \left[\frac{Z_T}{Z_q}(p)\right]\left[\frac{Z_q}{Z_A}(p)\right]. \tag{5.20}$$

Ultimately, we can then use the independent hadronic matrix element calculation of Z_A, which gives $Z_A = 0.7161(1)$ [113], to obtain Z_T. Since Z_A is just a number and does not have any scheme- or scale-dependence, we can quite freely convert back and forth between Z_T and $Z_T/Z_{A,V}$ in what follows. Table 5.4 shows the values obtained for $Z_T^{\mathrm{RI/MOM}}$ in the chiral limit for a range of lattice momenta. As discussed above we have performed the chiral extrapolation using a linear functional form, and figure 5.3 shows this linear extrapolation at the lattice momentum $(ap)^2 = 1.388$.

Having obtained lattice values for $Z_T^{\mathrm{RI/MOM}}$ at different momenta, we now calculate scale invariant values for Z_T in the chiral limit by dividing out the tensor current perturbative running factor. The three-loop running formula we use is:

$$Z_T^{\mathrm{SI}} = \frac{c(\alpha_s(\mu_0)/\pi)}{c(\alpha_s(\mu)/\pi)} Z_T^{\mathrm{RI/MOM}}(\mu) \tag{5.21}$$

where μ_0 is chosen such that $(a\mu_0)^2 = 2$, a value that lies within the fitting range used below. We give $c(\alpha_s)$, and present the details of the perturbative running and matching procedures, in the next section.

The SI values obtained in this way exhibit a dependence on the lattice momentum. We

Table 5.4: The non-perturbative factor $Z_T^{\mathrm{RI/MOM}}$ as a function of the scale μ calculated from Λ_T and the corresponding values for $Z_T^{\overline{\mathrm{MS}}}$. Note that the values for $Z_T^{\overline{\mathrm{MS}}}$ given in column three are obtained from those in column two by applying the $\mathrm{RI/MOM} - \overline{\mathrm{MS}}$ perturbative matching factors after the $\mathcal{O}(a\mu)^2$ lattice artifacts have been removed using an intermediate conversion to a scale-invariant scheme as described in the text.

μ(GeV)	$Z_T^{\mathrm{RI/MOM}}$	$Z_T^{\overline{\mathrm{MS}}}$
1.018	0.9121(74)	0.8812(38)
1.358	0.8583(46)	0.8355(36)
1.556	0.8380(32)	0.8194(35)
1.796	0.8177(27)	0.8048(34)
1.920	0.8118(27)	0.7986(34)
2.037	0.8037(22)	0.7935(34)
2.147	0.7981(21)	0.7892(34)
2.352	0.7899(18)	0.7821(33)
2.448	0.7862(17)	0.7791(33)
2.716	0.7779(16)	0.7719(33)

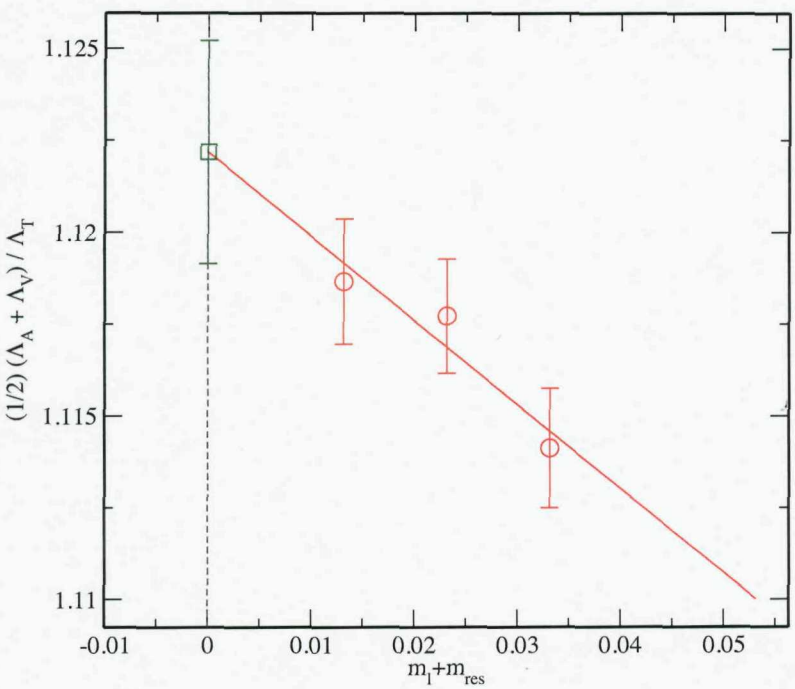

Figure 5.3: A plot of $\frac{1}{2}(\Lambda_A + \Lambda_V)/\Lambda_T$ as a function of quark mass as well as the linear extrapolation to the chiral limit, at $(ap)^2 = 1.388$, or $\mu = 2.04$ GeV

believe that the primary reason for this is the presence of lattice artifacts, with the lattice spacing introducing a small error of $\mathcal{O}\left((a\mu)^2\right)$. We therefore fit the momentum-dependent Z_T^{SI} to the form $A + B(a\mu)^2$ over the momentum range $1.3 < (a\mu)^2 < 2.5$ and extrapolate to $(a\mu)^2 \to 0$ to remove the lattice artifacts, as shown in figure 5.4. We interpret the result as the true Z_T^{SI}. We are of course ignoring possible μ dependence arising from the absence of higher order terms in the matching factor, but such scale dependence can only be removed by even higher order computation of the perturbative matching factor, and such a correction is expected to be very small. Finally, we run the scale-invariant Z_T/Z_A back to different scales in the RI/MOM scheme using eqn. 5.21, and use the perturbative matching factor (evaluated in the next section) to match to the $\overline{\mathrm{MS}}$ scheme. The $\overline{\mathrm{MS}}$ values are shown in figure 5.5 and table 5.4.

For the constant connecting the bare lattice tensor current operator to its continuum counterpart defined according to the $\overline{\mathrm{MS}}$ scheme at the renormalization scale $\mu = 2$ GeV, we obtain:

$$Z_T^{\overline{\mathrm{MS}}}(2\ \mathrm{GeV}) = 0.7950 \pm 0.0034(\mathrm{stat}) \pm 0.0150(\mathrm{sys}). \tag{5.22}$$

The systematic error is determined by adding in quadrature our estimates of three separate errors which we now discuss.

The effect on Z_T of the difference between determining Z_q/Z_A from $\frac{1}{2}(\Lambda_A + \Lambda_V)$ and from Λ_A contributes an error of ± 0.0054 to $Z_T^{\overline{\mathrm{MS}}}(2\ \mathrm{GeV})$. The use of a perturbative matching factor accurate to order α^2 contributes an error (0.014). This error is estimated from the magnitude of the final term in the perturbative expression. Finally, our use of a non-zero sea quark mass for the strange quark (when the renormalization condition should really be imposed in the SU(3) chiral limit) contributes an error (0.0003). This is estimated by taking half of the observed $\partial Z/\partial m$ (half since there is only one strange quark flavour, but two light quark flavours) and multiplying by $m_s = 0.04$.

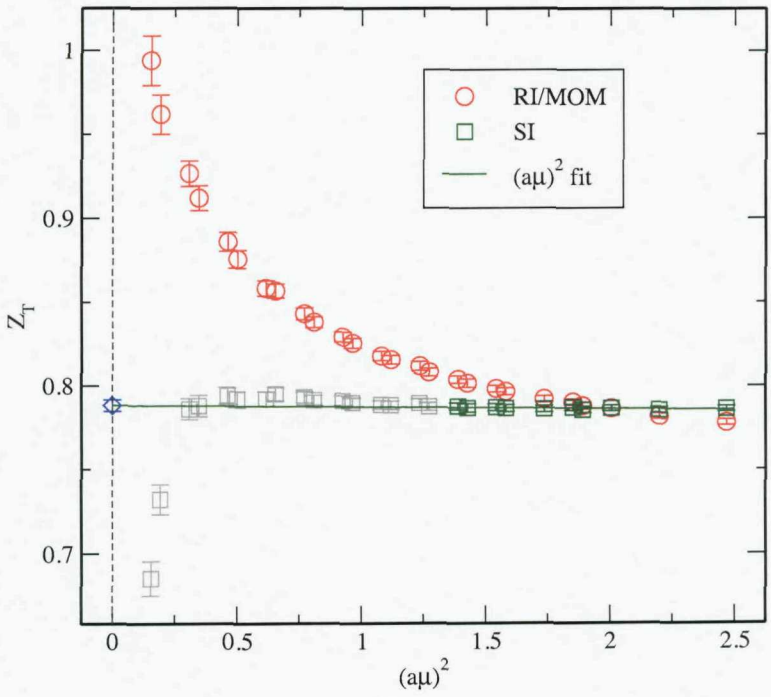

Figure 5.4: The quantities $Z_T^{\mathrm{RI/MOM}}(\mu)$ and $Z_T^{\mathrm{SI}}(\mu)$ plotted versus the square of the scale $a\mu$. Here $Z_T^{\mathrm{SI}}(\mu)$ is obtained by dividing $Z_T^{\mathrm{RI/MOM}}(\mu)$ by the predicted perturbative running factor. Shown also is the linear extrapolation of $Z_T^{\mathrm{SI}}(\mu) = Z_T^{\mathrm{SI}} + c(a\mu)^2$ using the momentum region $1.3 < (a\mu)^2 < 2.5$ to remove lattice artifacts.

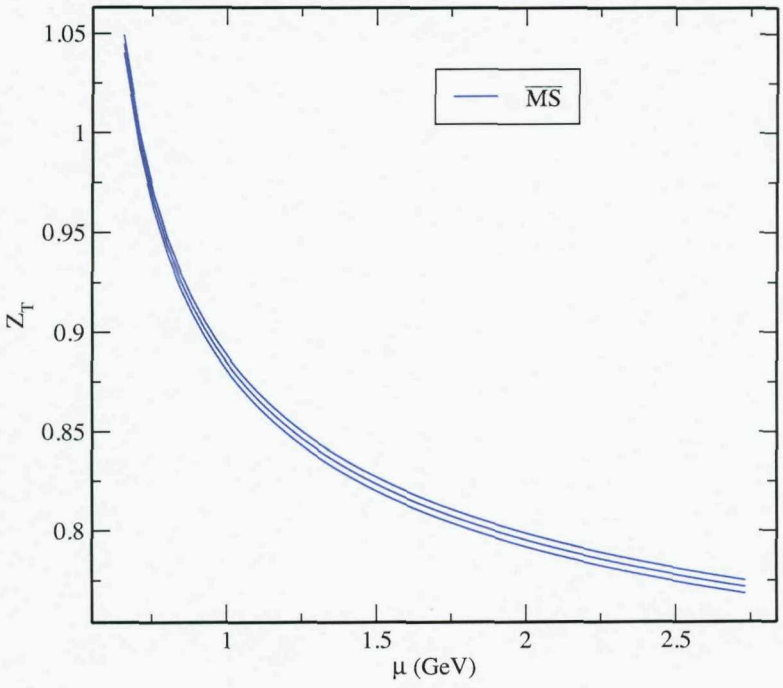

Figure 5.5: The renormalization factor Z_T expressed in the $\overline{\text{MS}}$ scheme. These results are obtained by applying the perturbative running factor to Z_T^{SI}. The value we are interested in is $Z_T^{\overline{\text{MS}}}(\mu = 2\,\text{GeV})$. The upper and lower curves show the statistical errors.

5.5 Perturbative Running and Scheme Matching for Z_T

In this section we give the details of the perturbative factors which have been used to perform the perturbative running and matching in the previous section. In what follows, we have made use of the four-loop QCD beta function calculated in [114], and the conventions we use are the same as in [115]:

$$\begin{aligned}
\beta_0 =& \frac{1}{4}\left(11-\frac{2}{3}n_f\right),\\
\beta_1 =& \frac{1}{16}\left(102-\frac{38}{3}n_f\right),\\
\beta_2 =& \frac{1}{64}\left(\frac{2857}{2}-\frac{5033}{18}n_f+\frac{325}{54}n_f^2\right),\\
\beta_3 =& \frac{1}{256}\left[\frac{149753}{6}+3564\zeta_3-\left(\frac{1078361}{162}+\frac{6508}{27}\zeta_3\right)n_f\right.\\
&\left.+\left(\frac{50065}{162}+\frac{6472}{81}\zeta_3\right)n_f^2+\frac{1093}{729}n_f^3\right].
\end{aligned} \tag{5.23}$$

To calculate the coupling constant $\alpha_s(\mu)$ at any scale, we have used the four-loop (NNNLO) running formula for α_s [114]:

$$\begin{aligned}
\frac{\partial a_s}{\partial \ln \mu^2} &= \beta(a_s)\\
&= -\beta_0 a_s^2-\beta_1 a_s^3-\beta_2 a_s^4-\beta_3 a_s^5+\mathcal{O}\left(a_s^6\right)
\end{aligned} \tag{5.24}$$

where $a_s = \alpha_s/\pi$. (We have changed the normalization of a_s to match the definition of the β-functions coefficients.) For a numerical implementation, we start from the world-average value at $\mu = M_Z$ [116],

$$\alpha_s^{(5)}(M_Z) = 0.1176 \pm 0.002, \tag{5.25}$$

where the superscript indicates that it is in the 5-flavour region, and run α_s across the m_b and m_c threshold with the matching conditions:

$$\alpha_s^{(5)}(m_b) = \alpha_s^{(4)}(m_b) \qquad \text{and} \qquad \alpha_s^{(4)}(m_c) = \alpha_s^{(3)}(m_c). \tag{5.26}$$

Having computed $\alpha_s^{(3)}(m_c)$, we can calculate the coupling constant at any scale in the 3-flavour theory. For example,

$$\alpha_s^{(3)}(\mu = 2\,\text{GeV}) = 0.2904. \tag{5.27}$$

$$Z_m^{\text{SI}} = \frac{c(\alpha_s(\mu_0)/\pi)}{c(\alpha_s(\mu)/\pi)} Z_m^{\text{RI/MOM}}(\mu) \tag{5.28}$$

where the function $c(x)$ is given by:

$$\begin{aligned} c(x) = (x)^{\bar{\gamma}_0} \Big\{ & 1 + (\bar{\gamma}_1 - \bar{\beta}_1\bar{\gamma}_0)\,x \\ & + \frac{1}{2}\left[(\bar{\gamma}_1 - \bar{\beta}_1\bar{\gamma}_0)^2 + \bar{\gamma}_2 + \bar{\beta}_1{}^2\bar{\gamma}_0 - \bar{\beta}_1\bar{\gamma}_1 - \bar{\beta}_2\bar{\gamma}_0\right] x^2 \\ & + \left[\frac{1}{6}(\bar{\gamma}_1 - \bar{\beta}_1\bar{\gamma}_0)^3 + \frac{1}{2}(\bar{\gamma}_1 - \bar{\beta}_1\bar{\gamma}_0)\left(\bar{\gamma}_2 + \bar{\beta}_1{}^2\bar{\gamma}_0 - \bar{\beta}_1\bar{\gamma}_1 - \bar{\beta}_2\bar{\gamma}_0\right)\right. \\ & \left. + \frac{1}{3}\left(\bar{\gamma}_3 - \bar{\beta}_1{}^3\bar{\gamma}_0 + 2\bar{\beta}_1\bar{\beta}_2\bar{\gamma}_0 - \bar{\beta}_3\bar{\gamma}_0 + \bar{\beta}_1{}^2\bar{\gamma}_1 - \bar{\beta}_2\bar{\gamma}_1 - \bar{\beta}_1\bar{\gamma}_2\right)\right] x^3 \\ & + \mathcal{O}(x^4)\Big\}, \end{aligned} \tag{5.29}$$

with $\bar{\beta}_i = \frac{\beta_i}{\beta_0}$ and

$$\bar{\gamma}_i = \frac{\gamma_m^{\text{RI/MOM}(i)}}{\beta_0} \tag{5.30}$$

When applying eq. (5.28), we need to choose a value of μ_0, where the SI value is calculated. The exact value of μ_0 is immaterial and for convenience we choose its value such that

$$(a\mu_0)^2 = 2. \tag{5.31}$$

The anomalous dimension of the tensor current in the $\overline{\text{MS}}$ scheme is given at three-loops in ref. [117],

$$\begin{aligned} \gamma_T^{\overline{\text{MS}}(0)} &= \frac{1}{3}, \\ \gamma_T^{\overline{\text{MS}}(1)} &= \frac{1}{16}\frac{2}{27}(543 - 26N_f), \\ \gamma_T^{\overline{\text{MS}}(2)} &= \frac{1}{64}\frac{2}{243}(\frac{1}{2}157665 - 4176\zeta_3 - (2160\zeta_3 + 7860)N_f - 54N_f^2). \end{aligned} \tag{5.32}$$

For consistency we have adjusted the normalization from that used in ref. [117] such that $\gamma_T^{\overline{\rm MS}}$ satisfies the generic RG-equation for the renormalization constant Z_Γ of the quark bilinear $\bar{\psi}\Gamma\psi$,

$$\begin{aligned} \frac{\partial \ln Z_\Gamma}{\partial \ln \mu^2} &= \gamma_\Gamma(a_s) \\ &= -\gamma_\Gamma^{(0)} a_s - \gamma_\Gamma^{(1)} a_s^2 - \gamma_\Gamma^{(2)} a_s^3 + \mathcal{O}(a_s^4), \end{aligned} \tag{5.33}$$

with $a_s = \alpha_s/\pi$.

The perturbative running for the tensor current has also been computed at three loops in the RI/MOM′ scheme [117], and we use it to obtain the RI/MOM scheme anomalous dimension as follows. We consider the conversion function $C_\Gamma^{\mathrm{RI/MOM}^{(\prime)}}$ used to match the RI/MOM or RI/MOM′ scheme to the $\overline{\rm MS}$ scheme:

$$Z_\Gamma^{\overline{\rm MS}} = C_\Gamma^{\mathrm{RI/MOM}^{(\prime)}} Z_\Gamma^{\mathrm{RI/MOM}^{(\prime)}}. \tag{5.34}$$

Applying the above renormalization group equation (5.33) we obtain

$$\gamma_\Gamma^{\mathrm{RI/MOM}^{(\prime)}} = \gamma_\Gamma^{\overline{\rm MS}} - \frac{\partial \ln C_\Gamma^{\mathrm{RI/MOM}^{(\prime)}}}{\partial \ln \mu^2}. \tag{5.35}$$

Since the only difference between the RI/MOM and RI/MOM′ schemes lies in the definition of the quark field renormalization constants $Z_2^{\mathrm{RI/MOM}'}$ and $Z_2^{\mathrm{RI/MOM}}$, we write $C_\Gamma^{\mathrm{RI/MOM}^{(\prime)}} = C_\Gamma C_2^{\mathrm{RI/MOM}^{(\prime)}}$. The vertex part C_Γ of the conversion function is common to both the RI/MOM and RI/MOM′ schemes. It follows that

$$\begin{aligned} \gamma_\Gamma^{\mathrm{RI/MOM}'} - \gamma_\Gamma^{\mathrm{RI/MOM}} &= \frac{\partial \ln C_2^{\mathrm{RI/MOM}}}{\partial \ln \mu^2} - \frac{\partial \ln C_2^{\mathrm{RI/MOM}'}}{\partial \ln \mu^2} \\ &= \gamma_2^{\mathrm{RI/MOM}} - \gamma_2^{\mathrm{RI/MOM}'}. \end{aligned} \tag{5.36}$$

Since both functions $\gamma_2^{\mathrm{RI/MOM}}$ and $\gamma_2^{\mathrm{RI/MOM}'}$ are known [115], we can now compute the anomalous dimension of the tensor current in the RI/MOM scheme from the known one in the RI/MOM′ scheme. We note that since the r.h.s. of (5.36) is valid for any choice of Γ on the

l.h.s., one may use the identity

$$\gamma_\Gamma^{\mathrm{RI/MOM}} = \gamma_\Gamma^{\mathrm{RI/MOM'}} - (\gamma_{\Gamma'}^{\mathrm{RI/MOM'}} - \gamma_{\Gamma'}^{\mathrm{RI/MOM}}). \tag{5.37}$$

In order to compute $\gamma_T^{\mathrm{RI/MOM}}$ here we have used $\gamma_2^{\mathrm{RI/MOM}}$ and $\gamma_2^{\mathrm{RI/MOM'}}$ from ref. [115]:

$$\begin{aligned}
\gamma_2^{\mathrm{RI/MOM'}(0)} &= 0, \\
\gamma_2^{\mathrm{RI/MOM'}(1)} &= \frac{N^2-1}{16N^2}\left\{\left[\frac{3}{8}+\frac{11}{4}N^2\right] + N_f\left[-\frac{1}{2}N\right]\right\}, \\
\gamma_2^{\mathrm{RI/MOM'}(2)} &= \frac{N^2-1}{64N^3}\left\{\left[\frac{3}{16}+\frac{233}{24}N^2+\frac{17129}{288}N^4-3N^2\zeta_3-\frac{197}{16}N^4\zeta_3\right]\right. \\
&+ N_f\left[-\frac{7}{12}N-\frac{743}{36}N^3+2N^3\zeta_3\right] \\
&+ \left. N_f^2\left[\frac{13}{9}N^2\right]\right\}, \\
\gamma_2^{\mathrm{RI/MOM'}(3)} &= \frac{N^2-1}{256N^4}\left\{\left[\frac{1027}{128}+\frac{8069}{384}N^2+\frac{240973}{1152}N^4+\frac{5232091}{3456}N^6\right.\right. \\
&\quad +25\zeta_3+31N^2\zeta_3-\frac{12031}{64}N^4\zeta_3-\frac{124721}{192}N^6\zeta_3 \\
&\quad \left.-40\zeta_5-60N^2\zeta_5+\frac{5465}{64}N^4\zeta_5+\frac{20625}{128}N^6\zeta_5\right] \\
&+ N_f\left[\frac{329}{12}N-\frac{1141}{144}N^3-\frac{113839}{144}N^5\right. \\
&\quad -4N\zeta_3+5N^3\zeta_3+\frac{2245}{12}N^5\zeta_3 \\
&\quad \left.-30N^3\zeta_5-\frac{125}{4}N^5\zeta_5\right] \\
&+ N_f^2\left[-\frac{515}{72}N^2+\frac{1405}{12}N^4+6N^2\zeta_3-\frac{32}{3}N^4\zeta_3\right] \\
&+ \left. N_f^3\left[-\frac{125}{27}N^3\right]\right\}.
\end{aligned} \tag{5.38}$$

In this way we obtain the anomalous dimension:

$$\begin{aligned}
\gamma_T^{\mathrm{RI/MOM}(0)} &= \frac{1}{3}, \\
\gamma_T^{\mathrm{RI/MOM}(1)} &= \frac{1}{16}\frac{2}{27}(543-26N_f), \\
\gamma_T^{\mathrm{RI/MOM}(2)} &= \frac{1}{64}\frac{1}{243}(478821-117648\zeta(3)+6(384\zeta(3)-8713)N_f+928N_f^2)
\end{aligned} \tag{5.39}$$

from which we compute the running of Z_T using (5.29).

Combining (5.24) and (5.33) we compute the expression for the matching factor $C_T^{\mathrm{RI/MOM}}$. After expanding in a_s we obtain:

$$\frac{Z_T^{\overline{\mathrm{MS}}}}{Z_T^{\mathrm{RI/MOM}}} = 1 + \frac{1}{81}(-4866 + 1656\zeta(3) + 259N_f)\left(\frac{\alpha_s}{4\pi}\right)^2. \tag{5.40}$$

5.6 Perturbative Estimates for Renormalization Coefficients

In this section, we outline the one-loop perturbative estimation of the renormalization constants for the quark bilinear operators, for comparison with the non-perturbative results. The details of performing perturbative calculations with domain-wall fermions are explained in [118–120], and the form of the Iwasaki gluon propagator is given in [84].

Our numerical simulations use a domain-wall height $M = 1.8$. For this value of M, with the Iwasaki gluon action, the one-loop coefficient in the physical quark normalization is $z_w \approx 112$ (extracted from [119]), making it clear that mean-field improvement is necessary. The prescription given in [119] is used.

Writing the domain wall height as $M = 1 - \omega_0$, the bare value of ω_0 in our simulation is $\omega_0 = -0.8$. The mean field improved value of ω_0 is then given by

$$\omega_0^{\mathrm{MF}} = \omega_0 + 4(1-u) \simeq -0.303, \tag{5.41}$$

where the link variable is defined by $u = \mathscr{P}^{1/4}$ and $\mathscr{P} = 0.588130692$ is the value of the plaquette in the chiral limit.

We define the renormalization constant, Z_{O_i}, which relates the bare lattice operator, $O_i^{\mathrm{Latt}}(a^{-1})$, to the corresponding renormalized one in the $\overline{\mathrm{MS}}$ scheme at a renormalization scale of $\mu = a^{-1}$ by:

$$O_i^{\overline{\mathrm{MS}}}(a^{-1}) = Z_i O_i^{\mathrm{Latt}}(a^{-1}). \tag{5.42}$$

Here $i = S, P, V, A, T$ for the scalar and pseudoscalar densities, vector and axial-vector currents

and tensor bilinear. The one-loop, mean field improved estimates for the Z_i are:

$$Z_{S,P} = \frac{u}{1-(\omega_0^{\rm MF})^2}\frac{1}{Z_\omega^{\rm MF}}\left(1-\frac{\alpha_s C_F}{4\pi}5.455\right) \tag{5.43}$$

$$Z_{V,A} = \frac{u}{1-(\omega_0^{\rm MF})^2}\frac{1}{Z_\omega^{\rm MF}}\left(1-\frac{\alpha_s C_F}{4\pi}4.660\right) \tag{5.44}$$

$$Z_T = \frac{u}{1-(\omega_0^{\rm MF})^2}\frac{1}{Z_\omega^{\rm MF}}\left(1-\frac{\alpha_s C_F}{4\pi}3.062\right), \tag{5.45}$$

where C_F is the second Casimir invariant $C_F = (N^2-1)/2N$ for the gauge group $SU(N)$. Here $\sqrt{Z_w}$ is the quantum correction to the normalization factor $\sqrt{1-\omega_0^2}$ of the physical quark fields. At one-loop order in perturbation theory

$$Z_w = 1+\frac{\alpha_s C_F}{4\pi}5.251. \tag{5.46}$$

The coefficients in eqs. (5.43) – (5.46) are obtained by linear interpolation between the entries for $M = 1.30$ and $M = 1.40$ in tables III and IV of ref. [119] to the mean-field value of $M = 1.303$. Since the mean-field value of M is so close to the quoted values at $M = 1.30$, this procedure should be no worse than using the general interpolation formula quoted in [119] (certainly the difference between the two procedures is negligible compared to the remaining systematic uncertainties).

In order to estimate the numerical values of the renormalization constants, a choice must be made for the expansion parameter, i.e. the coupling constant α_s. Here we consider two of the possible choices, the mean-field value as defined in eq.(62) of ref. [120] and the $\overline{\rm MS}$ coupling, both defined at $\mu = a^{-1}$. The mean field improved coupling constant is given by

$$\frac{1}{g^2_{\rm MF}(a^{-1})} = \frac{\mathscr{P}}{g_0^2}+d_g+c_p+N_f d_f, \tag{5.47}$$

where g_0 is the bare lattice coupling constant ($g_0^2 = 6/\beta$), and the remaining parameters are defined in ref. [120] and take the numerical values $d_g = 0.1053$, $c_p = 0.1401$ and for $\omega_0^{\rm MF} = -0.303$, $d_f = -0.00148$. We therefore obtain

$$\alpha_{\rm MF}(1.729\,{\rm GeV}) = 0.1769. \tag{5.48}$$

Such a value of the coupling is significantly lower than that in the $\overline{\text{MS}}$ scheme at the same scale, for which we take, $\alpha^{\overline{\text{MS}}}(1.729\ \text{GeV}) = 0.3138$.

The difference in the two values of the coupling constant leads to a significant uncertainty in the estimates of the renormalization constants at this order, as can be seen in table 5.5. The need to eliminate this large uncertainty is the principle motivation for the use of non-perturbative renormalization. The entries in table 5.5 are the factors by which the matrix elements of the bare lattice operators should be multiplied in order to obtain those in the $\overline{\text{MS}}$(NDR) scheme at the renormalization scale $\mu = 1.729\,\text{GeV}$.

Finally, the renormalization group running from $\mu = 1.729\,\text{GeV}$ is performed, in order to obtain the normalization constants at other scales, and in particular at the conventional reference scale of $\mu = 2\,\text{GeV}$ (see table 5.6). In each case, the highest order available for the anomalous dimension is used: three loops for the tensor operator and four loops for the scalar/pseudoscalar densities. Whenever required, the strong coupling $\alpha_s(\mu)$ is evaluated using the four-loop beta function. However, when the beta function is needed to solve the renormalization group equations, only those terms up to the same order as is available for the corresponding anomalous dimension are used. This is the same procedure that is used for the non-perturbatively determined renormalization constants. The numbers in table 5.6 are the factors by which the matrix elements of the bare lattice operators should be multiplied in order to obtain those in the $\overline{\text{MS}}$(NDR) scheme at $\mu = 2\,\text{GeV}$. The entries in the first column indicate which coupling was used in matching between the bare lattice operators and the $\overline{\text{MS}}$(NDR) scheme at $\mu = 1.729\,\text{GeV}$, i.e. before the running to other scales.

5.7 Final Results for the Vector Meson Couplings

For the necessary ratio of renormalization constants (evaluated by chirally-extrapolating the ratio, rather than taking the ratio after the chiral extrapolations) we find $Z_T/Z_A = Z_T/Z_V =$

Table 5.5: The factors, computed in perturbation theory, by which the matrix elements of the bare lattice operators should be multiplied in order to obtain those in the $\overline{\text{MS}}$(NDR) scheme at the renormalization scale $\mu = 1.729\,\text{GeV}$. This table shows that the difference in the choice of the strong coupling constant leads to large uncertainty in the renormalization constants.

Coupling	$Z_{S,P}(1.729\,\text{GeV})$	$Z_{V,A}$	$Z_T(1.729\,\text{GeV})$
$\alpha_{\text{MF}}(1.729\,\text{GeV})$	0.788	0.801	0.827
$\alpha^{\overline{\text{MS}}}(1.729\,\text{GeV})$	0.672	0.693	0.737

Table 5.6: The perturbative renormalization constants at the conventional scale of $\mu = 2\,\text{GeV}$ by renormalization group running from $\mu = 1.729\,\text{GeV}$. The entries in the first column indicate which coupling was used in matching between the bare lattice operators and the $\overline{\text{MS}}$(NDR) scheme at $\mu = 1.729\,\text{GeV}$. For comparison, the non-perturbative results (with statistical and systematic errors given in that order) are: $Z_{S,P}(2\text{ GeV}) = 0.604(18)(55)$, $Z_{V,A} = 0.7161(1)$, and $Z_T(2\text{ GeV}) = 0.7950(34)(150)$.

Coupling	$Z_{S,P}(2\,\text{GeV})$	$Z_{V,A}$	$Z_T(2\,\text{GeV})$
$\alpha_{\text{MF}}(1.729\,\text{GeV})$	0.822	0.801	0.813
$\alpha^{\overline{\text{MS}}}(1.729\,\text{GeV})$	0.701	0.693	0.725

Table 5.7: Previous quenched lattice results for the ratio of tensor and vector decay constants.

Reference	$\frac{f_\rho^T(2\text{GeV})}{f_\rho}$	$\frac{f_{K^*}^T(2\text{GeV})}{f_{K^*}}$	$\frac{f_\phi^T(2\text{GeV})}{f_\phi}$
Becirevic et al. [28]	$0.720(24)(^{+16}_{-00})$	$0.739(17)(^{+3}_{-0})$	0.759(9)(0)
Braun et al. [27]	0.742(14)	–	0.780(8)

$1.1101(92) \simeq 1.11(1)$. The relation between the ratios of bare and renormalized matrix elements is then:

$$\frac{f_V^T(2\,\text{GeV})}{f_V} = \frac{Z_T(2\,\text{GeV}a)}{Z_V}\,\frac{f_V^{T\,\text{bare}}(a)}{f_V^{\text{bare}}} = 1.11(1)\,\frac{f_V^{T\,\text{bare}}(a)}{f_V^{\text{bare}}}\,. \tag{5.49}$$

In the $\overline{\text{MS}}$ scheme with $\mu = 2\,\text{GeV}$ we finally obtain:

$$\frac{f_\rho^T}{f_\rho} = 0.687(27); \quad \frac{f_{K^*}^T}{f_{K^*}} = 0.717(12); \quad \frac{f_\phi^T}{f_\phi} = 0.750(8)\,. \tag{5.50}$$

These results can be compared with previous quenched lattice results which we summarize in table 5.7. The QCDSF/UKQCD collaboration has also presented the result $f_\rho^T = 168(3)\,\text{MeV}$ using an $N_f = 2$ $O(a)$ improved clover action with a range of lattice spacings ($0.07 < a < 0.11$ fm) [121]. Combining our result for the ratio from eq. (5.50) together with the experimental value for f_ρ discussed in sec. 2.3.1 we obtain a smaller value $f_\rho^T = 143(6)\,\text{MeV}$.

Chapter 6

Distribution Amplitude Moments: Bare Calculation

In chapter 2, we introduced hadronic light-cone distribution amplitudes, and discussed in some detail both their physical interpretation (as, in the leading-twist case, the overlap with the valence Fock state in an appropriate collinear configuration) and their phenomenological importance (the DA is the component of the hadronic wavefunction which, when soft effects can be neglected, controls hard exclusive processes). The DAs of the light mesons are the most well-studied case, and these quantities are important non-perturbative inputs in the analysis of both elastic and transition form factors such as $F_\pi(Q^2)$ and $F_{\gamma\gamma^*\pi}(Q^2)$, and for B-decays when described in either QCD factorization or the Soft Collinear Effective Theory.

As discussed in section 2.5, distribution amplitudes are usually parameterized in terms of their Gegenbauer moments, which renormalize multiplicatively (to leading order) and with an anomalous dimension hierarchy such that the lowest moments dominate at high momentum transfer. These lowest moments can be simply related to the ordinary moments, which can be expressed as decay-constant-type matrix elements of operators containing covariant derivatives, and are therefore calculable on the lattice.

In the present chapter, we present the bare lattice calculation of the non-vanishing first 2 moments of the leading-twist DAs, for both the pseudoscalar π and K mesons and the (longitudinally-polarized) vector mesons ρ, K^* and ϕ. Early results from the work presented here have been published in refs. [112, 122]. A complete set of results will appear in a forthcoming UKQCD/RBC publication.

6.1 Bare Moments from Lattice Correlation Functions

In this section, we describe our general strategy for the lattice calculation of the unrenormalized lowest moments of light meson DAs. We obtain expressions both for the moments $\langle \xi^1 \rangle$ and $\langle \xi^2 \rangle$ for the pseudoscalar meson, and for the longitudinal moments $\langle \xi^1 \rangle^{\parallel}$ and $\langle \xi^2 \rangle^{\parallel}$ for the vector meson, in terms of Euclidean lattice correlation functions which can then be estimated by Monte Carlo integration of the QCD path integral. In each case, we consider here a generic meson having valence quark content $(\bar{q}q')$ and select the flavour content at the lattice data level by contracting quark propagators with the appropriate masses. Since we can obtain all of these moments from ratios of lattice two-point functions, we can again expect to benefit from the cancellation of statistical fluctuations that tends to occur in such ratios.

6.1.1 Lattice Operators

We now define the local lattice operators appearing in the necessary correlation functions. In order to create the pseudoscalar and vector meson states, and to obtain their decay constants (which must be cancelled from the local matrix element expression for the moments), we will need the following quark bilinears:

$$P(x) \equiv \bar{q}(x)\gamma_5 q'(x), \quad V_\mu(x) \equiv \bar{q}(x)\gamma_\mu q'(x), \quad A_\mu(x) \equiv \bar{q}(x)\gamma_\mu\gamma_5 q'(x). \tag{6.1}$$

Although local interpolating operators are specified here, in the numerical simulations we again use smeared operators at the source of our correlation functions (in order to improve the overlap with the mesonic states and thereby to obtain better plateaus). Since the effects of smearing cancel in the ratios, the essentials of our discussion in this section hold for both the smeared and unsmeared cases. We give details of the smearing procedures used in the next section.

In constructing the lattice operators from whose hadronic matrix elements the distribution amplitude moments may be extracted, we use the following symmetric left- and right-acting covariant derivatives:

$$\vec{D}_\mu \psi(x) = \frac{1}{2a}\left\{U(x,x+\hat{\mu})\psi(x+\hat{\mu}) - U(x,x-\hat{\mu})\psi(x-\hat{\mu})\right\}, \tag{6.2}$$

and

$$\bar{\psi}(x)\overleftarrow{D}_\mu = \frac{1}{2a}\left\{\bar{\psi}(x+\hat{\mu})U(x+\hat{\mu},x) - \bar{\psi}(x-\hat{\mu})U(x-\hat{\mu},x)\right\}, \tag{6.3}$$

where $U(x,y)$ is the gauge link going from site x to site y, and $\hat{\mu}$ is a vector of length a in the direction μ (where a of course denotes the lattice spacing). The operators of interest are then defined by:

$$\begin{aligned} O_{\{\rho\mu\}}(x) &\equiv \bar{q}(x)\gamma_{\{\rho}\overleftrightarrow{D}_{\mu\}}q'(x), & O_{\{\rho\mu\nu\}}(x) &\equiv \bar{q}(x)\gamma_{\{\rho}\overleftrightarrow{D}_\mu\overleftrightarrow{D}_{\nu\}}q'(x), \\ O^5_{\{\rho\mu\}}(x) &\equiv \bar{q}(x)\gamma_{\{\rho}\gamma_5\overleftrightarrow{D}_{\mu\}}q'(x), & O^5_{\{\rho\mu\nu\}}(x) &\equiv \bar{q}(x)\gamma_{\{\rho}\gamma_5\overleftrightarrow{D}_\mu\overleftrightarrow{D}_{\nu\}}q'(x), \end{aligned} \tag{6.4}$$

where the braces in the subscripts indicate symmetrization of the enclosed free indices and the subtraction of traces.

6.1.2 Operator Mixing

In the continuum, the operators $O^{(5)}_{\rho\mu}$ and $O^{(5)}_{\rho\mu\nu}$ transform as second- or third-rank tensor representations of the Lorentz group, respectively. Since Lorentz symmetry is broken on the lattice, however, we must consider instead their transformation properties under the finite hypercubic group $\mathscr{H}_4$, consisting of reflections and $\pi/2$ rotations, as well as the discrete symmetries parity

P and charge-conjugation C, in order to understand the increased possibilities for operator mixing under renormalization. It is necessary to choose indices such that operator mixing is kept under control, but also desirable that a signal can be obtained with as few non-zero components of momentum as possible (in order to avoid the associated discretization effects and statistical degradation).

By decomposing the operators into the 20 irreducible representations of $\mathscr{H}_4$ [123], it is found that, with the indices symmetrized and traceless as shown above, lattice symmetries exclude mixing of the first moment operators with other operators of the same or lower dimension as long as the 2 indices are taken to be different. For the second moment operators, the same choice can be made but in this case there is mixing with a total derivative operator for the case of off-forward matrix elements.

6.1.3 $\langle \xi^1 \rangle_P$ and $\langle \xi^2 \rangle_P$ from Correlation Function Ratios

In order to obtain the first and second moments of the pseudoscalar meson distribution amplitude, $\langle \xi^1 \rangle$ and $\langle \xi^2 \rangle$, we consider the following two-point correlation functions:

$$C_{A_\nu P}(t,\vec{p}\,) \equiv \sum_{\vec{x}} e^{i\vec{p}\cdot\vec{x}} \langle 0|A_\nu(t,\vec{x})P^\dagger(0)|0\rangle, \tag{6.5}$$

$$C^5_{\{\rho\mu\}}(t,\vec{p}\,) \equiv \sum_{\vec{x}} e^{i\vec{p}\cdot\vec{x}} \langle 0|O^5_{\{\rho\mu\}}(t,\vec{x})P^\dagger(0)|0\rangle, \tag{6.6}$$

$$C^5_{\{\rho\mu\nu\}}(t,\vec{p}\,) \equiv \sum_{\vec{x}} e^{i\vec{p}\cdot\vec{x}} \langle 0|O^5_{\{\rho\mu\nu\}}(t,\vec{x})P^\dagger(0)|0\rangle. \tag{6.7}$$

For a generic pseudoscalar meson P, we define $Z_P \equiv \langle P(p)|P^\dagger|0\rangle$ and the bare decay constant by $\langle 0|A_\nu|P(p)\rangle \equiv ip_\nu f_P^{\text{bare}}$. Then, at large Euclidean times t and $T-t$, the correlation functions defined above tend towards:

$$C_{A_\nu P}(t,\vec{p}\,) \rightarrow \frac{Z_P f_P^{\text{bare}} e^{-E_P T/2} \sinh((t-T/2)E_P)}{E_P} \times (ip_\nu), \tag{6.8}$$

$$C^5_{\{\rho\mu\}}(t,\vec{p}\,) \rightarrow \frac{Z_P f_P^{\text{bare}} e^{-E_P T/2} \sinh((t-T/2)E_P)}{E_P} \times (ip_\rho)(ip_\mu)\langle \xi^1 \rangle^{\text{bare}}, \tag{6.9}$$

$$C^5_{\{\rho\mu\nu\}}(t,\vec{p}\,) \rightarrow \frac{Z_P f_P^{\text{bare}} e^{-E_P T/2} \sinh((t-T/2)E_P)}{E_P} \times (ip_\rho)(ip_\mu)(ip_\nu)\langle \xi^2 \rangle^{\text{bare}}. \tag{6.10}$$

We can now extract, from the following ratios of correlation functions, bare values for the first and second moments of the pseudoscalar meson distribution amplitudes:

$$R^P_{\{\rho\mu\};\nu}(t,\vec{p}\,) \equiv \frac{C^5_{\{\rho\mu\}}(t,\vec{p}\,)}{C_{A_\nu P}(t,\vec{p}\,)} \to i\frac{p_\rho p_\mu}{p_\nu}\langle\xi^1\rangle^{\rm bare}, \tag{6.11}$$

$$R^P_{\{\rho\mu\nu\};\sigma}(t,\vec{p}\,) \equiv \frac{C^5_{\{\rho\mu\nu\}}(t,\vec{p}\,)}{C_{A_\sigma P}(t,\vec{p}\,)} \to -\frac{p_\rho p_\mu p_\nu}{p_\sigma}\langle\xi^2\rangle^{\rm bare}. \tag{6.12}$$

The first moment can be obtained from $R^P_{\{\rho\mu\};\nu}(t,\vec{p}\,)$ by taking $\mu=\nu=4$[1], $\rho=1,2$ or 3 and a single non-zero momentum component, $|p_\rho| = 2\pi/L$. To extract the second moment from $R^P_{\{\rho\mu\nu\};\sigma}(t,\vec{p}\,)$ we must have two non-zero momentum components: we take $\nu=\sigma=4$, $\rho,\mu=1,2$ or 3 with $\rho\neq\mu$ and $|p_\rho| = |p_\mu| = 2\pi/L$. We give a more detailed description of our procedure for obtaining the bare values in the next section.

6.1.4 $\langle\xi^1\rangle^{\parallel}_V$ and $\langle\xi^2\rangle^{\parallel}_V$ from Correlation Function Ratios

For the calculation of the first two moments of the vector meson's longitudinal distribution amplitude, we begin by considering the following two-point correlation functions:

$$C_{V_\mu V_\nu}(t,\vec{p}\,) \equiv \sum_{\vec{x}} e^{i\vec{p}\cdot\vec{x}}\langle 0|V_\mu(t,\vec{x})V^\dagger_\nu(0)|0\rangle, \tag{6.13}$$

$$C_{\{\rho\mu\}\nu}(t,\vec{p}\,) \equiv \sum_{\vec{x}} e^{i\vec{p}\cdot\vec{x}}\langle 0|O_{\{\rho\mu\}}(t,\vec{x})V^\dagger_\nu(0)|0\rangle, \tag{6.14}$$

$$C_{\{\rho\mu\nu\}\sigma}(t,\vec{p}\,) \equiv \sum_{\vec{x}} e^{i\vec{p}\cdot\vec{x}}\langle 0|O_{\{\rho\mu\nu\}}(t,\vec{x})V^\dagger_\sigma(0)|0\rangle. \tag{6.15}$$

We define the bare longitudinal decay constant of a vector meson V, with polarization index λ and polarization vector $\varepsilon^{(\lambda)}_\mu$, through $\langle 0|V_\mu|V(p,\lambda)\rangle \equiv f_V^{\rm bare} m_V \varepsilon^{(\lambda)}_\mu$. Then, at large Euclidean

[1]The index 4 corresponds to the time-direction.

times t and $T-t$, the correlation functions defined above may be written:

$$C_{V_\mu V_\nu}(t,\vec{p}\,) \rightarrow \frac{-(f_V m_V)^2 e^{-E_V T/2}\cosh((t-T/2)E_V)}{E_V} \times \sum_\lambda \varepsilon_\mu^{(\lambda)} \varepsilon_\nu^{*(\lambda)} \tag{6.16}$$

$$= \frac{-(f_V m_V)^2 e^{-E_V T/2}\cosh((t-T/2)E_V)}{E_V} \times \left(-g_{\mu\nu} + \frac{p_\mu p_\nu}{m_V^2}\right),$$

$$C_{\{\rho\mu\}\nu}(t,\vec{p}\,) \rightarrow \frac{-i(f_V m_V)^2 e^{-E_V T/2}\langle \xi^1\rangle^{\|\text{ bare}} \sinh((t-T/2)E_V)}{E_V} \tag{6.17}$$

$$\times \frac{1}{2}\sum_\lambda \varepsilon_\nu^{*(\lambda)}(\varepsilon_\rho^{(\lambda)} p_\mu + \varepsilon_\mu^{(\lambda)} p_\rho)$$

$$= \frac{-i(f_V m_V)^2 e^{-E_V T/2}\langle \xi^1\rangle^{\|\text{ bare}} \sinh((t-T/2)E_V)}{E_V}$$

$$\times \frac{1}{2}\left(-g_{\rho\nu} p_\mu - g_{\mu\nu} p_\rho + \frac{2 p_\rho p_\mu p_\nu}{m_V^2}\right),$$

$$C_{\{\rho\mu\nu\}\sigma}(t,\vec{p}\,) \rightarrow \frac{(f_V m_V)^2 e^{-E_V T/2}\langle \xi^2\rangle^{\|\text{ bare}} \sinh((t-T/2)E_V)}{E_V} \tag{6.18}$$

$$\times \frac{1}{3}\sum_\lambda \varepsilon_\sigma^{*(\lambda)}(\varepsilon_\rho^{(\lambda)} p_\mu p_\nu + \varepsilon_\mu^{(\lambda)} p_\rho p_\nu + \varepsilon_\nu^{(\lambda)} p_\rho p_\mu)$$

$$= \frac{(f_V m_V)^2 e^{-E_V T/2}\langle \xi^2\rangle^{\|\text{ bare}} \sinh((t-T/2)E_V)}{E_V}$$

$$\times \frac{1}{3}\left(-g_{\rho\sigma} p_\mu p_\nu - g_{\mu\sigma} p_\rho p_\nu - g_{\nu\sigma} p_\rho p_\mu + \frac{3 p_\rho p_\mu p_\nu p_\sigma}{m_V^2}\right),$$

where we have made use of the completeness relation for the polarization vectors of massive vector particles, $\sum_\lambda \varepsilon_\mu^{(\lambda)} \varepsilon_\nu^{*(\lambda)} = -g_{\mu\nu} + p_\mu p_\nu / m_V^2$.

We may now extract bare values for the first and second moments from the following ratios:

$$R^V_{\{\rho\mu\}\nu}(t,\vec{p}\,) \equiv \frac{C_{\{\rho\mu\}\nu}(t,\vec{p}\,)}{\frac{1}{3}\sum_i C_{V_i V_i}(t,\vec{p}=0\,)} \rightarrow -i\langle \xi^1\rangle^{\|\text{ bare}} \tanh((t-T/2)E_V) \tag{6.19}$$

$$\times \frac{1}{2}\left(-g_{\rho\nu} p_\mu - g_{\mu\nu} p_\rho + \frac{2 p_\rho p_\mu p_\nu}{m_V^2}\right),$$

$$R^V_{\{\rho\mu\nu\}\sigma}(t,\vec{p}\,) \equiv \frac{C_{\{\rho\mu\nu\}\sigma}(t,\vec{p}\,)}{\frac{1}{3}\sum_i C_{V_i V_i}(t,p_i=0,|\vec{p}|=\frac{2\pi}{L}\,)} \rightarrow \langle \xi^2\rangle^{\|\text{ bare}} \tanh((t-T/2)E_V) \tag{6.20}$$

$$\times \frac{1}{3}\left(-g_{\rho\sigma} p_\mu p_\nu - g_{\mu\sigma} p_\rho p_\nu - g_{\nu\sigma} p_\rho p_\mu + \frac{3 p_\rho p_\mu p_\nu p_\sigma}{m_V^2}\right),$$

where the index i runs over spatial dimensions only. We obtain the first moment from $R^V_{\{\rho\mu\}\nu}(t,\vec{p}\,)$ at $\vec{p}=0$ by taking $\mu=4, \rho=\nu=1,2$ or 3. The second moment is obtained from $R^V_{\{\rho\mu\nu\}\sigma}(t,\vec{p}\,)$ by taking, for example, $\nu=4, \rho=1, \mu=\sigma=2$ and a single non-zero component of $\vec{p}$ in the 1-direction.

6.2 Bare Results

The correlation functions are estimated using the same sets of UKQCD/RBC $N_f = 2+1$ DWF gauge configurations as the vector meson couplings, i.e. the 16^3 dataset of table 3.2 and the UNI 24^3 dataset of table 3.3. The smearings used are those described as GL-GL and HL-HL, i.e. both quark propagators are smeared at the source of the 2-point function, using either hydrogen-like wavefunction smearing or gauge-invariant Gaussian smearing. We again average over the available number of sources, and use the usual jackknife procedure to estimate statistical uncertainties.

In order to extract $\langle \xi^1 \rangle_K$ from the ratio $R^P_{\{\rho\mu\};\nu}(t,\vec{p}\,)$ defined in (6.11), we need the two correlation functions to be measured at $|\vec{p}| \neq 0$. Since hadronic observables with larger lattice momenta have larger lattice artefacts and statistical errors, we restrict the choice of indices to $\rho = \nu = 4$ and $\mu = 1,2$ or 3 with $|\vec{p}| = 2\pi/L$ (i.e., $p_\mu = \pm 2\pi/L$ with the remaining two components of $\vec{p}$ equal to 0). $\langle \xi^1 \rangle_K$ can then be obtained from the ratio at large times:

$$R^P_{\{4k\};4}(t, p_k = \pm 2\pi/L) = \pm i \frac{2\pi}{L} \langle \xi^1 \rangle, \quad |\vec{p}| = \frac{2\pi}{L}, \quad k = 1,2,3. \tag{6.21}$$

The plots in figure 6.1 show our results for $\langle \xi^1 \rangle_K$ as a function of t obtained from the ratio $R^P_{\{4k\};4}(t, p_k = \pm 2\pi/L)$ for the four values of the light-quark mass, and combining the results at t with those at $T-t-1$. The results have been averaged over the three values for k and, in total, the 6 equivalent lattice momenta with $|\vec{p}| = 2\pi/L$.

To obtain $\langle \xi^2 \rangle_{\pi,K}$ from the ratio $R^P_{\{\rho\mu\nu\};\sigma}(t,\vec{p}\,)$ defined in (6.12) we need two non-zero components of momentum. We consider the cases:

$$R^P_{\{4jk\};4}(t, p_j = \pm 2\pi/L, p_k = \pm 2\pi/L) = -(\pm\frac{2\pi}{L})(\pm\frac{2\pi}{L})\langle \xi^2 \rangle, \quad |\vec{p}| = \sqrt{2}\frac{2\pi}{L}, \quad k,j = 1,2,3, \tag{6.22}$$

with $k \neq j$. We average over all 4 momentum combinations appropriate to each of the 3 possible Lorentz index choices.

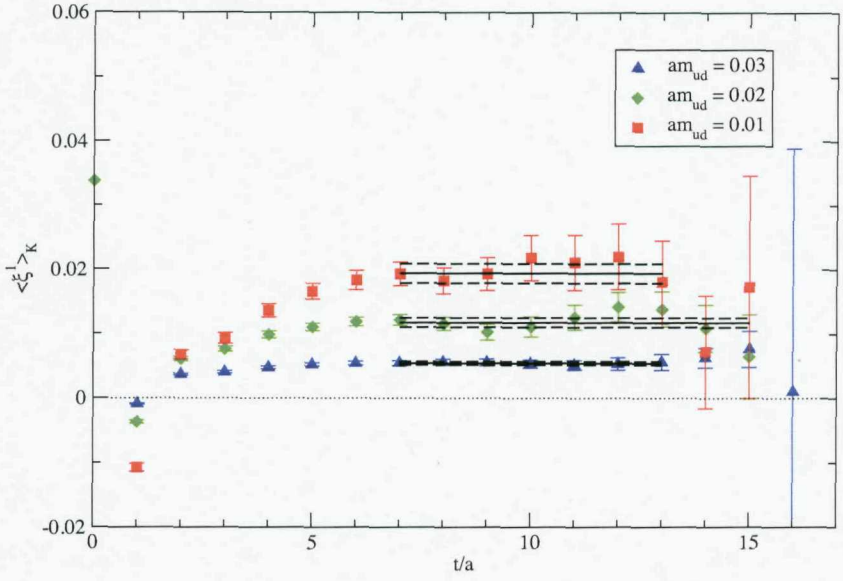

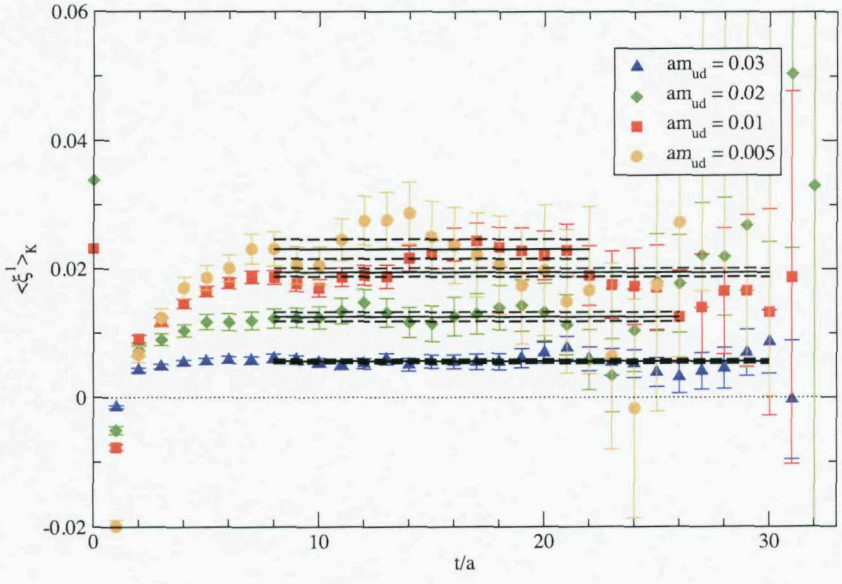

Figure 6.1: Results for $\langle \xi^1 \rangle_K$ as a function of the time, on the 16^3 and 24^3 lattices.

We may extract $\langle \xi^1 \rangle^{\parallel}_{K^*}$ from the ratio $R^V_{\{\rho\mu\}\nu}(t,\vec{p}\,)$ defined in (6.19) by considering only zero-momentum correlation functions. In the denominator, we average $C_{V_iV_i}(t,\vec{p}=0)$ over all 3 spatial directions. In the numerator, we average over $C_{\{41\}1}(t,\vec{p}=0)$, $C_{\{42\}2}(t,\vec{p}=0)$ and $C_{\{43\}3}(t,\vec{p}=0)$. Results are shown in figure 6.2.

$\langle \xi^2 \rangle^{\parallel}_{K^*,\rho,\phi}$ is extracted from the ratio defined in (6.20) by averaging $C_{V_iV_i}(t,p_i=0,|\vec{p}|=\frac{2\pi}{L}\,)$ over all 4 appropriate momenta for all 3 spatial directions, in the denominator. In the numerator, we average over all possible combinations of $C_{\{4ij\}i}(t,p_j=\pm\frac{2\pi}{L},|\vec{p}|=\frac{2\pi}{L})$ with $i\neq j$.

Tables 6.1 and 6.2 show the 16^3 and 24^3 results respectively, complete with linear chiral extrapolations which, as we shall discuss in the next section, can be justified using chiral perturbation theory (at least in the pseudoscalar case).

6.3 Quark Mass Extrapolations

According to leading-order chiral perturbation theory [124], $\langle \xi^1 \rangle_K$ is proportional to $m_s - m_q$ without logarithms:

$$\langle \xi^1 \rangle_K = \frac{8B_0}{f^2}(m_s - m_{u/d})b_{1,2}\,, \tag{6.23}$$

where f and B_0 denote the usual chiral perturbation theory parameters and $b_{1,2}$ is a Wilson coefficient introduced in ref. [124].

Our data shows clearly the effects of SU(3) symmetry breaking, and is compatible with this expectation. Therefore, we perform a linear extrapolation in $m_s - m_q$, to the physical point $a(m_s - m_q) = 0.0356(16)$ [108] (shown in fig. 6.3). The second error quoted in the results table is due to the uncertainty in this extrapolation point. In this way we deal simultaneously with the usual light-quark mass extrapolation and with the strange quark mass extrapolation which is necessitated by our strange quark mass being approximately 15% too heavy. Unfortunately,

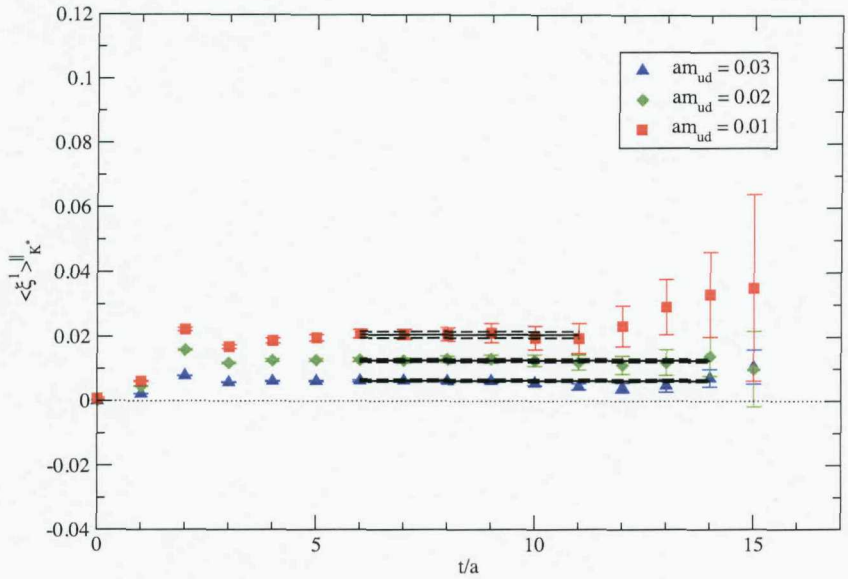

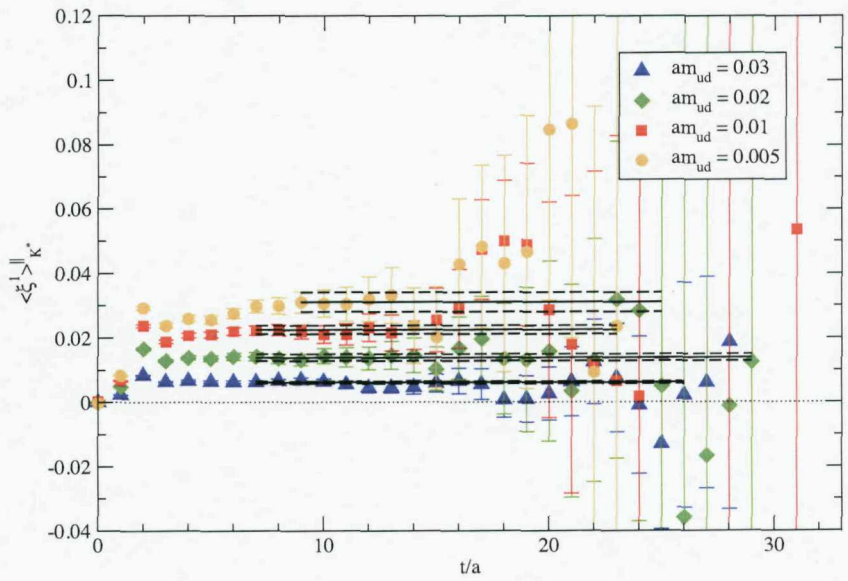

Figure 6.2: Results for $\langle \xi^1 \rangle^{\parallel}_{K^*}$ as a function of the time, on the 16^3 and 24^3 lattices.

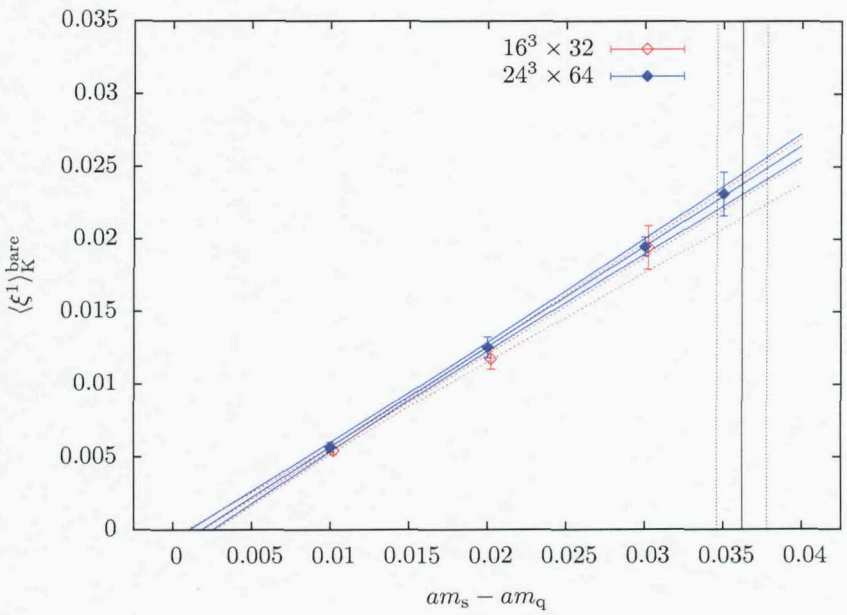

Figure 6.3: Chiral extrapolation for $\langle \xi^1 \rangle_K$. The extrapolation is to the physical point, the uncertainty in which is indicated by the dotted lines.

our extrapolation does not vanish in the SU(3) limit, since in order to have a reasonable number of data points in the fit we have had to include the results for the heaviest light-quark masses, which can hardly be said to be in the chiral region.

As a similar linear behaviour is seen for $\langle \xi^1 \rangle^{\parallel}_{K^*}$ (see fig. 6.4), we follow the same procedure for that quantity. We note that we seem to see a hint of a finite volume effect in the K^* case, but not in the K case, which is contrary to what we would expect. Where we do have K^* results for both volumes at the same light-quark mass, however, they agree within the statistical uncertainties. It may therefore be that this observation should not yet be taken too seriously.

For the second moments, we also have some guidance from chiral perturbation theory [125] - there should be no non-analytic dependence to 2-loops, and we should fit linearly in m_π^2. The dependence on the quark masses appears to be very mild in any case, and in fact our results for the ρ, K^* and ϕ agree within the statistical errors. In this case, therefore, we perform a linear extrapolation in the light quark masses and neglect the effect of the heavy strange quark mass

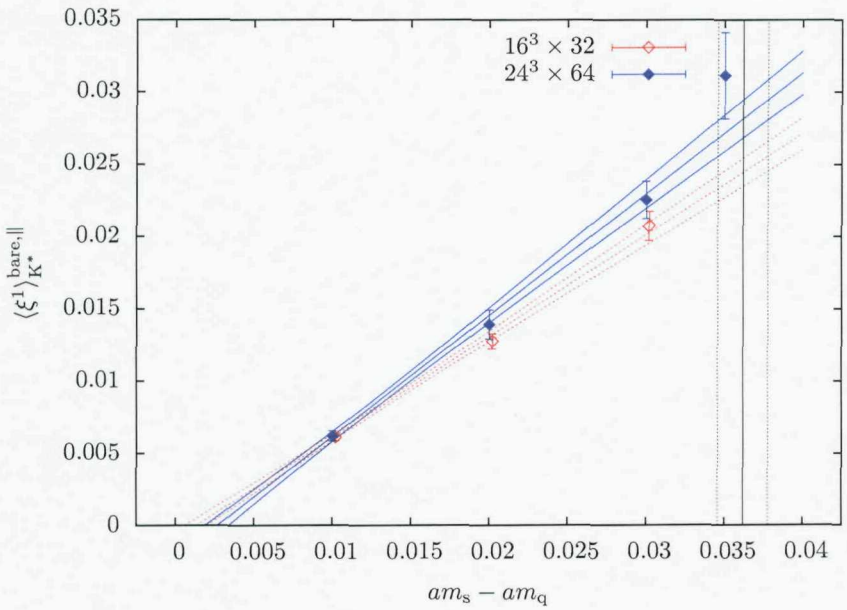

Figure 6.4: Chiral extrapolation for $\langle \xi^1 \rangle^{\parallel}_{K^*}$.

(see figs. 6.5 - 6.9).

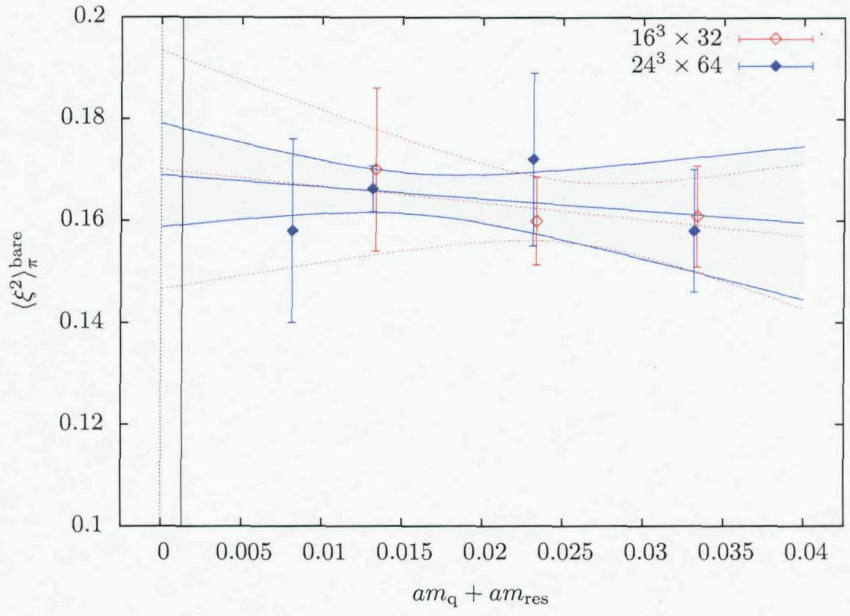

Figure 6.5: Chiral extrapolation for $\langle \xi^2 \rangle_\pi$.

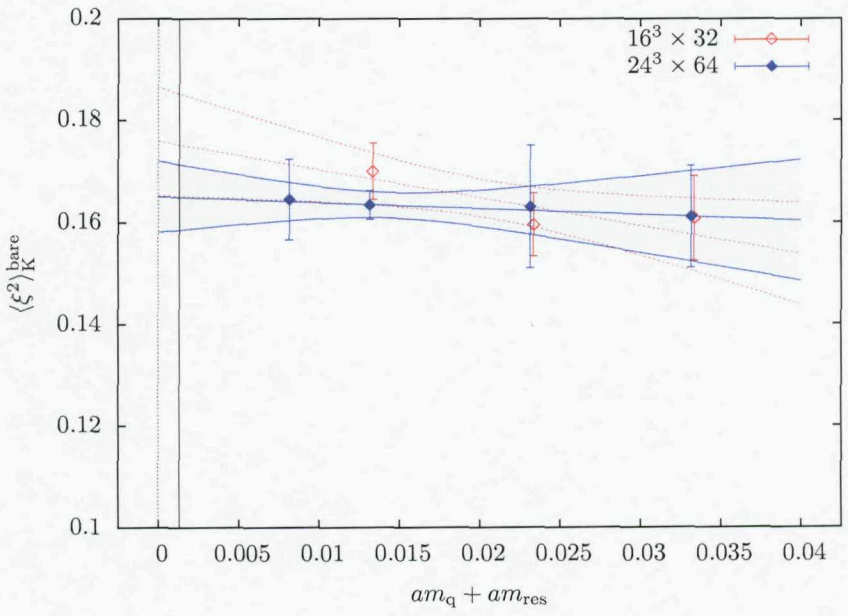

Figure 6.6: Chiral extrapolation for $\langle \xi^2 \rangle_K$.

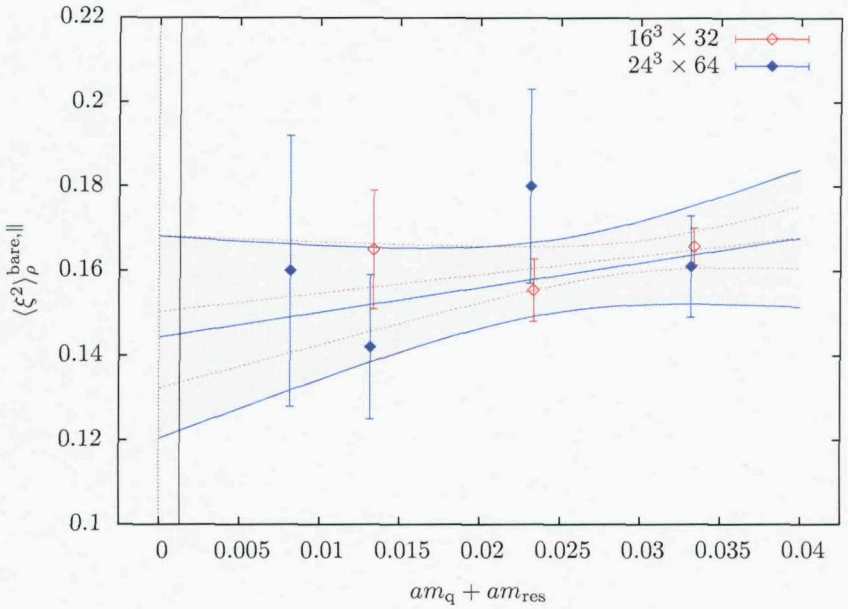

Figure 6.7: Chiral extrapolation for $\langle \xi^2 \rangle_\rho^{\parallel}$.

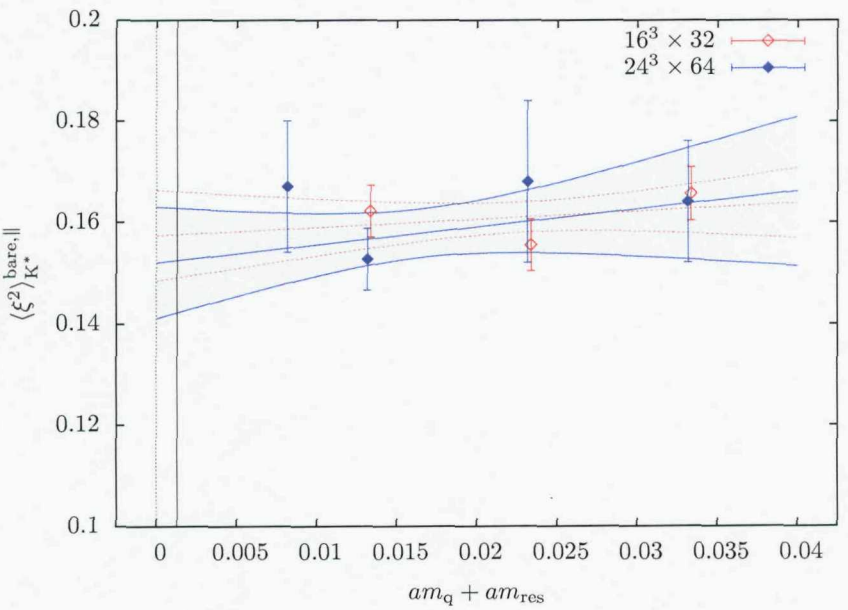

Figure 6.8: Chiral extrapolation for $\langle \xi^2 \rangle_{K^*}^{\parallel}$.

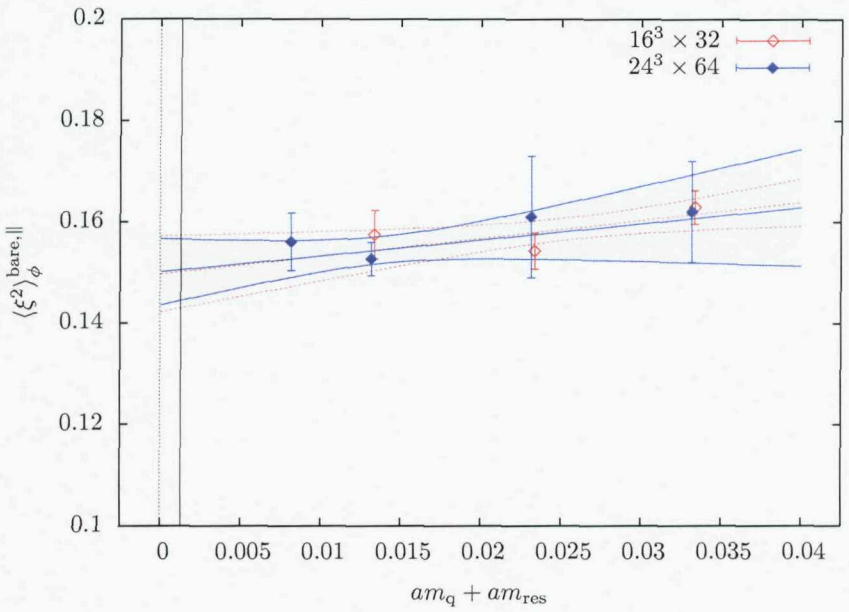

Figure 6.9: Chiral extrapolation for $\langle \xi^2 \rangle_\phi^\parallel$.

Table 6.1: Summary of results for the bare values of the distribution amplitude moments on the 16^3 lattices. The chiral extrapolations are discussed in section 6.3, and the errors are statistical and (in the first moment case) due to the uncertainty in the physical point for the chiral extrapolation.

am_{ud}	0.03	0.02	0.01	0.005	χ-limit
$\langle \xi^2 \rangle_\pi$	0.1608(99)	0.1599(86)	0.170(16)	-	0.170(23)
$\langle \xi^1 \rangle_K$	0.00543(27)	0.01174(71)	0.0194(15)	-	0.0228(14)(11)
$\langle \xi^2 \rangle_K$	0.1607(83)	0.1595(62)	0.1700(55)	-	0.176(11)
$\langle \xi^2 \rangle_\rho^\parallel$	0.1657(44)	0.1554(74)	0.165(14)	-	0.150(18)
$\langle \xi^1 \rangle_{K^*}^\parallel$	0.00610(24)	0.01275(51)	0.0207(10)	-	0.02443(96)(107)
$\langle \xi^2 \rangle_{K^*}^\parallel$	0.1656(53)	0.1555(51)	0.1622(51)	-	0.1573(89)
$\langle \xi^2 \rangle_\phi^\parallel$	0.1629(33)	0.1543(36)	0.1575(48)	-	0.1497(75)

Table 6.2: Summary of results for the bare values of the distribution amplitude moments on the 24^3 lattices.

am_{ud}	0.03	0.02	0.01	0.005	χ-limit
$\langle\xi^2\rangle_\pi$	0.158(12)	0.172(17)	0.1662(45)	0.158(18)	0.169(10)
$\langle\xi^1\rangle_K$	0.00566(33)	0.01254(72)	0.01946(65)	0.0231(15)	0.02377(71)(110)
$\langle\xi^2\rangle_K$	0.161(10)	0.163(12)	0.1634(28)	0.1645(79)	0.1651(70)
$\langle\xi^2\rangle_\rho^\parallel$	0.161(12)	0.180(23)	0.142(17)	0.160(32)	0.144(24)
$\langle\xi^1\rangle_{K^*}^\parallel$	0.00619(35)	0.0139(10)	0.0225(13)	0.0311(30)	0.0281(13)(14)
$\langle\xi^2\rangle_{K^*}^\parallel$	0.164(12)	0.168(16)	0.1527(61)	0.167(13)	0.152(11)
$\langle\xi^2\rangle_\phi^\parallel$	0.162(10)	0.161(12)	0.1527(33)	0.1561(57)	0.1501(66)

Chapter 7

Distribution Amplitude Moments: Renormalization

Having extracted, from Monte Carlo simulation of ratios of lattice correlation functions, bare values for the lowest moments of several light-meson distribution amplitudes, we must renormalize the relevant lattice operators in order to obtain physical results. Because of the chiral symmetry of the domain-wall fermion action, the renormalization of operators which differ only by a factor of γ_5 will be identical, and so we do not need separate calculations for the pseudoscalar and vector meson cases. Numerically, of course, one can obtain different results from the non-perturbative calculations for the two cases, due to the spontaneous chiral symmetry breaking (the effects of which persist even at relatively high momenta for our exceptional-momentum vertex amplitudes), as discussed in sec. 5.3.

As explained in section 6.1.2, with our choice of indices the first-moment operators renormalize multiplicatively. Therefore we define:

$$O^{\overline{\mathrm{MS}}}_{\{\rho\mu\}}(\mu) = Z_{O_{\{\rho\mu\}}} O^{\mathrm{latt}}_{\{\rho\mu\}}(a) \,. \tag{7.1}$$

For the second moment calculation, we must take account of the mixing with a total derivative

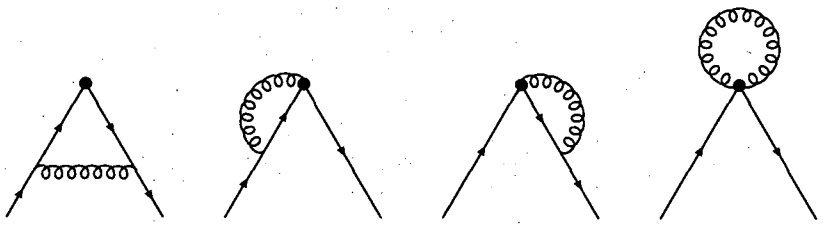

Figure 7.1: One-loop vertex diagrams evaluated in the perturbative renormalization of the 1st and 2nd moment operators.

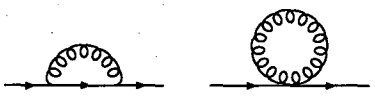

Figure 7.2: One-loop diagrams for the quarks' wavefunction renormalization.

operator that occurs for off-forward matrix elements. We adopt the notation:

$$\mathcal{O}_{DD} = \bar{\psi}\gamma_{\{\mu}\gamma_5 \overleftrightarrow{D}_{\nu} \overleftrightarrow{D}_{\kappa\}}\psi, \qquad \mathcal{O}_{\partial\partial} = \partial_{\{\nu}\partial_{\kappa}\bar{\psi}\gamma_{\mu\}}\gamma_5\psi, \tag{7.2}$$

with all Lorentz indices distinct and symmetrized. We then have the relationship:

$$\mathcal{O}_{DD}^{\overline{\rm MS}}(\mu) = Z_{DD,DD}\mathcal{O}_{DD}^{\rm latt}(a) + Z_{DD,\partial\partial}\mathcal{O}_{\partial\partial}^{\rm latt}(a). \tag{7.3}$$

7.1 Perturbative Calculation

As explained in section 3.7.2, the perturbative matching from the lattice 'scheme' to the $\overline{\rm MS}$ scheme can be done by comparing the corresponding one-loop calculations of a quark two-point function with an insertion of the relevant operator. This requires the evaluation of both the vertex diagrams shown in figure 7.1 and the wavefunction renormalization factor represented by the diagrams in figure 7.2.

The perturbative renormalization factors for the first moment operator corresponding to alternative lattice formulations can be found in [126] (domain-wall fermions and plaquette action), [127] (overlap fermions and Lüscher–Weisz action) and [128] (clover fermions and

plaquette action). The second moment calculations with clover and Wilson fermions have been performed in [128] and [129] respectively (in both cases using the plaquette gauge action). We have already outlined mean-field improved perturbative calculations with domain-wall fermions and Iwasaki gauge fields in sec. 5.6.

For the first-moment operator, the renormalization factor is given at one-loop by:

$$Z_{O_{\{\rho\mu\}}} = \frac{1}{(1-w_0^2)Z_w}\left[1+\frac{\alpha C_F}{4\pi}\left(-\frac{8}{3}\ln(\mu^2a^2)+\Sigma_1^{\overline{\rm MS}}-\Sigma_1+V^{\overline{\rm MS}}-V\right)\right], \tag{7.4}$$

whilst for the second moment calculation, the one-loop perturbative expressions are:

$$Z_{DD,DD} = \frac{1}{(1-w_0^2)Z_w}\left[1+\frac{\alpha C_F}{4\pi}\left(-\frac{25}{6}\ln(\mu^2a^2)+\Sigma_1^{\overline{\rm MS}}-\Sigma_1+V_{DD}^{\overline{\rm MS}}-V_{DD}\right)\right], \tag{7.5}$$

$$Z_{DD,\partial\partial} = \frac{1}{(1-w_0^2)Z_w}\frac{\alpha C_F}{4\pi}\left(\frac{5}{6}\ln(\mu^2a^2)+V_{\partial\partial}^{\overline{\rm MS}}-V_{\partial\partial}\right), \tag{7.6}$$

where $(1-w_0^2)Z_w$ is a characteristic normalization factor for the physical quark fields in the domain-wall formalism, as described in section 5.6.

The terms labelled with $\overline{\rm MS}$ superscripts must be evaluated by calculations within that scheme, whilst the other terms require calculations using lattice perturbation theory. For compactness of notation we define:

$$c = \Sigma_1^{\overline{\rm MS}}-\Sigma_1+V^{\overline{\rm MS}}-V, \tag{7.7}$$

$$c_{DD} = \Sigma_1^{\overline{\rm MS}}-\Sigma_1+V_{DD}^{\overline{\rm MS}}-V_{DD}, \tag{7.8}$$

$$c_{\partial\partial} = V_{\partial\partial}^{\overline{\rm MS}}-V_{\partial\partial}. \tag{7.9}$$

The terms $\Sigma_1^{\overline{\rm MS}}$ and Σ_1 come from the renormalization of the quark wavefunction, while $V^{\overline{\rm MS}}$, $V_{DD}^{\overline{\rm MS}}$, $V_{\partial\partial}^{\overline{\rm MS}}$ and V, V_{DD}, $V_{\partial\partial}$ come from the one-loop corrections to the amputated two-point function. They are given by "vertex" and "sail" diagrams, plus (in the lattice case) an operator tadpole diagram. Since, for incoming quark momentum p_1 and outgoing quark momentum p_2, an external derivative leads to a factor proportional to p_1-p_2 and an internal two-sided derivative leads to a factor proportional to p_1+p_2, $V_{DD}^{\overline{\rm MS}}$ and V_{DD} can be isolated by computing

the one-loop correction with equal incoming and outgoing quark momenta. Similarly, $V_{\partial\partial}^{\overline{\rm MS}}$ and $V_{\partial\partial}$ are found by setting the incoming and outgoing quark momenta equal and opposite (the lattice tadpole diagram does not contribute in this case).

Using naive dimensional regularization (NDR) in Feynman gauge with a gluon mass infrared (IR) regulator, the continuum terms are:

$$\Sigma_1^{\overline{\rm MS}} = \frac{1}{2}, \qquad V^{\overline{\rm MS}} = -\frac{25}{18}, \qquad V_{DD}^{\overline{\rm MS}} = -\frac{121}{72}, \qquad V_{\partial\partial}^{\overline{\rm MS}} = \frac{41}{72}. \tag{7.10}$$

The lattice contributions must be evaluated for domain-wall fermions with the Iwasaki gluon action ($c_1 = -0.331$), also using Feynman gauge and a gluon mass IR regulator. Σ_1 is given in [119], while the vertex term V was calculated for the first moment operator in [122]. The calculation for the 2nd moment will appear in a forthcoming UKQCD/RBC publication.

For the operator $\mathcal{O}_{DD}$ with two covariant derivatives, mean-field improvement introduces a factor $u_{\rm pt}/u$ where u is the mean link (here taken to be $u = P^{1/4}$) and

$$u_{\rm pt} = 1 - \frac{\alpha C_{\rm F}}{4\pi} 8\pi^2 T_{\rm MF}$$

is its perturbative expansion. For the operator $\mathcal{O}_{\partial\partial}$ with two ordinary derivatives, in contrast, the extra factor is $u/u_{\rm pt}$. The mean-field-improved matching factors are thus:

$$Z_{O_{\{\rho\mu\}}}^{\rm MF} = \frac{1}{1-(w_0^{\rm MF})^2}\frac{1}{Z_w^{\rm MF}}\left[1 + \frac{\alpha C_{\rm F}}{4\pi}\left(-\frac{8}{3}\ln(\mu^2 a^2) + c^{\rm MF}\right)\right] \tag{7.11}$$

$$Z_{DD,DD}^{\rm MF} = \frac{1}{u}\frac{1}{1-(w_0^{\rm MF})^2}\frac{1}{Z_w^{\rm MF}}\left[1 + \frac{\alpha C_{\rm F}}{4\pi}\left(-\frac{25}{6}\ln(\mu^2 a^2) + c_{DD}^{\rm MF} - 8\pi^2 T_{\rm MF}\right)\right] \tag{7.12}$$

$$Z_{DD,\partial\partial}^{\rm MF} = u\frac{1}{1-(w_0^{\rm MF})^2}\frac{1}{Z_w^{\rm MF}}\frac{\alpha C_{\rm F}}{4\pi}\left(\frac{5}{6}\ln(\mu^2 a^2) + c_{\partial\partial}^{\rm MF}\right) \tag{7.13}$$

with $c^{\rm MF} = -0.6713$, $c_{DD}^{\rm MF} - 8\pi^2 T_{\rm MF} = 0.7408$ and $c_{\partial\partial}^{\rm MF} = 0.7391$.

To evaluate these expressions, we again make two choices for the coupling. The first is a mean-field improved coupling defined using the measured plaquette value P, according to [120]

$$\frac{1}{g_{\rm MF}^2(a^{-1})} = \frac{\mathcal{P}}{g_0^2} + d_g + c_p + N_f d_f, \tag{7.14}$$

where N_f is the number of dynamical quark flavours. For the Iwasaki gauge action with $c_1 = -0.331$, the values $d_g = 0.1053$ and $c_p = 0.1401$ are given in [119], while values for d_f as a function of M were calculated in [120]. In our simulations, $\beta = 6/g_0^2 = 2.13$ with $N_f = 3$ and $a^{-1} = 1.729\,\mathrm{GeV}$. The second choice is the continuum $\overline{\mathrm{MS}}$ coupling. At $\mu a = 1$, we find $\alpha_{\mathrm{MF}} = 0.1769$ and $\alpha^{\overline{\mathrm{MS}}} = 0.3138$. We use these two values to evaluate the renormalization factors above. We also evaluate the mean-field improved expression for the axial vector current renormalization [119], interpolating to our mean-field M^{MF}.

$$\begin{array}{lcccc} & Z^{\mathrm{MF}}_{O_{\{\rho\mu\}}} & Z^{\mathrm{MF}}_{DD,DD} & Z^{\mathrm{MF}}_{DD,\partial\partial} & Z^{\mathrm{MF}}_{\mathrm{A}} \\ \alpha_{\mathrm{MF}} & 0.9896 & 1.1604 & 0.0122 & 0.8009 \\ \alpha^{\overline{\mathrm{MS}}} & 0.9162 & 1.0966 & 0.0202 & 0.6934 \end{array} \tag{7.15}$$

The ratios of the renormalization factors, from which the factor $1/(1-(w_0^{\mathrm{MF}})^2)Z_w^{\mathrm{MF}}$ cancels, are then given by:

$$\begin{array}{lccc} & \frac{Z^{\mathrm{MF}}_{O_{\{\rho\mu\}}}}{Z^{\mathrm{MF}}_{\mathrm{A}}} & \frac{Z^{\mathrm{MF}}_{DD,DD}}{Z^{\mathrm{MF}}_{\mathrm{A}}} & \frac{Z^{\mathrm{MF}}_{DD,\partial\partial}}{Z^{\mathrm{MF}}_{\mathrm{A}}} \\ \alpha_{\mathrm{MF}} & 1.2356 & 1.4488 & 0.0152 \\ \alpha^{\overline{\mathrm{MS}}} & 1.3214 & 1.5815 & 0.0291 \end{array} \tag{7.16}$$

7.2 Non-Perturbative Renormalization

It would of course be preferable to obtain the desired renormalization constants without recourse to lattice perturbation theory, given the attendant worries about its precision at the one-loop level and the often large and difficult-to-estimate uncertainties. Before embarking upon this calculation, however, we confront some fundamental issues concerning the RI/MOM method.

7.2.1 The Momentum-Source Approach

In chapter 5, we described the successful use of the RI/MOM non-perturbative renormalization technique with our simulations, ultimately obtaining $\overline{\text{MS}}$-scheme renormalization coefficients for the quark bilinear operators. Disregarding the data in the low-momentum region, due to its contamination by non-perturbative effects such as QCD's dynamical chiral symmetry breaking, we relied upon the high-momentum ($1.3 < (a\mu)^2 < 2.5$) region in which it is instead discretization errors which threaten the applicability of the RI/MOM method. By evolving the high-momentum data to a common reference scale using the appropriate perturbative RG-running (where necessary), and thereby defining a scale invariant RI/MOM renormalization constant, it seemed possible to control these effects by performing a linear $(a\mu)^2 \to 0$ extrapolation. Thus, with some work the existence of a usable 'window' in lattice momenta could be established.

With the 'point-source' approach of chapter 5, the quark propagators which are used to construct the amputated vertices are obtained by inverting the fermion matrix with a point source located on a chosen site. By performing a Fourier transform, it is then possible to calculate the momentum-space propagator for a very wide variety of lattice momenta. Data is therefore obtained easily for many 4-momenta, but it is expensive to average over possible positions of the operator. Since we effectively throw out the data that falls outside of a restricted momentum range, however, and since the operator's position can actually be significant (see figure 7.3), it is not clear that this is the most computationally-efficient approach.

Alternatively, we can obtain directly the momentum-space propagator $S(p)_x = \sum_y S(x|y)e^{ipy}$ for a given 4-momentum p, by inverting with a plane-wave source [130]:

$$\sum_{x'} D(x|x')S(p)_{x'} = e^{ipx} \,. \tag{7.17}$$

By proceeding in this way, we effectively gain volume-averaging for the operator's position in

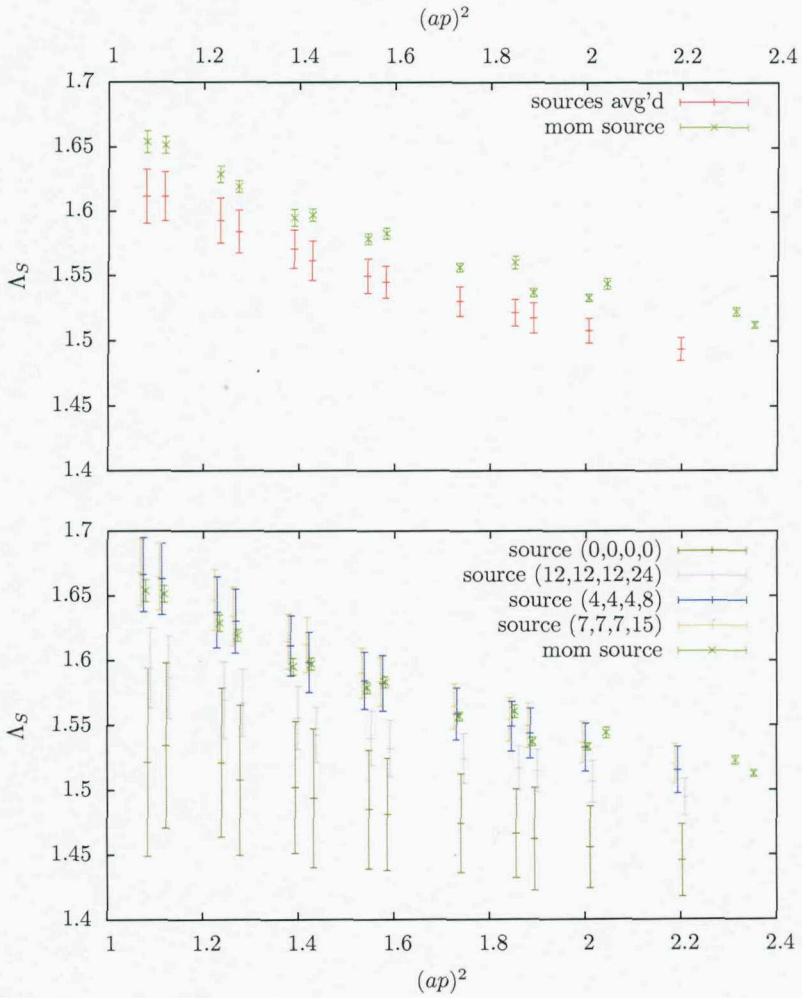

Figure 7.3: A comparison of results obtained for Λ_S using the point source approach (with each source treated separately) and the momentum source approach. The number and position of the point sources is clearly important: two of the point sources are in reasonable agreement with the momentum source, but the others cause a significant disagreement between the source-averaged and momentum source results.

the amputated correlation function, but the disadvantage of course is that we can afford data for fewer 4-momenta. Results obtained using the momentum-source approach do indeed show a drastic reduction in the statistical errors. Unfortunately, however, this serves largely to reveal structure in the discretization effects which previously was hidden by noise (see fig. 7.4).

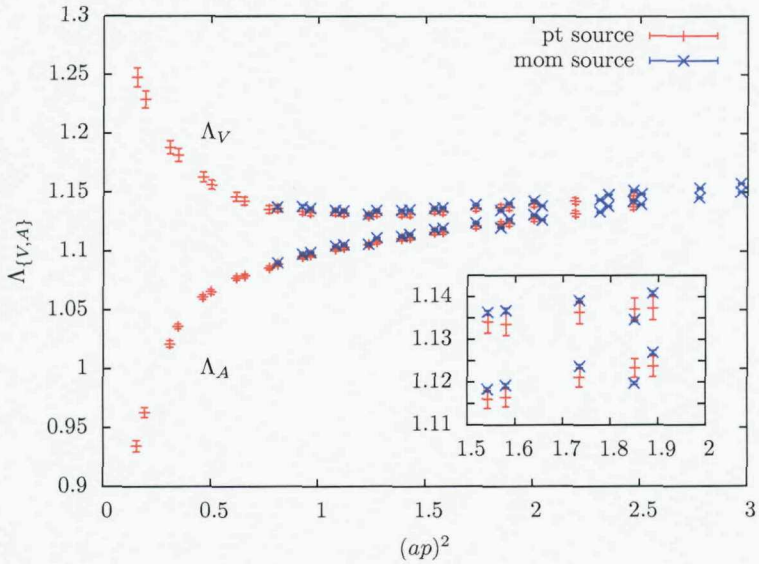

Figure 7.4: A comparison of results obtained for $\Lambda_{\{V,A\}}$ using the point source approach and the momentum source approach. The results are essentially in agreement and the momentum source results have much smaller statistical errors, but as the inset shows, the momentum source results do not behave smoothly.

In chapter 5, we simply averaged over the many different 4-momenta which contributed at a given $(ap)^2$, but with the momentum-source approach we have far fewer 4-momenta and see a very strong dependence on the size of the individual components, with deviations which are now well outside the statistical fluctuations. For a 4-momentum $p_\mu = (2\pi/L_\mu)n_\mu$, we define the quantity:

$$\mathscr{G} \equiv \sum_\mu p_\mu^4 = \sum_\mu \left(\frac{2\pi}{L_\mu} n_\mu\right)^4 , \tag{7.18}$$

which seems to be a reasonable guide to the size of the discretization effects, as figs. 7.5 and

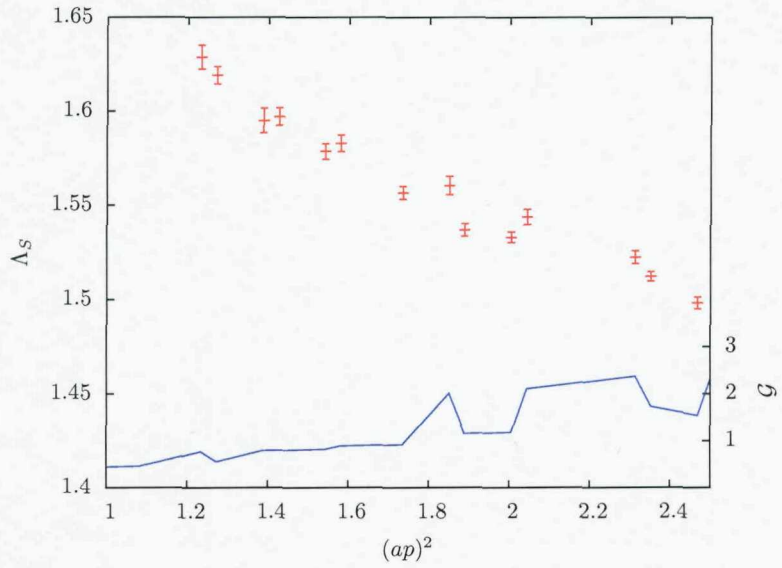

Figure 7.5: Results for Λ_S, with only a single 4-momentum p_μ at each $(ap)^2$, showing the correlation with the discretization error estimate $\mathcal{G}$.

7.6 demonstrate.

At the present time, efforts to establish the optimum way to proceed in the light of these discretization effects are ongoing. Therefore, we do not present non-perturbative results for the renormalization of the derivative operators. Fig. 7.7 shows why these effects could be ignored with the earlier, point source approach.

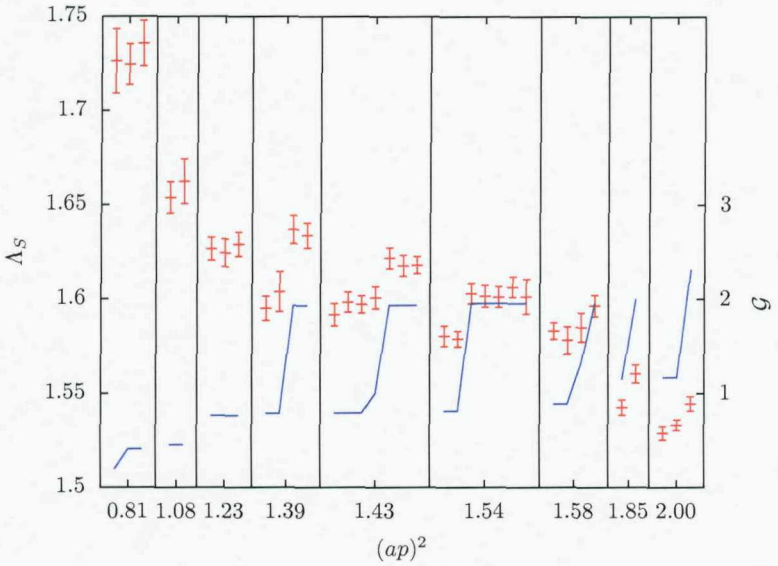

Figure 7.6: Results for Λ_S, showing how discretization effects that are roughly parameterized by the quantity $\mathscr{G}$ split the different 4-momenta contributing at a given $(ap)^2$.

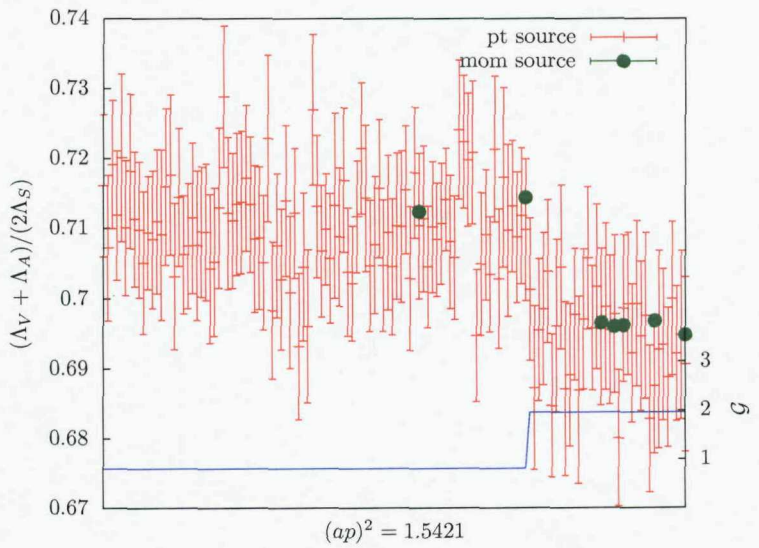

Figure 7.7: Results for the combination of renormalization constants $(\Lambda_V + \Lambda_A)/(2\Lambda_S)$ at a single scale $(ap)^2 = 1.5421$, calculated using the available 4-momenta using both the point and momentum source approaches.

Chapter 8

Conclusions and Outlook

Since the analysis of the momentum-source NPR data is still evolving, and we do not yet have a satisfactory means of extrapolating away the discretization effects or of quantifying the uncertainty due to them, we quote our final results for the low moments of the light-meson DAs using the perturbative values for the renormalization constants. Those final results, quoted at 2 GeV in the $\overline{\text{MS}}$ scheme, are given in table 8.1. In addition to the errors quoted there, we estimate an additional 5% due to discretization effects.

We are able to obtain all of the desired DA moments with an acceptable precision, and in particular for the first moments we see very clear evidence of SU(3) flavour symmetry breaking and the expected chiral behaviour for $\langle \xi^1 \rangle_K$. Where comparable, our results are in reasonable agreement both with those from sum rules calculations (but with smaller errors) and with those from the QCDSF collaborations' complementary programme [47].

It is clear that the first priority should be to bring the uncertainties on these results under better control by non-perturbatively renormalizing the derivative operators. If, as seems likely, we will ultimately have to accept that discretization effects will significantly limit the extent to which we can profit from the smaller statistical uncertainties of the momentum-source approach, we at least have the consolation that data at a finer lattice spacing will be available in

Table 8.1: Summary of final results for the renormalized values of the DA moments, at 2 GeV in the $\overline{\text{MS}}$ scheme. The quoted errors are (statistical)(systematic). There is in addition a discretization effect which we estimate to be $\sim 5\%$. We include the $N_f = 2$ QCDSF results [47,131] for comparison.

	16^3	24^3	QCDSF
$\langle \xi^2 \rangle_\pi$	0.274(34)(13)	0.272(15)(13)	0.269(39)
$\langle \xi^1 \rangle_K$	0.0277(17)(16)	0.02893(87)(166)	0.0272(5)(17)
$\langle \xi^2 \rangle_K$	0.282(17)(14)	0.267(11)(13)	0.260(6)(16)
$\langle \xi^2 \rangle_\rho^\parallel$	0.245(27)(12)	0.237(36)(12)	-
$\langle \xi^1 \rangle_{K^*}^\parallel$	0.0297(11)(16)	0.0342(16)(21)	0.033(2)(4)
$\langle \xi^2 \rangle_{K^*}^\parallel$	0.255(13)(13)	0.248(17)(12)	-
$\langle \xi^2 \rangle_\phi^\parallel$	0.245(11)(12)	0.246(10)(12)	-

the very near future. The new, finer dataset being generated by UKQCD/RBC should also allow for some control to be gained over the discretization effects in the bare DA moments. Furthermore, tests with partially-twisted boundary conditions (which, as discussed in sec. 3.2, help us to evade the problem of the lattice's large, minimum non-vanishing hadronic momentum component) will enable a check on the size of the current discretization errors to be made.

In order to go significantly beyond the refinement of the numerical results presented above, however, and to broaden the research programme beyond the moments studied here, a definite increase in the complexity of the lattice calculations is required. The transversely-polarized vector mesons would be a natural next step, and perhaps also the nucleon distribution amplitudes (for which the QCDSF/UKQCD collaboration have recently presented results [132]), but beyond that the quantities that one really wants to determine begin to present imposing

techincal difficulties.

Studying higher moments of DAs on the lattice, for example, would be desirable: in the continuum, the conformal expansion is generally truncated at around $n = 4$ (beyond which the sum rules are no longer stable). This would require obtaining the matrix elements of operators with more covariant derivatives, however, which makes it increasingly difficult to control operator mixing, as well as generally requiring more non-zero momentum components to be induced (and thereby leading to larger discretization errors and a worse signal). In fact, the operators with more than 3 covariant derivatives necessarily mix with lower dimensional operators, and therefore power divergences will arise, with the associated technical complications.

It would also be very interesting to study the higher-twist distribution amplitudes, which are particularly important for applications to B and D decays, and even give rise to leading order corrections in special cases such as the CP asymmetry in $B \to K^*\gamma$. In this case, however, we must add a gluonic part to the operator, and so there too we will have more Lorentz indices to consider and the problems caused by the loss of Lorentz symmetry will again be severe.

Of course, it would be particularly interesting to study B-meson DAs on the lattice. Aside from the usual difficulties of putting b quarks onto the lattice, however, the problem there is that it is the first inverse moment which is really phenomenologically interesting [133, 134], rather than the ordinary moments that we can obtain on the lattice by inserting covariant derivatives into bilinear operators, which turn out not to be so useful in this case.

There are a variety of ideas which, by using less-standard techniques, can in principle allow for the direct calculation of DAs on the lattice [135–137]. So far, however, only a limited amount of numerical work has been done in this direction [138, 139]. There are essentially two approaches: either light-cone quantization is used in order to try to construct a lattice formulation with a light-cone, or else a non-local but non-light-cone operator matrix element which can be related to the DA using perturbation theory is calculated in a standard simulation. Whilst

these approaches offer the possibility of new, interesting, original and complementary calculations, however, the parameterization via moments was not adopted purely for the convenience of lattice simulations, but has also a physical origin. In terms of producing phenomenologically useful numbers, therefore, it is not yet clear that such approaches will be able to compete with the 'standard' technique used here and in most other lattice studies so far.

Bibliography

[1] Michael Edward Peskin and Daniel V. Schroeder. An Introduction to quantum field theory. Reading, USA: Addison-Wesley (1995) 842 p.

[2] Rajan Gupta. Introduction to lattice QCD. 1997.

[3] Martin Luscher. Advanced lattice QCD. 1998.

[4] Thomas DeGrand and Carleton E. Detar. Lattice methods for quantum chromodynamics. New Jersey, USA: World Scientific (2006) 345 p.

[5] C. Amsler et al. Review of particle physics. *Phys. Lett.*, B667:1, 2008.

[6] J. Gasser and H. Leutwyler. Chiral Perturbation Theory to One Loop. *Ann. Phys.*, 158:142, 1984.

[7] J. Gasser and H. Leutwyler. Chiral Perturbation Theory: Expansions in the Mass of the Strange Quark. *Nucl. Phys.*, B250:465, 1985.

[8] John C. Collins, Davison E. Soper, and George Sterman. Factorization of hard processes in qcd. *ADV.SER.DIRECT.HIGH ENERGY PHYS.*, 5:1, 1988.

[9] George Sterman. Partons, factorization and resummation. 1995.

[10] V. L. Chernyak and A. R. Zhitnitsky. Asymptotic Behavior of Exclusive Processes in QCD. *Phys. Rept.*, 112:173, 1984.

[11] George Sterman and Paul Stoler. Hadronic form factors and perturbative QCD. *Ann. Rev. Nucl. Part. Sci.*, 47:193–233, 1997.

[12] R. Devenish and A. Cooper-Sarkar. Deep inelastic scattering. Oxford, UK: Univ. Pr. (2004) 403 p.

[13] G. Peter Lepage and Stanley J. Brodsky. Exclusive Processes in Perturbative Quantum Chromodynamics. *Phys. Rev.*, D22:2157, 1980.

[14] S. J. Brodsky. Perspectives on exclusive processes in QCD. 2002.

[15] V. L. Chernyak, A. R. Zhitnitsky, and V. G. Serbo. Asymptotic hadronic form-factors in quantum chromodynamics. *JETP Lett.*, 26:594–597, 1977.

[16] A. V. Efremov and A. V. Radyushkin. Factorization and Asymptotical Behavior of Pion Form- Factor in QCD. *Phys. Lett.*, B94:245–250, 1980.

[17] Glennys R. Farrar and Darrell R. Jackson. The Pion Form-Factor. *Phys. Rev. Lett.*, 43:246, 1979.

[18] M. Diehl. Generalized parton distributions. *Phys. Rept.*, 388:41–277, 2003.

[19] A. V. Belitsky and A. V. Radyushkin. Unraveling hadron structure with generalized parton distributions. *Phys. Rept.*, 418:1–387, 2005.

[20] M. Beneke, G. Buchalla, M. Neubert, and Christopher T. Sachrajda. QCD factorization for b $\rightarrow$ pi pi decays: Strong phases and cp violation in the heavy quark limit. *Phys. Rev. Lett.*, 83:1914–1917, 1999.

[21] M. Beneke, G. Buchalla, M. Neubert, and Christopher T. Sachrajda. QCD factorization for exclusive, non-leptonic B meson decays: General arguments and the case of heavy-light final states. *Nucl. Phys.*, B591:313–418, 2000.

[22] M. Beneke, G. Buchalla, M. Neubert, and Christopher T. Sachrajda. QCD factorization in B → pi K, pi pi decays and extraction of Wolfenstein parameters. *Nucl. Phys.*, B606:245–321, 2001.

[23] Christian W. Bauer, Sean Fleming, Dan Pirjol, and Iain W. Stewart. An effective field theory for collinear and soft gluons: Heavy to light decays. *Phys. Rev.*, D63:114020, 2001.

[24] Christian W. Bauer, Dan Pirjol, and Iain W. Stewart. Soft-collinear factorization in effective field theory. *Phys. Rev.*, D65:054022, 2002.

[25] Christian W. Bauer, Sean Fleming, Dan Pirjol, Ira Z. Rothstein, and Iain W. Stewart. Hard scattering factorization from effective field theory. *Phys. Rev.*, D66:014017, 2002.

[26] Patricia Ball, Vladimir M. Braun, Y. Koike, and K. Tanaka. Higher twist distribution amplitudes of vector mesons in QCD: Formalism and twist three distributions. *Nucl. Phys.*, B529:323–382, 1998.

[27] V. M. Braun et al. A lattice calculation of vector meson couplings to the vector and tensor currents using chirally improved fermions. *Phys. Rev.*, D68:054501, 2003.

[28] Damir Becirevic, Vittorio Lubicz, Federico Mescia, and Cecilia Tarantino. Coupling of the light vector meson to the vector and to the tensor current. *JHEP*, 05:007, 2003.

[29] Patricia Ball, Gareth W. Jones, and Roman Zwicky. B –¿ V gamma beyond QCD factorisation. *Phys. Rev.*, D75:054004, 2007.

[30] Patricia Ball and Roman Zwicky. New results on B –¿ pi, K, eta decay formfactors from light-cone sum rules. *Phys. Rev.*, D71:014015, 2005.

[31] M. Beneke, T. Feldmann, and D. Seidel. Systematic approach to exclusive B –¿ V l+ l-, V gamma decays. *Nucl. Phys.*, B612:25–58, 2001.

[32] Stefan W. Bosch and Gerhard Buchalla. The radiative decays B –¿ V gamma at next-to-leading order in QCD. *Nucl. Phys.*, B621:459–478, 2002.

[33] Ahmed Ali, Ben D. Pecjak, and Christoph Greub. $B \to V\gamma$ Decays at NNLO in SCET. *Eur. Phys. J.*, C55:577–595, 2008.

[34] Martin Beneke and Matthias Neubert. QCD factorization for B –¿ P P and B –¿ P V decays. *Nucl. Phys.*, B675:333–415, 2003.

[35] Stanley J. Brodsky, Hans-Christian Pauli, and Stephen S. Pinsky. Quantum chromodynamics and other field theories on the light cone. *Phys. Rept.*, 301:299–486, 1998.

[36] Thomas Heinzl. Light-cone quantization: Foundations and applications. *Lect. Notes Phys.*, 572:55–142, 2001.

[37] Paul A. M. Dirac. Forms of Relativistic Dynamics. *Rev. Mod. Phys.*, 21:392–399, 1949.

[38] Stanley J. Brodsky, Y. Frishman, G. Peter Lepage, and Christopher T. Sachrajda. Hadronic Wave Functions at Short Distances and the Operator Product Expansion. *Phys. Lett.*, B91:239, 1980.

[39] V. M. Braun, G. P. Korchemsky, and Dieter Mueller. The uses of conformal symmetry in QCD. *Prog. Part. Nucl. Phys.*, 51:311–398, 2003.

[40] Patricia Ball and M. Boglione. SU(3) breaking in K and K* distribution amplitudes. *Phys. Rev.*, D68:094006, 2003.

[41] G. Peter Lepage and Stanley J. Brodsky. Exclusive Processes in Quantum Chromodynamics: Evolution Equations for Hadronic Wave Functions and the Form-Factors of Mesons. *Phys. Lett.*, B87:359–365, 1979.

[42] A. V. Efremov and A. V. Radyushkin. Asymptotical Behavior of Pion Electromagnetic Form-Factor in QCD. *Theor. Math. Phys.*, 42:97–110, 1980.

[43] V. N. Gribov and L. N. Lipatov. Deep inelastic e p scattering in perturbation theory. *Sov. J. Nucl. Phys.*, 15:438–450, 1972.

[44] L. N. Lipatov. The parton model and perturbation theory. *Sov. J. Nucl. Phys.*, 20:94–102, 1975.

[45] Yuri L. Dokshitzer. Calculation of the Structure Functions for Deep Inelastic Scattering and e+ e- Annihilation by Perturbation Theory in Quantum Chromodynamics. (In Russian). *Sov. Phys. JETP*, 46:641–653, 1977.

[46] Guido Altarelli and G. Parisi. Asymptotic Freedom in Parton Language. *Nucl. Phys.*, B126:298, 1977.

[47] V. M. Braun et al. Moments of pseudoscalar meson distribution amplitudes from the lattice. *Phys. Rev.*, D74:074501, 2006.

[48] G. Martinelli and Christopher T. Sachrajda. A LATTICE CALCULATION OF THE SECOND MOMENT OF THE PION'S DISTRIBUTION AMPLITUDE. *Phys. Lett.*, B190:151, 1987.

[49] D. Daniel, Rajan Gupta, and D. G. Richards. A Calculation of the pion's quark distribution amplitude in lattice QCD with dynamical fermions. *Phys. Rev.*, D43:3715–3724, 1991.

[50] L. Del Debbio, Massimo Di Pierro, A. Dougall, and Christopher T. Sachrajda. The second moment of the pion's distribution amplitude. *Nucl. Phys. Proc. Suppl.*, 83:235–237, 2000.

[51] Luigi Del Debbio, Massimo Di Pierro, and Alex Dougall. The second moment of the pion light cone wave function. *Nucl. Phys. Proc. Suppl.*, 119:416–418, 2003.

[52] Mikhail A. Shifman, A. I. Vainshtein, and Valentin I. Zakharov. QCD and Resonance Physics. Sum Rules. *Nucl. Phys.*, B147:385–447, 1979.

[53] Mikhail A. Shifman, A. I. Vainshtein, and Valentin I. Zakharov. QCD and Resonance Physics: Applications. *Nucl. Phys.*, B147:448–518, 1979.

[54] Pietro Colangelo and Alexander Khodjamirian. QCD sum rules: A modern perspective. 2000.

[55] A. Khodjamirian, Th. Mannel, and M. Melcher. Kaon distribution amplitude from QCD sum rules. *Phys. Rev.*, D70:094002, 2004.

[56] V. M. Braun and A. Lenz. On the SU(3) symmetry-breaking corrections to meson distribution amplitudes. *Phys. Rev.*, D70:074020, 2004.

[57] Patricia Ball and Roman Zwicky. SU(3) breaking of leading-twist K and K* distribution amplitudes: A reprise. *Phys. Lett.*, B633:289–297, 2006.

[58] Patricia Ball and Roman Zwicky. Operator relations for SU(3) breaking contributions to K and K* distribution amplitudes. *JHEP*, 02:034, 2006.

[59] Kenneth G. Wilson. CONFINEMENT OF QUARKS. *Phys. Rev.*, D10:2445–2459, 1974.

[60] Kenneth G. Wilson. The origins of lattice gauge theory. *Nucl. Phys. Proc. Suppl.*, 140:3–19, 2005.

[61] Michael Creutz, Laurence Jacobs, and Claudio Rebbi. Experiments with a Gauge Invariant Ising System. *Phys. Rev. Lett.*, 42:1390, 1979.

[62] L. Maiani and M. Testa. Final state interactions from Euclidean correlation functions. *Phys. Lett.*, B245:585–590, 1990.

[63] Laurent Lellouch and Martin Luscher. Weak transition matrix elements from finite-volume correlation functions. *Commun. Math. Phys.*, 219:31–44, 2001.

[64] Paulo F. Bedaque. Aharonov-Bohm effect and nucleon nucleon phase shifts on the lattice. *Phys. Lett.*, B593:82–88, 2004.

[65] C. T. Sachrajda and G. Villadoro. Twisted boundary conditions in lattice simulations. *Phys. Lett.*, B609:73–85, 2005.

[66] Paulo F. Bedaque and Jiunn-Wei Chen. Twisted valence quarks and hadron interactions on the lattice. *Phys. Lett.*, B616:208–214, 2005.

[67] J. M. Flynn, A. Juttner, and C. T. Sachrajda. A numerical study of partially twisted boundary conditions. *Phys. Lett.*, B632:313–318, 2006.

[68] K. Symanzik. Continuum Limit and Improved Action in Lattice Theories. 1. Principles and phi**4 Theory. *Nucl. Phys.*, B226:187, 1983.

[69] Holger Bech Nielsen and M. Ninomiya. No Go Theorem for Regularizing Chiral Fermions. *Phys. Lett.*, B105:219, 1981.

[70] Paul H. Ginsparg and Kenneth G. Wilson. A Remnant of Chiral Symmetry on the Lattice. *Phys. Rev.*, D25:2649, 1982.

[71] David B. Kaplan. A method for simulating chiral fermions on the lattice. *Phys. Lett.*, B288:342–347, 1992.

[72] Yigal Shamir. Chiral fermions from lattice boundaries. *Nucl. Phys.*, B406:90–106, 1993.

[73] Vadim Furman and Yigal Shamir. Axial symmetries in lattice QCD with Kaplan fermions. *Nucl. Phys.*, B439:54–78, 1995.

[74] Rajamani Narayanan and Herbert Neuberger. Infinitely many regulator fields for chiral fermions. *Phys. Lett.*, B302:62–69, 1993.

[75] Herbert Neuberger. Exactly massless quarks on the lattice. *Phys. Lett.*, B417:141–144, 1998.

[76] Herbert Neuberger. A practical implementation of the overlap-Dirac operator. *Phys. Rev. Lett.*, 81:4060–4062, 1998.

[77] Herbert Neuberger. More about exactly massless quarks on the lattice. *Phys. Lett.*, B427:353–355, 1998.

[78] P. Hasenfratz. Prospects for perfect actions. *Nucl. Phys. Proc. Suppl.*, 63:53–58, 1998.

[79] Peter Hasenfratz; Victor Laliena, and Ferenc Niedermayer. The index theorem in QCD with a finite cut-off. *Phys. Lett.*, B427:125–131, 1998.

[80] Martin Luscher. Exact chiral symmetry on the lattice and the Ginsparg- Wilson relation. *Phys. Lett.*, B428:342–345, 1998.

[81] Ferenc Niedermayer. Exact chiral symmetry, topological charge and related topics. *Nucl. Phys. Proc. Suppl.*, 73:105–119, 1999.

[82] Michael Creutz. Aspects of chiral symmetry and the lattice. *Rev. Mod. Phys.*, 73:119–150, 2001.

[83] Herbert Neuberger. Exact chiral symmetry on the lattice. *Ann. Rev. Nucl. Part. Sci.*, 51:23–52, 2001.

[84] Y. Iwasaki. RENORMALIZATION GROUP ANALYSIS OF LATTICE THEORIES AND IMPROVED LATTICE ACTION. 2. FOUR-DIMENSIONAL NONABELIAN SU(N) GAUGE MODEL. UTHEP-118.

[85] Y. Iwasaki and T. Yoshie. RENORMALIZATION GROUP IMPROVED ACTION FOR SU(3) LATTICE GAUGE THEORY AND THE STRING TENSION. *Phys. Lett.*, B143:449, 1984.

[86] Y. Iwasaki. Renormalization Group Analysis of Lattice Theories and Improved Lattice Action: Two-Dimensional Nonlinear O(N) Sigma Model. *Nucl. Phys.*, B258:141–156, 1985.

[87] D. J. Antonio et al. First results from 2+1-flavor domain wall QCD: Mass spectrum, topology change and chiral symmetry with L(s) = 8. *Phys. Rev.*, D75:114501, 2007.

[88] Justin Foley et al. Practical all-to-all propagators for lattice QCD. *Comput. Phys. Commun.*, 172:145–162, 2005.

[89] A. D. Kennedy. Algorithms for dynamical fermions. 2006.

[90] Rainer Sommer. Non-perturbative renormalization of QCD. 1997.

[91] Stefano Capitani. Lattice perturbation theory. *Phys. Rept.*, 382:113–302, 2003.

[92] Stefan Sint. Non-perturbative renormalization in lattice field theory. *Nucl. Phys. Proc. Suppl.*, 94:79–94, 2001.

[93] Martin Luscher, Peter Weisz, and Ulli Wolff. A Numerical method to compute the running coupling in asymptotically free theories. *Nucl. Phys.*, B359:221–243, 1991.

[94] G. Martinelli, C. Pittori, Christopher T. Sachrajda, M. Testa, and A. Vladikas. A general method for nonperturbative renormalization of lattice operators. *Nucl. Phys.*, B445:81–108, 1995.

[95] Martin Luscher, Rajamani Narayanan, Peter Weisz, and Ulli Wolff. The Schrodinger functional: A Renormalizable probe for nonAbelian gauge theories. *Nucl. Phys.*, B384:168–228, 1992.

[96] Stefan Sint. The Schrodinger functional in QCD. *Nucl. Phys. Proc. Suppl.*, 42:835–837, 1995.

[97] V. N. Gribov. Quantization of non-Abelian gauge theories. *Nucl. Phys.*, B139:1, 1978.

[98] Maria Luigia Paciello, Silvano Petrarca, Bruno Taglienti, and Anastassios Vladikas. Gribov noise of the lattice axial current renormalization constant. *Phys. Lett.*, B341:187–194, 1994.

[99] T. Blum et al. Non-perturbative renormalisation of domain wall fermions: Quark bilinears. *Phys. Rev.*, D66:014504, 2002.

[100] D. J. Antonio et al. Neutral kaon mixing from 2+1 flavor domain wall QCD. *Phys. Rev. Lett.*, 100:032001, 2008.

[101] Y. Aoki et al. Non-perturbative renormalization of quark bilinear operators and B_K using domain wall fermions. 2007.

[102] Shu Li, Robert D. Mawhinney, and UKQCD Collaborations. Kaon Weak Matrix Elements in 2+1 flavor DWF QCD. *PoS*, LAT2007:359, 2007.

[103] M. A. Clark and A. D. Kennedy. Accelerating dynamical fermion computations using the rational hybrid Monte Carlo (RHMC) algorithm with multiple pseudofermion fields. *Phys. Rev. Lett.*, 98:051601, 2007.

[104] P. Boyle et al. The QCDOC project. *Nucl. Phys. Proc. Suppl.*, 140:169–175, 2005.

[105] P. A. Boyle et al. Hardware and software status of QCDOC. *Nucl. Phys. Proc. Suppl.*, 129:838–843, 2004.

[106] P. A. Boyle, C. Jung, and T. Wettig. The QCDOC supercomputer: Hardware, software, and performance. *ECONF*, C0303241:THIT003, 2003.

[107] C. Allton et al. 2+1 flavor domain wall QCD on a (2 fm)^3 lattice: light meson spectroscopy with Ls = 16. *Phys. Rev.*, D76:014504, 2007.

[108] C. Allton et al. Physical Results from 2+1 Flavor Domain Wall QCD and SU(2) Chiral Perturbation Theory. 2008.

[109] Robert G. Edwards and Balint Joo. The Chroma software system for lattice QCD. *Nucl. Phys. Proc. Suppl.*, 140:832, 2005.

[110] P Boyle. A novel gauge invariant multi-state smearing technique. *J. Comput. Phys.*, 179:349–370, 2002.

[111] C. R. Allton et al. Gauge invariant smearing and matrix correlators using Wilson fermions at Beta = 6.2. *Phys. Rev.*, D47:5128–5137, 1993.

[112] M. A. Donnellan et al. Lattice Results for Vector Meson Couplings and Parton Distribution Amplitudes. *PoS*, LAT2007:369, 2007.

[113] Meifeng Lin and Enno E. Scholz. Chiral Limit and Light Quark Masses in 2+1 Flavor Domain Wall QCD. *PoS*, LAT2007:120, 2007.

[114] T. van Ritbergen, J. A. M. Vermaseren, and S. A. Larin. The four-loop beta function in quantum chromodynamics. *Phys. Lett.*, B400:379–384, 1997.

[115] K. G. Chetyrkin and A. Retey. Renormalization and running of quark mass and field in the regularization invariant and MS-bar schemes at three and four loops. *Nucl. Phys.*, B583:3–34, 2000.

[116] W. M. Yao et al. Review of particle physics. *J. Phys.*, G33:1–1232, 2006.

[117] J. A. Gracey. Three loop anomalous dimension of non-singlet quark currents in the RI' scheme. *Nucl. Phys.*, B662:247–278, 2003.

[118] Sinya Aoki, Taku Izubuchi, Yoshinobu Kuramashi, and Yusuke Taniguchi. Perturbative renormalization factors of quark bilinear operators for domain-wall QCD. *Phys. Rev.*, D59:094505, 1999.

[119] Sinya Aoki, Taku Izubuchi, Yoshinobu Kuramashi, and Yusuke Taniguchi. Perturbative renormalization factors in domain-wall QCD with improved gauge actions. *Phys. Rev.*, D67:094502, 2003.

[120] Sinya Aoki and Yoshinobu Kuramashi. The lattice Lambda parameter in domain wall QCD. *Phys. Rev.*, D68:034507, 2003.

[121] Melnulf Gockeler et al. Meson decay constants from N(f) = 2 clover fermions. *PoS*, LAT2005:063, 2006.

[122] P. A. Boyle et al. A lattice computation of the first moment of the kaon's distribution amplitude. *Phys. Lett.*, B641:67–74, 2006.

[123] M. Gockeler et al. Lattice Operators for Moments of the Structure Functions and their Transformation under the Hypercubic Group. *Phys. Rev.*, D54:5705–5714, 1996.

[124] Jiunn-Wei Chen and Iain W. Stewart. Model independent results for SU(3) violation in light- cone distribution functions. *Phys. Rev. Lett.*, 92:202001, 2004.

[125] Jiunn-Wei Chen, Hung-Ming Tsai, and Ke-Chuan Weng. Model-independent results for SU(3) violation in twist-3 light-cone distribution functions. *Phys. Rev.*, D73:054010, 2006.

[126] Stefano Capitani. Perturbative renormalization of the first moment of structure functions for domain-wall QCD. *Phys. Rev.*, D73:014505, 2006.

[127] R. Horsley, H. Perlt, Paul E. L. Rakow, G. Schierholz, and A. Schiller. Renormalisation of one-link quark operators for overlap fermions with Luescher-Weisz gauge action. *Phys. Lett.*, B628:66–72, 2005.

[128] M. Gockeler et al. Renormalisation of composite operators in lattice perturbation theory with clover fermions: Non-forward matrix elements. *Eur. Phys. J.*, C48:523–530, 2006.

[129] M. Gockeler et al. Perturbative renormalisation of the second moment of generalised parton distributions. *Nucl. Phys.*, B717:304–323, 2005.

[130] M. Gockeler et al. Nonperturbative renormalisation of composite operators in lattice QCD. *Nucl. Phys.*, B544:699–733, 1999.

[131] V. M. Braun et al. Distribution Amplitudes of Vector Mesons. *PoS*, LAT2007:144, 2007.

[132] Meinulf Gockeler et al. Nucleon distribution amplitudes from lattice QCD. 2008.

[133] Seung J. Lee and Matthias Neubert. Model-independent properties of the B-meson distribution amplitude. *Phys. Rev.*, D72:094028, 2005.

[134] Patricia Ball and Roman Zwicky. —V(td)/V(ts)— from B –¿ V gamma. *JHEP*, 04:046, 2006.

[135] U. Aglietti et al. Model independent determination of the light-cone wave functions for exclusive processes. *Phys. Lett.*, B441:371–375, 1998.

[136] M. Burkardt and S. K. Seal. A study of light mesons on the transverse lattice. *Phys. Rev.*, D65:034501, 2002.

[137] V. Braun and Dieter Mueller. Exclusive processes in position space and the pion distribution amplitude. *Eur. Phys. J.*, C55:349–361, 2008.

[138] A. Abada et al. Preliminaries on a lattice analysis of the pion light cone wave function: A partonic signal? *Phys. Rev.*, D64:074511, 2001.

[139] Simon Dalley and Brett van de Sande. Transverse lattice calculation of the pion light-cone wavefunctions. *Phys. Rev.*, D67:114507, 2003.